

TABLE OF CONTENTS

LIST OF ABBREVIATIONS	III
CHAPTER 1: INTRODUCTION	1
1.1 Background	4
CHAPTER 2: SITE, INSTRUMENTATION, DATA, AND METHODOLOGY	8
2.1 Haukeliseter site	8
2.2 Climate at Haukeliseter	10
2.3 Instruments	11
2.3.1 Double Fence Snow gauge	13
2.3.2 MRR - Micro Rain Radar	15
2.3.3 PIP - Precipitation Imaging Package	17
2.3.4 MASC - Multi-Angular Snowfall Camera	18
2.4 Optimal Estimation Retrieval Algorithm	18
2.4.1 Snowfall retrieval scheme	18
2.4.2 Environmental masks for the optimal estimation retrieval	22
2.5 Operational weather forecast model - MEPS	24
2.5.1 MetCoOP Ensemble Prediction System - MEPS	24
2.5.2 Meso-NH and the ICE3 scheme	26
2.5.3 Adjustment of ICE3 inside AROME-MetCoOp	29
2.6 Numerical data transformation	29
2.6.1 Layer thickness in MEPS	29
2.6.2 Snow water content	30
2.6.3 Snow water path	31
2.6.4 Ensemble mean and Coefficient of Variation	31
2.6.5 Mean error and mean absolute error	32
2.6.6 Percent difference and average difference	32

CHAPTER 3: ANALYSIS OF THE CHRISTMAS STORM 2016	33
3.1 Extreme weather	34
3.2 Dynamic Tropopause map	35
3.3 Thickness, Sea Level Pressure, Total Precipitable Water, and wind at 250 hPa	37
3.4 Integrated Vapour Transport	37
3.5 Observations at the weather mast	40
3.6 Large scale circulation	41
CHAPTER 4: HAUKELISETER: OBSERVATION AND MEPS COMPARISON	50
4.1 Meteorological Investigation of the Christmas storm 2016	51
4.1.1 Surface comparison	51
4.2 Snowfall comparison	67
4.2.1 Sensitivity of the optimal estimation retrieval	67
4.2.2 Comparison of surface observations	69
4.2.3 MEPS forecast and surface observation comparison	73
4.2.4 Comparison of Snow Water Content in the vertical	83
4.2.5 Orographic influence on precipitation	98
CHAPTER 5: SUMMARY AND OUTLOOK	106
5.1 Outlook	107
REFERENCES	109
APPENDIX A: FORWARD MODEL	120
A.1 Scattering Model	120
APPENDIX B: RESULTS	123
B.1 Hourly averages ensemble member zero and one	123
B.2 Vertical SWC - all ensemble member	126

LIST OF ABBREVIATIONS

ACC	Accretion
AGG	Aggregation
AR	Atmospheric River
AROME	Applications of Research to Operations at Mesoscale
AUT	Autoconversion
BER	Bergeron-Findeisen process
C3VP	Canadian CloudSat-CALIPSO Validation Project
CFR	Contact Freezing of Raindrops
CPR	Cloud Profiling Radar
CV	Coefficient of Variation
CVM	Conversion-melting
DDA	Discrete Dipole Approximation
DEP	Deposition
DRY	Dry processes
DT	Dynamic Tropopause
ECMWF	European Centre for Medium-Range Weather Forecasts

EPS	Ensemble Prediction System
FMI	Finnish Meteorological Institute
HEN	Heterogeneous Nucleation
HON	Homogeneous Nucleation
IVT	Integrated Vapour Transport
LWC	Liquid Water Content
MASC	Multi-Angular Snowfall Camera
MEPS	MetCoOp Ensemble Prediction System
Meso-NH	Mesoscale Non-Hydrostatic model
Met-Norway	Norwegian Meteorological Institute
MetCoOp	Meteorological Co-operation on Operational NWP
MLT	Melting
MRR	Micro Rain Radar
MSLP	Mean Sea Level Pressure
NSF	National Science Foundation
NWP	Numerical Weather Prediction
PIP	Precipitation Imaging Package
PSD	Particle Size distribution
RIM	Riming
SMHI	Swedish Meteorological and Hydrological Institute
SWC	Snow Water Content

SWP	Snow Water Path
WCB	Warm Conveyor Belt
WET	Wet processes
WMO	World Meteorological Organization

CHAPTER 4: HAUKELISETER: OBSERVATION AND MEPS COMPARISON

In this chapter the results of the surface observation, the optimal estimation retrieval and the regional mesoscale forecast model are presented. On the basis of the methodology described in Chapter 2 it should be evaluated if a regional mesoscale forecast model predicts the same synoptic patterns as observed at the measurement site. Also, vertical SWC forecasted by MEPS is being compared with the retrieved vertical SWC at Haukeliseter. Attention should be paid to the fact, that this study is unique. The motivation to compare regional model forecasts with vertical snowfall measurements resulted from a study by Joos and Wernli [2012]. They did sensitivity studies on the microphysical scheme of COSMO (COncsortium for Small-scale MODelling) and found that the storm development depends on the correct vertical placement of the precipitation inside a modeled storm. Vertical precipitation placement determines the vertical profile of latent heating, and hence the generation of potential vorticity which in return shows if a storm strengthens or weakens. Correct vertical precipitation observations can then help to correctly assess model vertical precipitation patterns.

This study will give a first insight into comparing snowfall model forecasts with observed snowfall, for one particular extreme event, the 2016 Christmas storm.

4.1 METEOROLOGICAL INVESTIGATION OF THE CHRISTMAS STORM 2016

One of the main factors, that made the Christmas 2016 storm so interesting is the fact that fronts passed over Norway during the six-day period. One aim of this thesis is to identify if large scale phenomena were observed at the measurement site and if MEPS predicted the same measured pressure, temperature, wind, and precipitation patterns during the extreme event.

4.1.1 SURFACE COMPARISON

The large scale weather situation was discussed in Section 3.6. It has shown, that two low pressure systems affecte Norway around Christmas 2016. Figure 4.1.1 display the observations and intialisations for pressure, temperature, wind, and precipitation on 21 to 27 December 2016.

A comparison between the surface observations at Haukeliseter and the ECMWF analysis of the dynamic tropopause and geopotential thickness maps show that frontal transitions occurred on three days during the 2016 Christmas storm, 23, 25, and 26 December 2016 (Section 3.6). These show in the measurements and MEPS ensemble forecasts on 23, 25, and 26 December 2016 (Figure 4.1.1).

Figure 4.1.1 shows the different parameters forecasts initialised at 0 UTC for 23, 25, and 26 December 2016, as well as the observations at the Haukeliseter measurement site. During all days the MEPS forecast seems to be able to predict similar pressure, temperature, wind, and precipitation as is observed. Overestimations are seen for wind speed and surface precipiation amount in Figure 4.1.1c, h, m, r, e, j,o, and t.

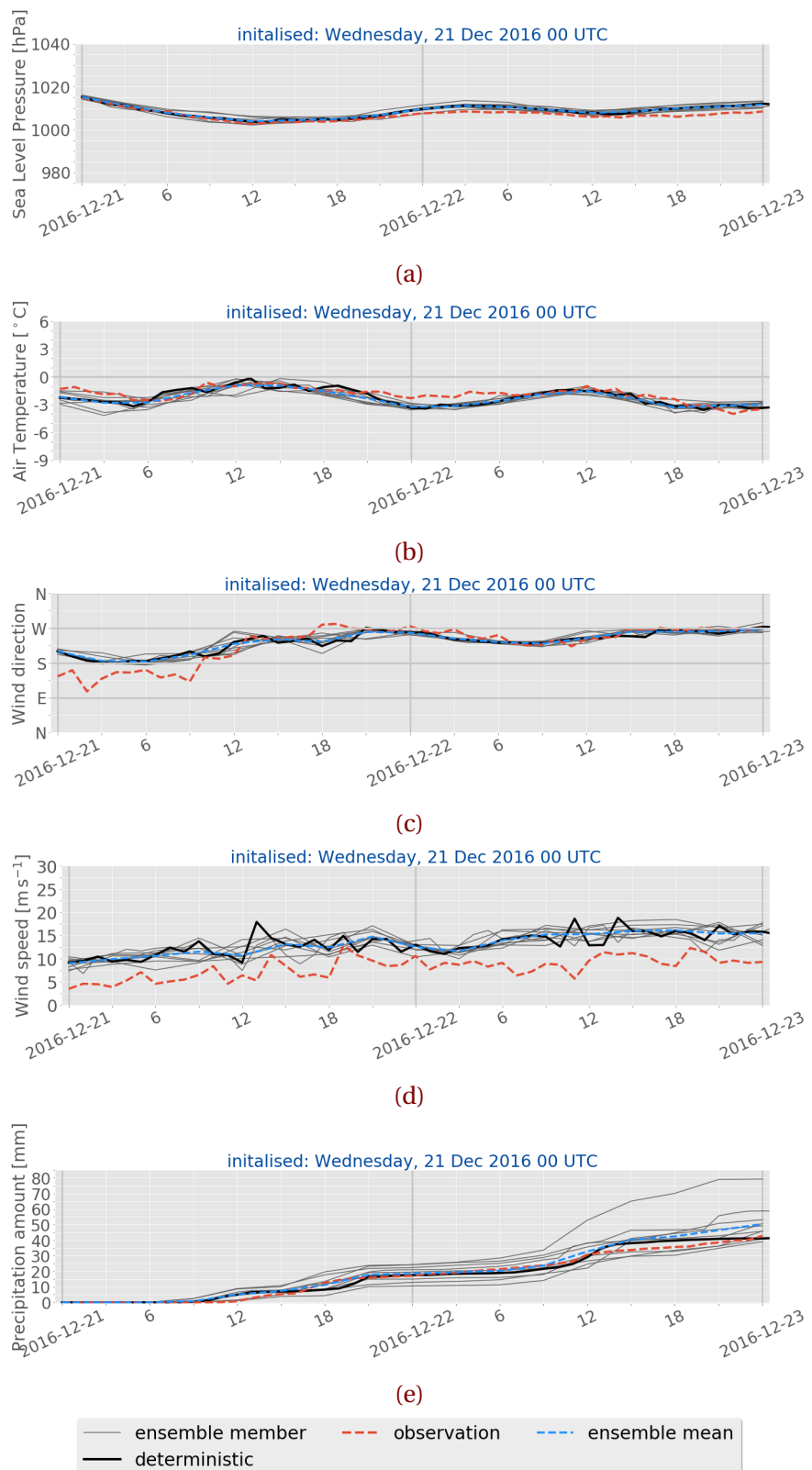


Figure 4.1.1: 48 h surface observations and MEPS ensemble forecasts initialised on 21 December 2016 at 0 UTC. Line representation according to the label. Upper to low panel: sea level pressure, 2 m air temperature, 10 m wind direction and speed, and precipitation amount. *Continued on next page.*

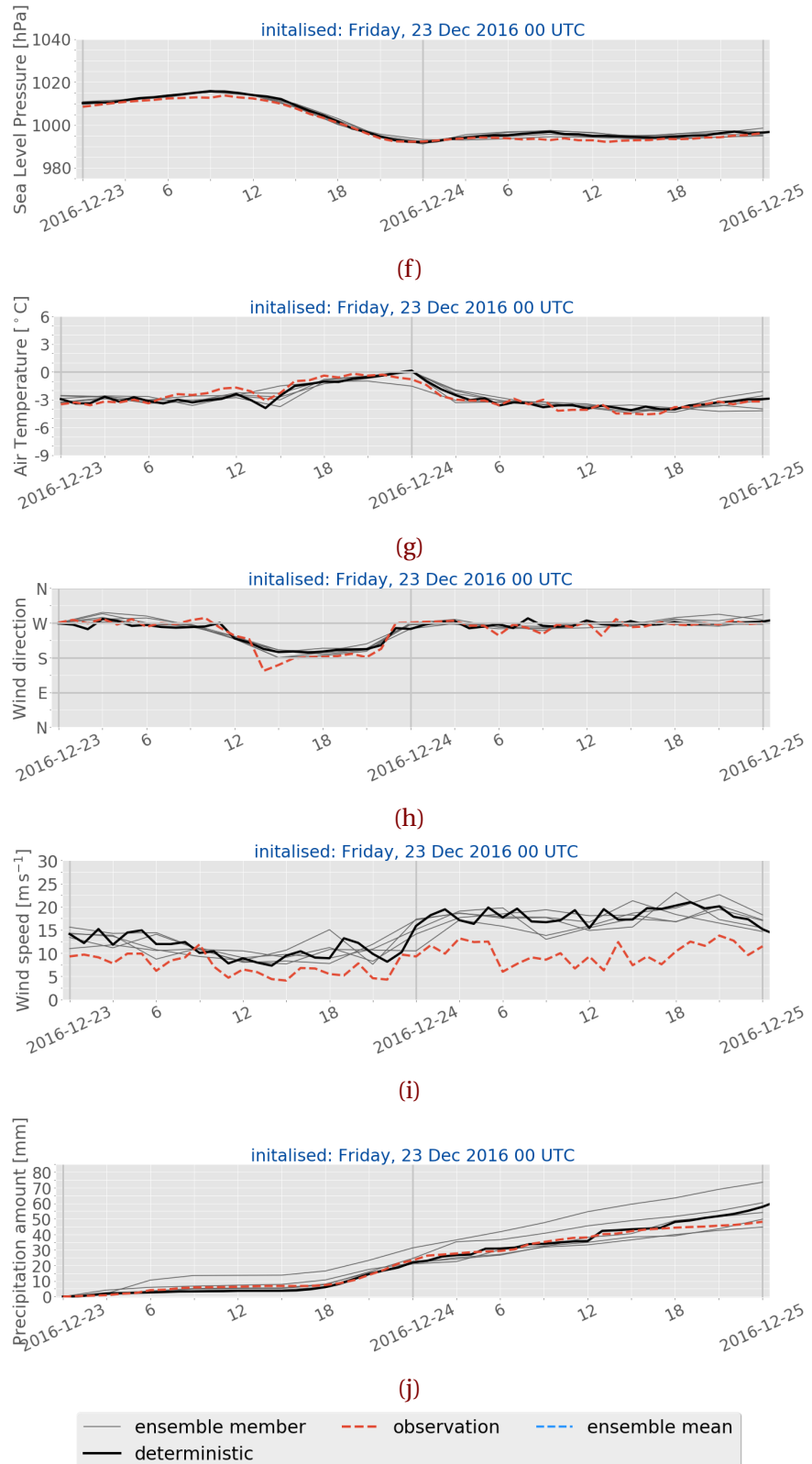


Figure 4.1.1: (Continued from previous page.) Initialisation on 23 December 2016 at 0 UTC.

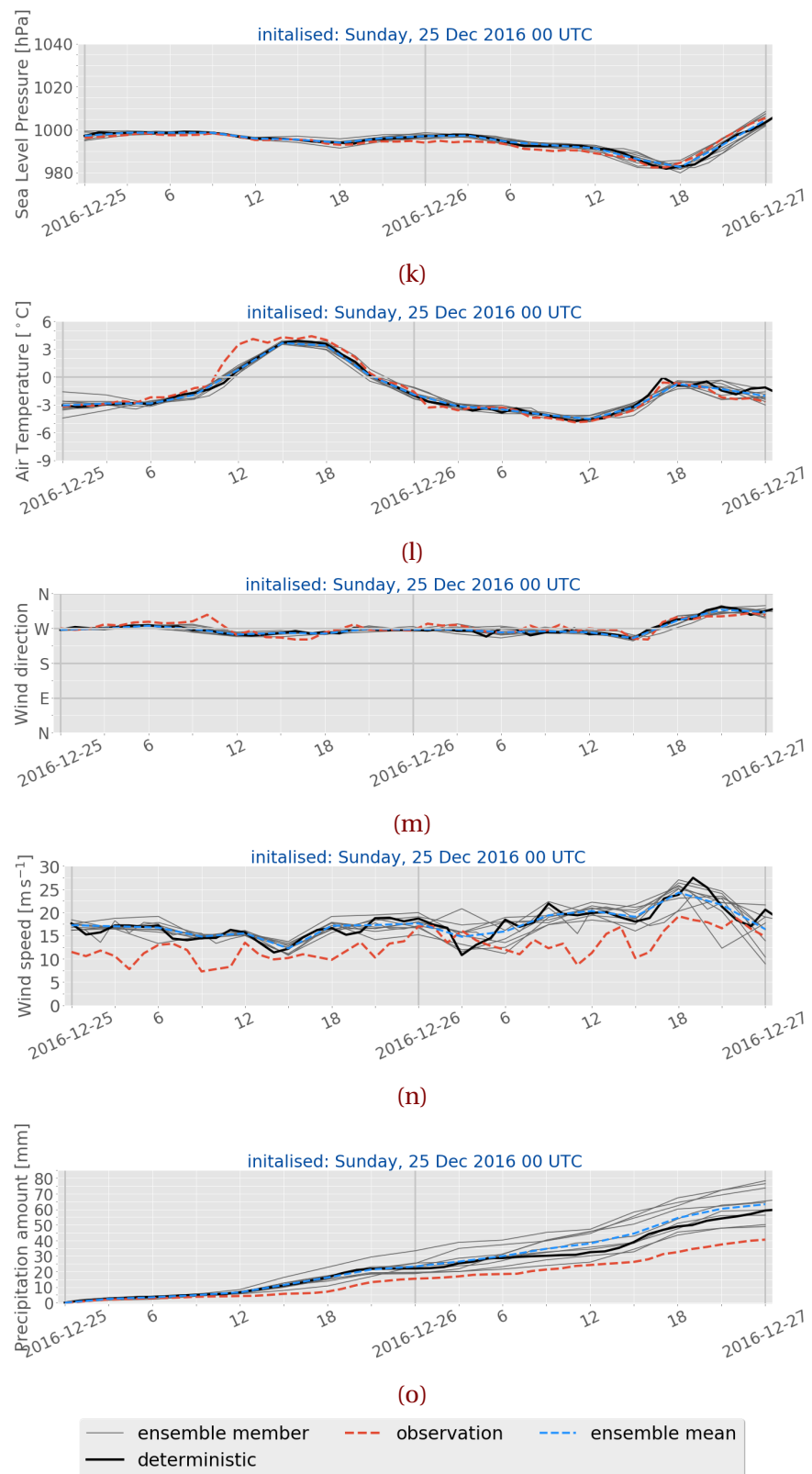


Figure 4.1.1: (Continued from previous page.) Initialisation on 25 December 2016 at 0 UTC.

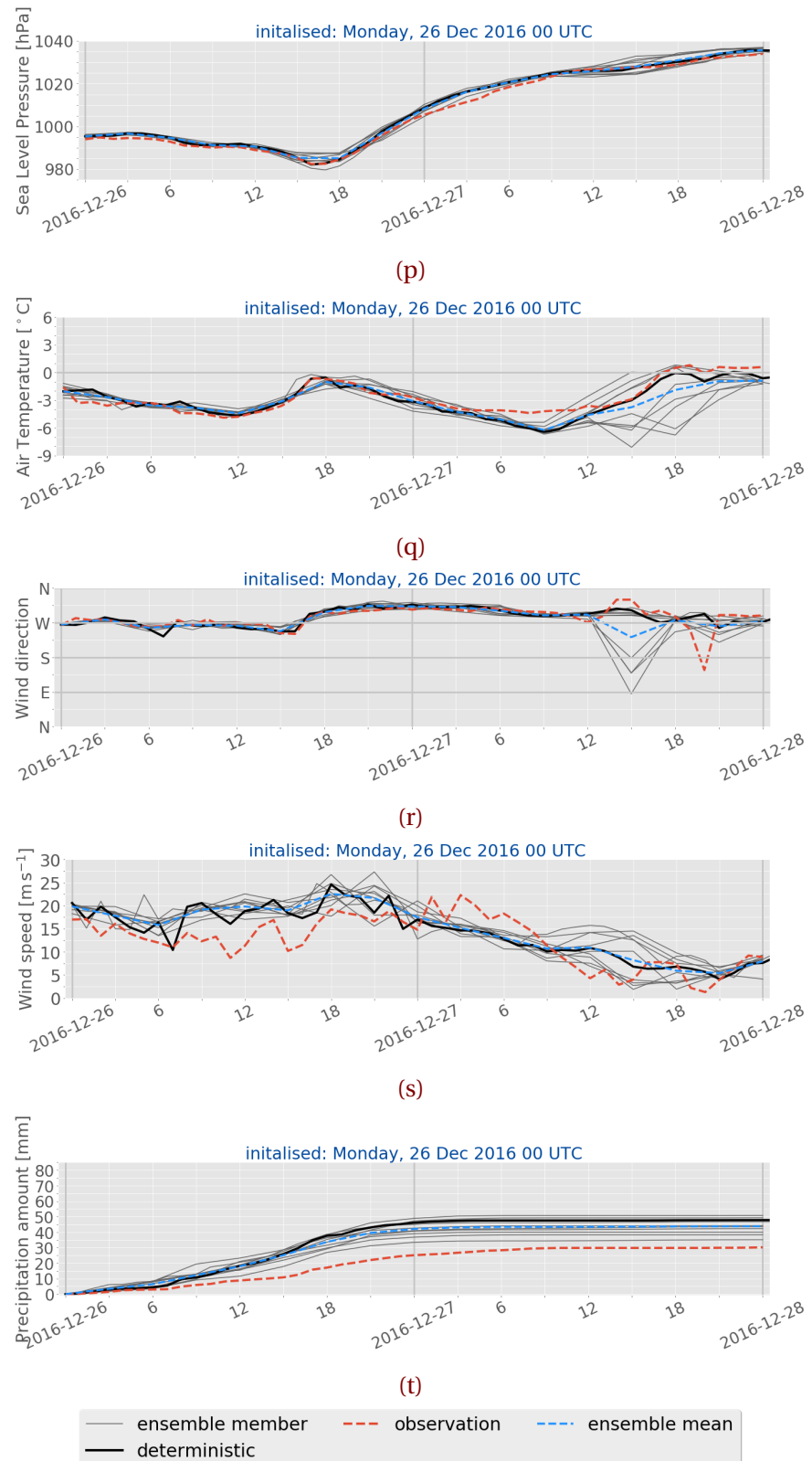


Figure 4.1.1: (Continued from previous page.) Initialisation on 26 December 2016 at 0 UTC.

include R-coefficient Figure 4.1.2 presents the correlation between the observations and the 48 h MEPS ensemble forecast. The relation for Haukeliseter observations and the MEPS forecast members is indicated with the regression calculated for each day. Sea level pressure has the best correlation of all variables. The scatter plots in Figure 4.1.2 show a good correlation for pressure and temperature. Wind direction (Figure 4.1.2f) displays good agreement for 24 to 26 December 2016, but the MEPS forecast imply a disagreement with southerly observed winds in Figure 4.1.2e, between 21 and 23 December 2016. Wind speed is overestimated throughout the event and will be further assessed in Section 4.2.5 (Figure 4.1.2g, h). Surface precipitation amount disagree more between 24 and 26 December 2016 than on 21 to 23 December 2016 (Figure 4.1.2i, j). Figure 4.1.2i suggests a better correlation below 20 mm, for 21 to 23 December 2016 than above. A detailed discussion about the precipitation overestimation at the surface is given in Section 4.2.3. On 23 and 26 December 2016, pressure decreases and increases, as well as temperature increases, and wind changes are present. Since these changes show in the surface observations in Figures 4.1.1f to 4.1.1j and, Figures 4.1.1p to 4.1.1t, it is assumed that frontal boundaries passed through Haukelieseter. The 25 December 2016 shows an increase of temperature between 15 UTC and 17 UTC leading to the assumption of a warm air evolution in Figure 4.1.1l. The overall weather situation, described in Section 3.6, showed that a warm front as well as cold front influenced Norway, on 25 December 2016. Since pressure and wind do not indicate a change related to frontal development, it is assumed that only the warm air section between the warm and cold front is shown in the surface measurements at Haukeliseter (Figure 4.1.1l).

As described in Section 3.6 the ECMWF dynamic tropopause analysis (Figure 3.6.2a) shows more ridging at the DT level on 23 December 2016, than on the previous days. Warm air is advected closer over to Southern Norway (Figure 3.6.2a). The low-pressure system approaches in the course of the day south-east of Iceland and hence stronger west to south west wind are associated with the cyclone (Figure 3.6.2c). The MEPS forecast, initialised on 23 December 2016 at 0 UTC in Figure 4.1.1f follows the observations and shows the decrease in pressure after 12 UTC due to the shift of the occluded front with a constant pressure after the transition. Since warmer air is more advected to the north and the DT in Figure 3.6.2a shows a warm low-pressure core, an increase in temperature is observed and predicted at the measurement site (Figure 4.1.1g). **Include L, H in the surface pressure**

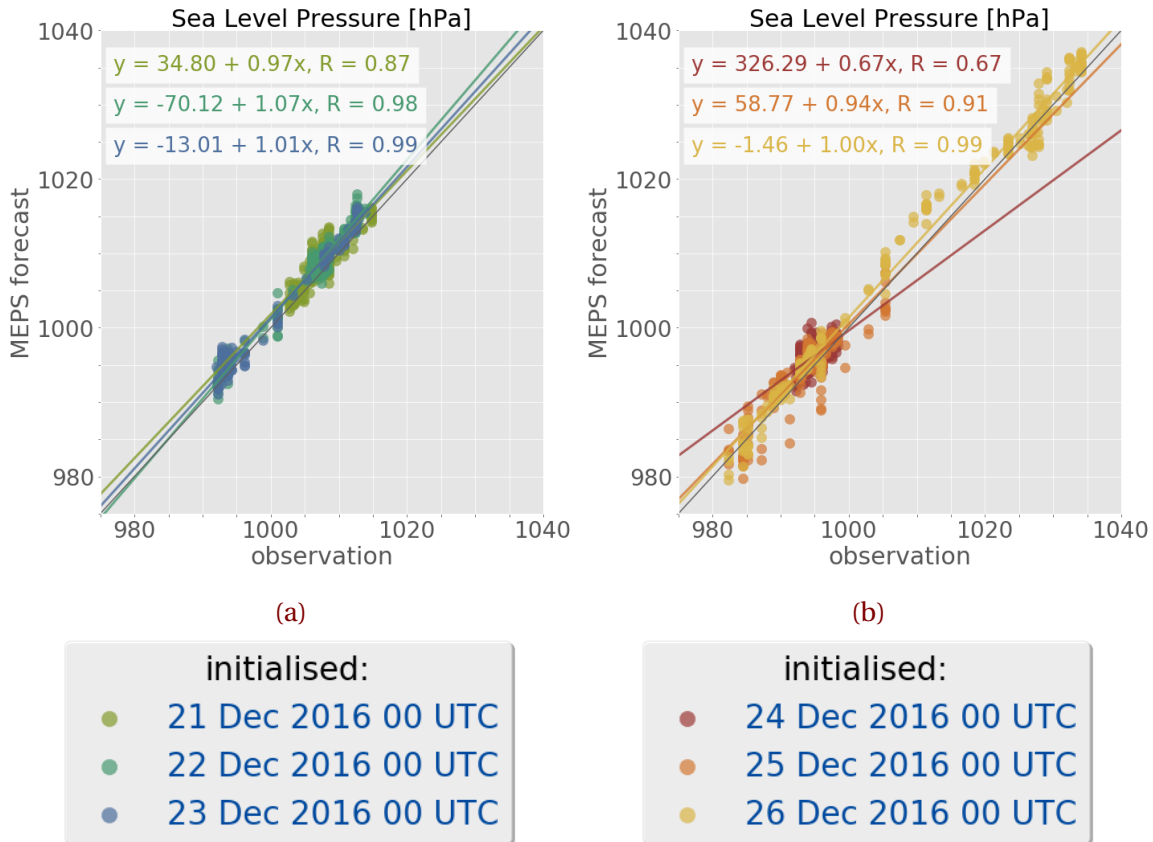


Figure 4.1.2: Scatter plots for surface observations and ensemble forecasts initialised for 21 to 23 December 2016 (left column, **a, c, e, g, i**) and for 24 to 26 December 2016 (right column, **b, d, f, h, j**). The 48 h scatter values indicate each day, showing the 1 h and 3 h forecasts respectively for 48 h. *Continued on next page.*

images

As the cyclone is advected to the north-east, closer into the Norwegian Sea, a wind change is seen in the ECMWF analysis (Figure 3.6.2c). First west wind and later south-west wind is associated with the low-pressure system. The MEPS forecast and observations in Figure 4.1.1h and i indicate a wind change from west to south with a slight decrease in wind speed.

On 23 December 2016, the evolution of the occlusion is also observed by an increase in precipitation. Before 18 UTC the surface accumulation shows light precipitation (Figure 4.1.1j). During the passage of the occlusion, the observed surface accumulation increases which is associated to continuous, heavy precipitation shown in Figure 4.1.1j.

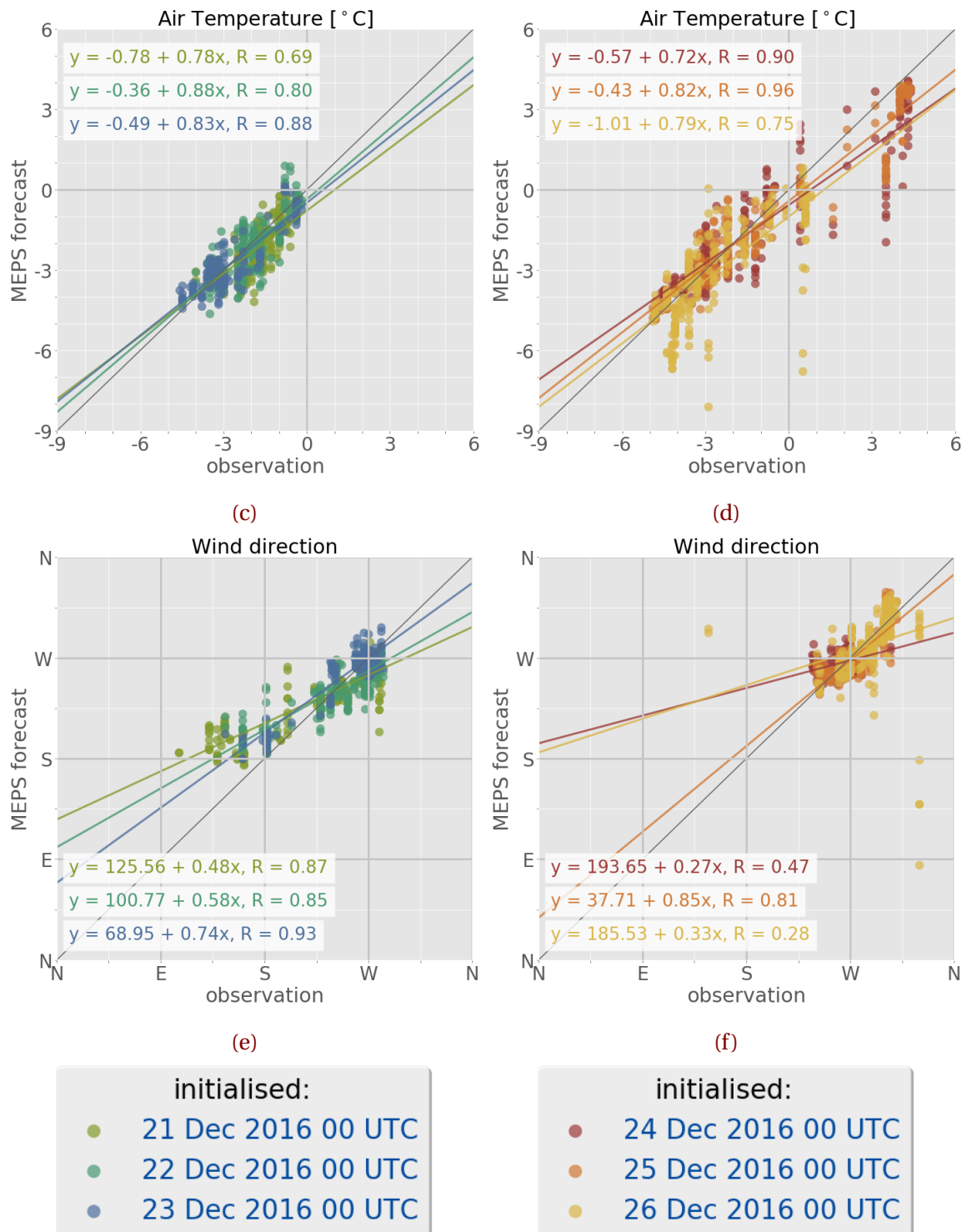


Figure 4.1.2: (Continued from previous page.) Upper panel 2 m air temperature, second panel 10 m wind direction.

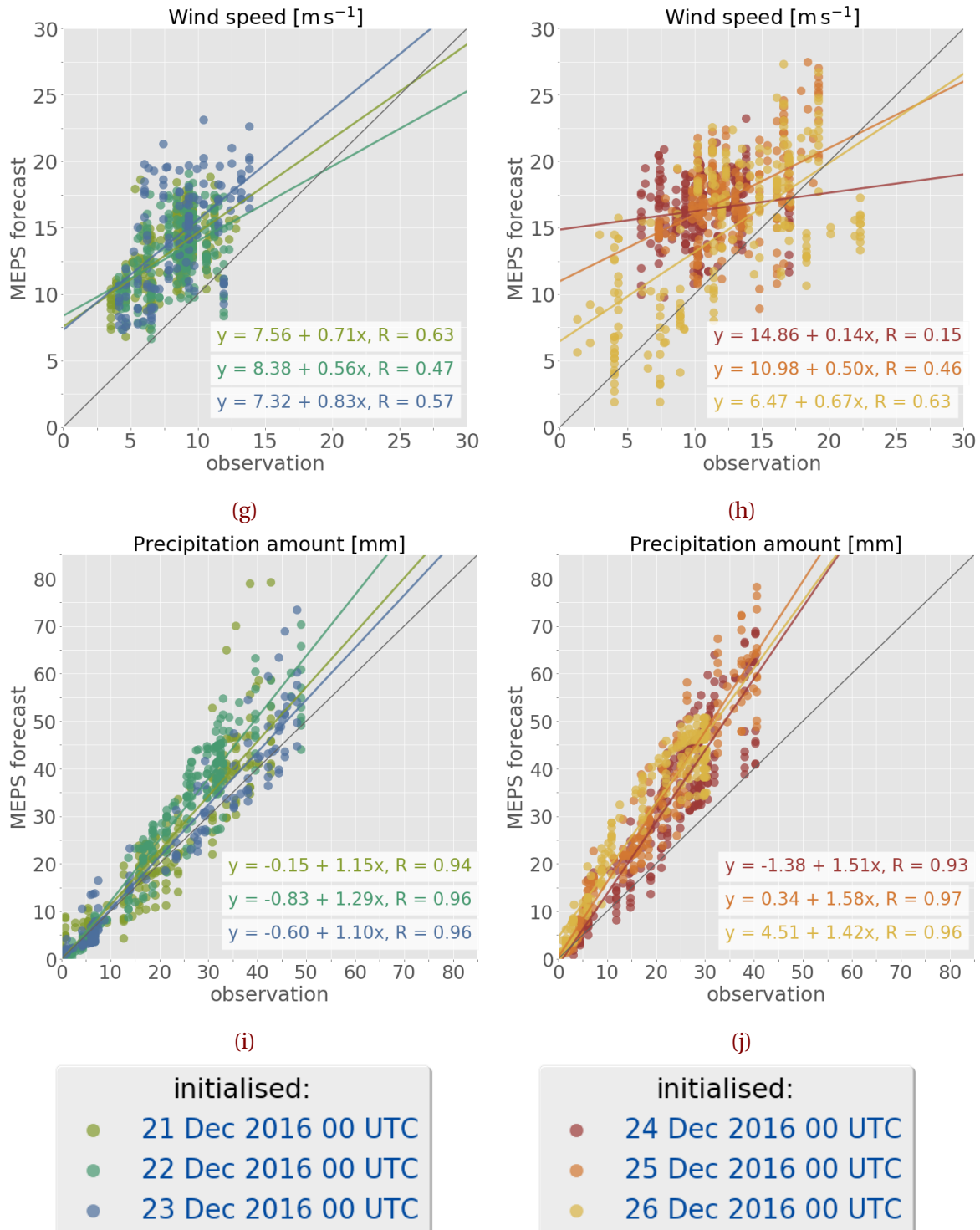


Figure 4.1.2: (Continued from previous page.) Upper panel 10 m wind speed, lower panel surface precipitation amount comparing double fence observations to 48 h MEPS forecasts.

Similar patterns as on 23 December 2016 were seen for the evolution of the occluded front on 26 December 2016 in the ECMWF analysis Figure 3.6.2n and 3.6.2p. In this case the low-pressure system was located north of Møro and Romsdal in the Norwegian Sea. In the morning the cyclone is located east of Iceland and in the course of the day it moves closer to the coast of Norway (Figure 3.6.2o and 3.6.2q). Before landfall at 16 UTC, a pressure decrease occurs at Haukeliseter (Figure 4.1.1p). During the development of the occluded front, the sea level pressure reaches its lowest point of 985 hPa (Figure 4.1.1p) and increases afterwards during the dissipation of the 2016 Christmas storm.

Since the cyclone was surrounded by colder air (south of the low-pressure system in Figure 3.6.2n), first a drop and then an increase of temperature were observed and forecasted by MEPS (Figure 4.1.1q). An indication of the occlusion evolution is also visible in the 10 m wind observations and MEPS predictions in Figure 4.1.1r and s. On 26 December 2016 at 0 UTC, the low pressure system is east of Iceland (not shown), moving closer into the Norwegian Sea by 12 UTC (Figure 3.6.2n and 3.6.2p). Surface west winds are associated to the cyclone in the Norwegian Sea, and impinging on the West coast of Norway Figure 3.6.2p. The wind measurement and MEPS forecast in Figure 4.1.1r and 4.1.1s, show a gentle west breeze of up to 17 ms^{-1} at Haukeliseter before 12 UTC. The centre of the occluded front is located over Norway at 18 UTC, and the pronounced surface pressure gradient, in Figure 3.6.2q, indicate an increase in surface wind with a north-west wind direction. During this transition of the occlusion, the wind direction changes to north-west with higher observed wind speeds up to 20 ms^{-1} (Figure 4.1.1r and 4.1.1s).

Precipitation is continuing throughout the day, with light to moderate precipitation before the occlusion passage seen in Figure 4.1.1t. Heavy precipitation related to the occlusion, around 16 UTC, is followed by moderate to light deposition on 26 December 2016.

While on 23 and 26 December 2016 precipitation was associated with a transition respectively landfall of an occlusion, the 25 December 2016 was marked by the transition of a warm sector. The ECMWF analysis shows a ridging of warm air at the dynamic tropopause (Figure 3.6.2i). The cyclone core is south east of Iceland in Figure 3.6.2i with two associated frontal boundaries. While the warm front is approaching the west coast, the cold front is north-west of Great Britain. In Figure 3.6.2k, the tail of the cold front moved into lower latitudes, following the slowdown of front, leading to a stationary frontal boundary.



Figure 4.1.3: MASC images of falling water drops observed on 25 December 2016 at 17 UTC from three different angles. Not all parts of the liquid sphere are equally illuminated.

Furthermore, the mid-latitude jet is aligned with the surface frontal boundaries (??), while the Haukeliseter site is located below the the midlatitudal jet (??).

Neither pressure nor wind observations and forecasts in Figure 4.1.1k, m, and n, indicate the evolution of any frontal boundary. The only indication of a transition could be seen in the increase and then decrease of temperature at 11 UTC until 21 UTC (Figure 4.1.1l). In Figure 4.1.1m, a small wind change from west to north-west is observed by the wind mast at 10 UTC, which is not forecasted by MEPS, it rather estimated strong westerly winds.

Particle images taken by the MASC are available on 25 December 2016, during the transition of the warm sector in Figure 4.1.3. Without theses images taken around 17 UTC it would only be possible to verify that liquid precipitation occurred with the optical precipitation detectors at the Haukeliseter site. Together with the increase in surface temperature (Figure 4.1.1l) it can be concluded that the warm sector of the Christmas 2016 event passed by the measurement site. **KICKI: Should I include the DIANA analysis maps? But the meteorologist also use ECMWF to make them!**

The comparison between the ECMWF analysis (Section 3.6) and the observations at the measurement site (Figure 4.1.1), led conclude that the ensemble member forecast system MEPS covers the prediction of large scale phenomena like occlusions and fronts, as well as liquid precipitation at the surface.

The scatter plots for observations and MEPS forecast show good correlation for most variables (Figures 4.1.2a to 4.1.2d, and f). The best agreement for pressure is reached on 26 December 2016 (Figure 4.1.1p), when the Christmas storm hit land and dissipated

after the evolution of the occlusion at 16 UTC. Dahlgren [2013] showed an improvement of sea level pressure forecast for AROME, by including large scale boundary conditions for ECMWF into the regional model. The observation-model comparison by Dahlgren [2013] showed a decrease of pressure bias with lead time after 24 h with the use of pressure mixing. Since surface pressure is in good agreement with the observations, it is assumed that the warm front did not pass through Haukeliseter on 25 December 2016 and only the warm sector associated with the 2016 Christmas storm is observed. This shows a quite detailed forecast ability of MEPS, as from the ECMWF analysis, in Figure 3.6.2i, it is not quite clear if the warm front could have passed through. To be sure that the warm front did not pass through Haukeliseter, or whether it is a predictive error of MEPS, surface pressure, temperature and wind should be compared to the nearest grid point of the global forecast model ECMWF to verify this result.

Figure 4.1.2d displays a moderate correlation between observation and the 48 h MEPS ensemble member forecast system. In general, MEPS underestimates the observed 2 m air temperature, but MEPS estimated the surface temperature changes at the correct occurrence for 23, 25, and 26 December 2016.

Figure 4.1.4b shows warm and cold biases for 23 and 26 December 2016, respectively. On 25 December 2016, within the warm sector a cold bias was observed, underestimating the temperature when compared to the observation. The forecasts for 23, 25, and 26 December 2016 show calculated mean absolute error values (Equation (2.6.11)) of up to 0.61 K, 0.77 K and 1.44 K in Figure 4.1.5b. The previous operational deterministic forecast model AROME-MetCoOp showed a cold bias of 2 m temperature for the Norwegian mean, during winter 2013 with the introduction of AROME-Norway and later AROME-MetCoOp [Müller et al., 2017]. The mean error for the Norwegian model domain of AROME-MetCoOP estimated by Müller et al. [2017] is smaller than 1.8 K for the surface 2 m temperature in December 2014. The new ensemble forecast system MEPS shows a reduction of mean errors for the Christmas 2016 extreme event, when compared to the Norwegian mean of AROME-MetCoOp.

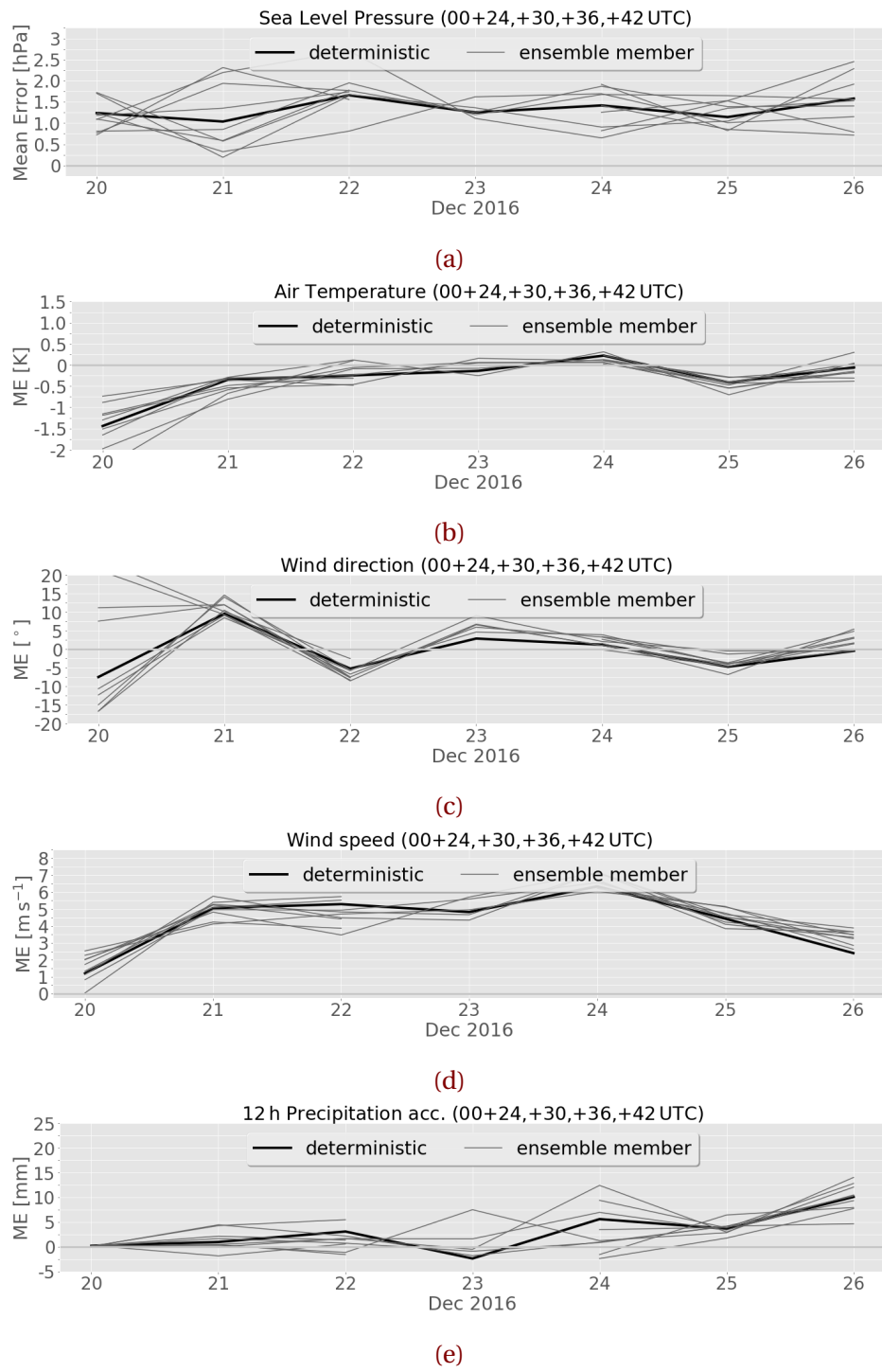


Figure 4.1.4: Mean error (a, b, c, d, e) of surface variables for all ten ensemble members at Haukeliseter, initialisations at 0 UTC, valid for 48 h. From top to bottom, sea level pressure (a), 2 m air temperature (b), 10 m wind direction (c), 10 m wind speed (d), precipitation accumulation for 12 h surface accumulation (e).

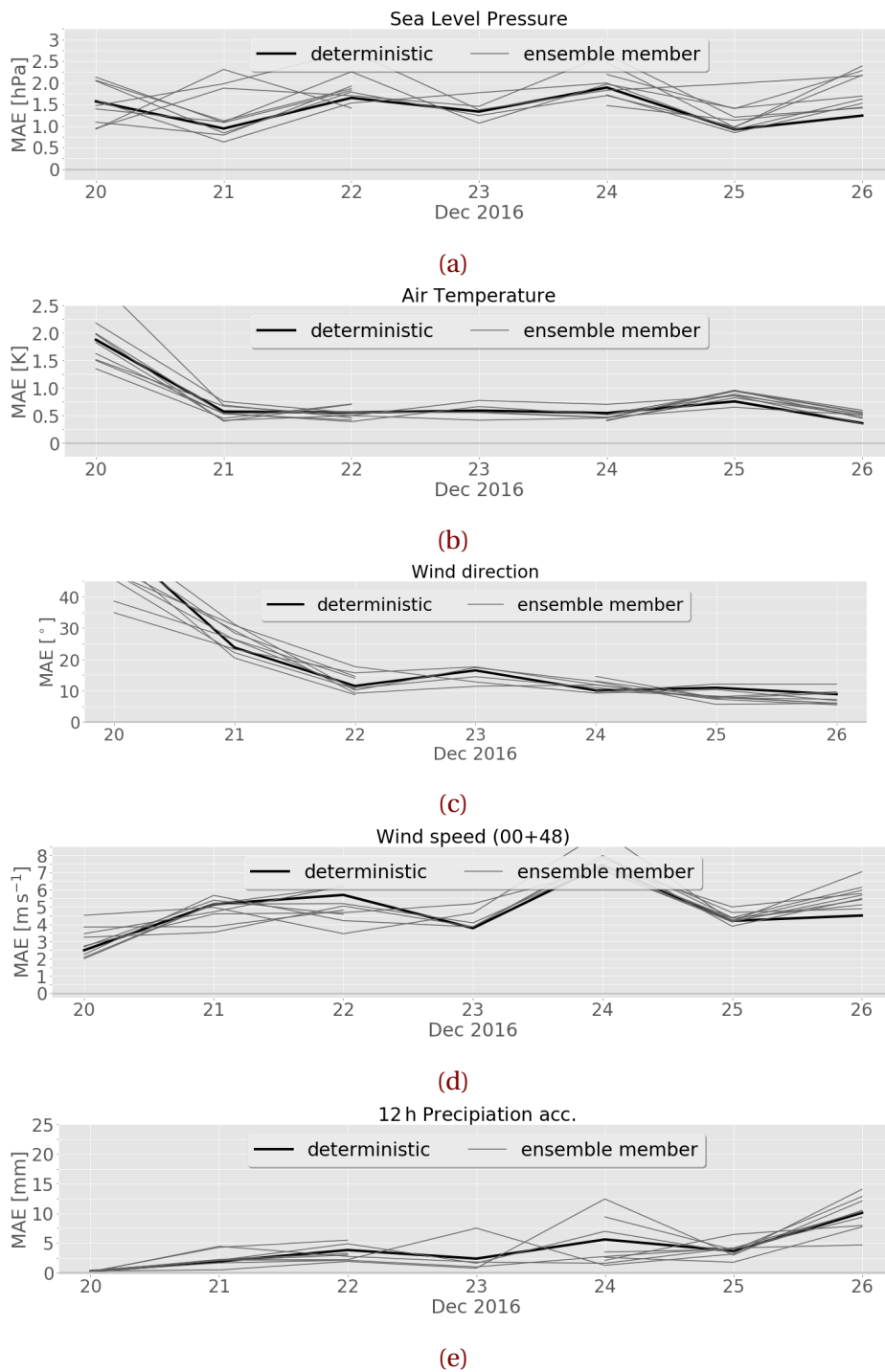


Figure 4.1.5: Mean absolute error (a, b, c, d, e) of surface variables for all ten ensemble members at Haukeliseter, initialisations at 0 UTC, valid for 48 h. From top to bottom, sea level pressure (a), 2 m air temperature (b), 10 m wind direction (c), 10 m wind speed (d), precipitation accumulation for 12 h surface accumulation (e).

During the Christmas storm 2016, high wind speeds were observed at the Haukeliseter site (Figure 4.1.1i, n and s). According to Müller et al. [2017] high wind speeds are significantly better simulated for AROME-MetCoOp compared to ECMWF's forecast for the model domain. Wind speed MEPS predictions in Figure 4.1.1i, n, and s displays still an overestimation of wind speeds throughout the event. Furthermore, the correlation of observations and wind speed in Figure 4.1.2g and h show an overestimation for stronger wind speeds on 24 to 26 December 2016 than for 21 to 23 December 2016. The mean absolute error for wind speed during the Christmas storm is ranging from 3 m s^{-1} to 7 m s^{-1} for 48 h lead time. During the three days of frontal transitions, the highest mean absolute error of 6.5 m s^{-1} occurs for initialisations on 23 December 2016. The inaccuracy for wind speeds is an already known difficulty in the deterministic version of MEPS [Müller et al., 2017]. Müller et al. [2017] presented, that AROME-MetCoOp wind speed prediction generally agreed better with observations for wind speeds between 3 m s^{-1} to 13 m s^{-1} than ECMWF forecasts did, showing the advantage of a high-resolution weather model. Furthermore, with increasing wind speed the forecast accuracy for the Norwegian mean decreased with a mean absolute error below 2 m s^{-1} for 6 h to 24 h lead times, in December 2014 in AROME-MetCoOp. Müller et al. [2017] study case showed a slight underestimation of ECMWF 10 m wind compared to the Norwegian AROME-MetCoOp forecast for February 2015. On 23 December 2016, the mean absolute error is more than three times as high as the monthly averaged value for the Norwegian forecast domain (2 m s^{-1} for 6 h to 24 h forecast time) from Müller et al. [2017]. The larger mean absolute error during the event is firstly related to the comparison of a long term study of Müller et al. [2017], secondly their mean absolute error monthly average for 6 h to 24 h lead times, and third to the location of Haukeliester.

Haukeliseter is a measurement site exposed to high wind speeds [Wolff et al., 2013, 2015]. The ensemble prediction system MEPS seems to still have issues forecasting the wind speed correctly in mountainous terrain. A detailed insight to the orographical wind influence will be assessed in Section 4.2.5.

Pressure, temperature, and wind changes for the occlusion transition on 26 December 2016 were already forecasted for initialisations on 25 December 2016 (Figure 4.1.1k, l, m, n), only wind speed and precipitation seem not to agree with the observations at Haukeliseter. The same is true for 25 December 2016, when the warm sector passes through Haukelis-

eter.

Figure 4.1.1e, j, o, and t illustrate the surface precipitation amount observed and predicted by MEPS for Haukeliseter. MEPS overestimation is shown for precipitation when the cyclone intensifies and gets closer to Norway on 24, 25 and 26 December 2016. The surface observations and MEPS predictions in Figure 4.1.2i and j show an overestimate for 24, 25 and 26 December 2016, whereas on 21, 22, and 23 December 2016 the surface accumulation is balanced for predictions up to 30 mm. Any reasons for the overestimation of precipitation accumulation on the ground will be further analysed and discussed in Section 4.2.3. What could be still a weakness that the model overestimates the wind speed? In Müller et al. [2017]: change from ECOCLIMAP1 because the surface roughness was too low and followed high wind speeds? Is this still the case for MEPS? High wind speeds followed also from wrongly addressed 'permanent snow'. Do not use 'orographic drag' in AROME-MetCoOp, could that lead to the too high estimated wind? When 'canopy drag' was changed saw increase in SBL drag which followed a decrease in wind speed. But AROME-MetCoOp is able to forecast high wind speeds, while ECMWF is not.

Overall, for initialisations on 21 to 23 December 2016 (Figure 4.1.2a, c, e, g) the forecast is best for all variables. The large-scale weather pattern seems to be more predictable as long as the weather situation is not extreme. Figure 4.1.2b, d, f, h suggest as if MEPS has difficulties predicting the intensification and associated pressure decrease of the Christmas 2016 storm at Haukeliseter. The prediction of pressure fits well on all days (Figure 4.1.2a, b) compared to temperature, wind direction, wind speed, and precipitation (Figures 4.1.2c to 4.1.2j). The greatest difficulty has MEPS with the prediction of wind speed during the entire extreme event. The rainfall, however, fit well for 23 December 2016 (Figure 4.1.1j and 4.1.2i), but MEPS has problems predicting the accumulation of surface precipitation amount correctly for the extreme days of the 2016 Christmas storm, 24 to 26 December 2016 (Figure 4.1.1o, t and Figure 4.1.2j).

Figures 4.1.2a to 4.1.2d have shown good agreement of ensemble members. It is not expected that ensemble members agree they should just give a variability around the observations, that is why ensemble member prediction exists (Section 2.5). Based on the uncertainty in observations the solution space that is possible has to be understood. During extreme events the model is not adjusted to present the extreme event particularly

well.

4.2 SNOWFALL COMPARISON

Get some text to flow

4.2.1 SENSITIVITY OF THE OPTIMAL ESTIMATION RETRIEVAL

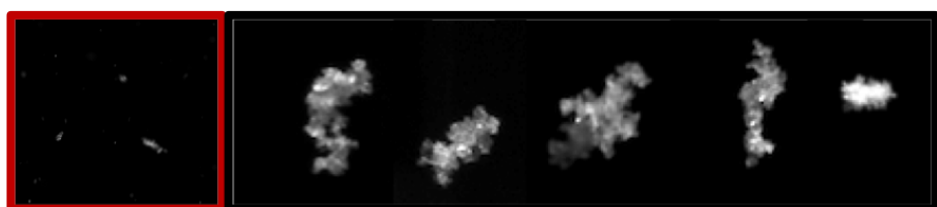


Figure 4.2.1: MASC observations during the Christmas storm 2016. Left (red frame), small ground up blowing snow particles. Five images on the right, rimed particles.

The optimal estimation retrieval scheme was applied to the six-day Christmas 2016 storm event. MASC images of snowfall during the event were used to guide the selection of the appropriate particle model and PSD input for the retrieval scheme. In this section, the sensitivity of retrieval results to these inputs is explored. Such an exercise should also allow an identification of those properties that yield the best match with Met-Norway snow gauge measurements at Haukeliseter.

The majority of the MASC images from Haukeliseter contained snow particles that looked like the left image Figure 4.2.1 (red frame). Such images suggest small ground-up blowing snow particles that are consistent with the high winds observed during the event. However, a careful examination of the MASC images also finds the presence of rimed aggregates such as those in the right five images (Figure 4.2.1). Pristine crystals such as plates and columns were not observed during the christmas 2016 event. As such, the use of two different aggregate particle models developed for the CloudSat mission were explored.

Figure 4.2.2 presents hourly measured snowfall accumulations on 22 December 2016 plotted against retrieved values for the two different aggregate assumptions. The 'B8' aggregate is a low reflectivity per unit mass aggregate that worked well for the cold, dry conditions observed at Barrow as described in [Cooper et al. \[2017\]](#). The 'B6' aggregate is a high

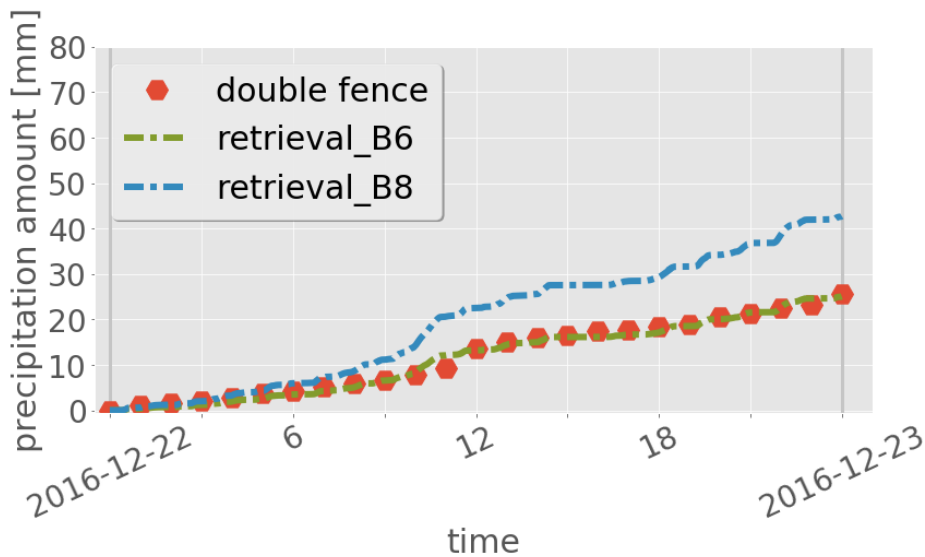


Figure 4.2.2: Hourly double fence snowfall accumulations [mm] plotted against retrieved values for the 22 December 2016 for different retrieval assumptions permutations. Double fence snowfall accumulation, red hexagons, retrieved precipitation amount for the here used study (B6), green, dash-dotted, and for small aggregates (B8), blue dashed.

reflectivity per unit mass particle. As such, the 'B6' aggregate would seem more physically consistent with the observed rimed particles and high water environment found in the coastal mountains at Haukeliseter. The presence of a water or rimed coating on the aggregates aloft would greatly enhance their effective reflectivity. Indeed, Figure 4.2.2 suggests that the reflective 'B6' aggregate agreed much better than the less reflective 'B8' aggregate with the snow gauge.

Table 4.2.1 presents the percentage differences between snow gauge and retrieved estimates found when using these particle model assumptions for 22 December 2016. Use of the 'B6' aggregate agreed within 5 % of the double fence observations (Table 4.2.1) for both 12 h and 24 h surface accumulations. Admittedly, use of the 'B6' aggregate produced slightly too little snowfall relative to the gauges for the remaining days of the event as discussed in Section 4.2.2. The use of the 'B8' aggregate, however, overestimated snowfall by at least 65 % for both the 12 h and 24 h surface accumulations (Table 4.2.1). Since this aggregate had low reflectivity per unit mass, it required significantly more SWC in the for-

Table 4.2.1: Observations (obs.) and retrieved (ret.) snowfall amounts for 22 December 2016 for different particle model assumptions. B6 indicating the here uses particle model (Appendix A.1) and B8 indicating the retrieved snowfall amounts for small particles.

Particle model	12 h accumulation				24 h accumulation			
	Snowfall		Difference	Snowfall		Difference		
	obs.	ret.		obs.	ret.			
	[mm]		[%]	[mm]		[%]		
B6	13.6	13.2	-3.0	23.1	25.1	-2.1		
B8	13.6	22.5	+65.5	23.1	42.7	+66.9		

ward model calculations to match MRR reflectivities. The retrieval therefore overestimates snowfall rate for these meteorological conditions.

The discussion here has focused on MASC estimates of habit instead of PSD or fall speed. The reason is that the MASC and PIP saw primarily blowing snow particles at the surface that likely were much smaller than the particles that the MRR remotely sensed aloft. The use of the PSD measured by the MASC or PIP in the retrieval therefore produced snowfall totals much greater than those measured by the double fence snow gauges. Essentially, it takes a much greater mass of small particles than large particles to match a given reflectivity. These results contrast with those found for low wind speed events at Haukeliseter where the use of MASC habit, PSD, and fall speed observations resulted in retrieved snowfall accumulations very close to Met-Norway double fence gauge observations. Regardless, for this high wind event, the [Wood \[2011\]](#) a priori temperature PSD relationship and a climatological average fallspeed of 0.85 ms^{-1} [private communication, [Schirle, 2018](#)] were employed.

4.2.2 COMPARISON OF SURFACE OBSERVATIONS

To be able to compare the vertical predicted snow water content with the retrieved snow water content a verification of the surface accumulation is made. If the retrieved surface accumulation is confident in comparison to the double fence measurement, then the vertical measurements can be trusted.

The correlation in Figure 4.2.3a demonstrates a good agreement between the 48 h accumulation measured by the double fence and the retrieved surface accumulation. The black line in Figure 4.2.3a presents a linear correlation with a regression coefficient of $R = 0.97$. In general, the retrieved surface snowfall accumulation is underestimated when compared to the double fence measurements, but not to a large degree.

Figure 4.2.3b shows the difference between retrieved accumulation and observed accumulation by the double fence. For the time period 20 to 24 December 2016, Figure 4.2.3b indicates an underestimation of retrieved snow accumulation of less than -5 mm for the first 24 h. Snow accumulation calculated on 23 December 2016 at 0 UTC show after 24 h an underestimation by the retrieval of up to -6.5 mm. On 24 December 2016, larger underestimation after 43 h is related to the observation of liquid precipitation on 25 December 2016 between 12 UTC to 21 UTC. On 25 December 2016 no fair comparison to the double fence measurement can be performed after 12 UTC because of the neglection of liquid precipitation when temperatures exceed 2°C .

For a 12 h accumulation follows for the Christmas storm (21 to 26 December 2016) an average difference of 85.5 % (Table 4.2.2). For longer, 24 h accumulation decreases the average difference to be -4.7 % (excluding values on 25 December 2016 after 12 UTC and on 26 December 2016 after 17 UTC because of attenuation at the MRR). The daily surface snowfall accumulation difference between retrieval and observation in Table 4.2.2 show almost always a well agreement to the double fence. The only well pronounced mismatch is seen on 21 December 2016, where it measures much more than the double fence gauge (+435.8 %).

Similar to this study, Cooper et al. [2017] used a CloudSat snow particle model, PSD and fall speed from MASC observations for five snow events at Barrow, Alaska. The comparison to the weather station revealed an difference between National Weather Service observations and retrieved accumulations of -18 % for five snow events.

Table 4.2.2 shows the difference for each individual day and the average difference for six and four days, depending on the accumulation of 12 h or 24 h. The choice of the correct PSD model, slope parameters and fall speed in the optimal estimation snowfall retrieval, shows a good agreement with the observations at Haukeliseter for the 2016 Christmas storm in contrast to the 200 % difference when only using the CloudSat snowfall algorithm (Section 2.4). It indicates also a reduction of the non-uniqueness of snow accumulation is

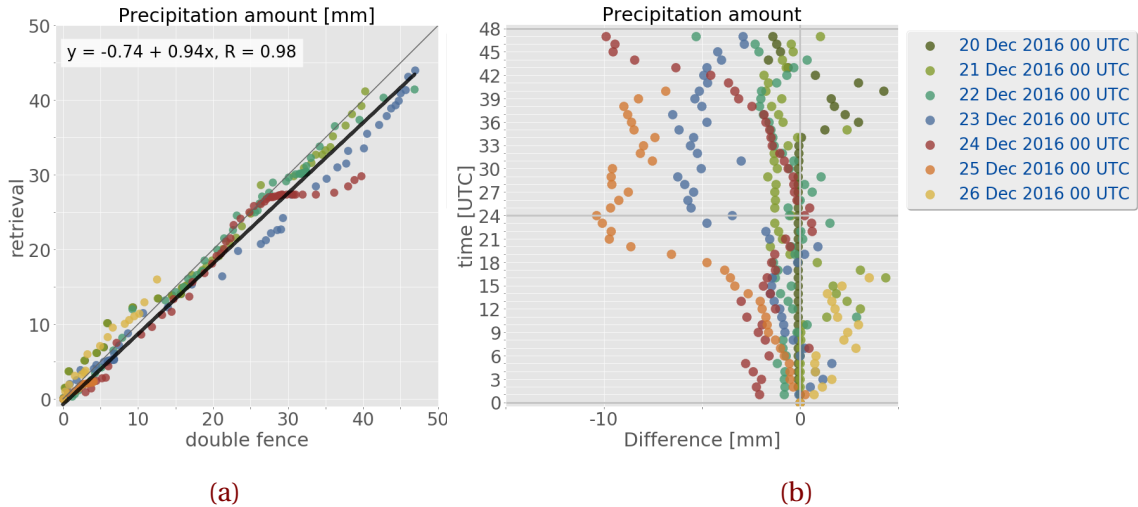


Figure 4.2.3: **a:** Surface precipitation amount comparison between the double fence observations and the retrieved surface accumulation of precipitation for 48 h. In black the linear correlation between the double fence observations and retrieved surface snow. **b:** Difference between the retrieved and the observed accumulation by the double fence. The colours represent the different starting days at 0 UTC for the 48 h accumulation.

reduced, when using a combination of ground-based observations instead of only Ze-S relationships.

It turns out that there is no relation between high and low precipitation events since the differences vary daily. [Cooper et al. \[2017\]](#) showed also different combinations of PSD assumptions and snow fall speed. For Barrow, best agreements between observations and retrieved snowfall were found by using the CloudSat particle model, slope parameters and snowfall speeds from the MASC. In the here presented study, the best assumption for surface snowfall accumulation was found by using a particle model for rimed aggregates (Section 2.4 and 4.2.1) such as in Figure 4.2.1.

On 20 and 21 December 2016, the difference error is large (-97.8% and 435.8% , respectively). This is probably related to an observation of precipitation at the double fence, even though no precipitation was observed. On 20 December 2016, observation at the double fence might be related to some particles stirred up by wind into the orifice of the gauge. Since no manual observations are done at the Haukeliseter site, is it difficult to say if blowing snow occurred or if it was snowing. This introduces additional errors

Table 4.2.2: Comparison of observed (obs.) and retrieved (ret.) snowfall amounts for the Christmas storm 2016. Difference refers to the difference of the retrieved and observed snow accumulation after 12 h and 24 h. The average difference is the value over all six/four days. Excluding values after 12 UTC on 25 December 2016 and after 17 UTC on 26 December 2016.

Day in 2016	12 h accumulation				24 h accumulation			
	Snowfall		Difference	Average difference	Snowfall		Difference	Average difference
	obs.	ret.			obs.	ret.		
	[mm]		[%]	[%]	[mm]		[%]	[%]
20 Dec	0.1	0.0	-97.8		0.1	0.0	-97.8	
21 Dec	0.7	3.8	+435.8		17.1	16.6	-2.7	
22 Dec	13.6	13.2	-3.0		25.6	25.1	-2.1	
23 Dec	6.3	5.2	-16.8		23.3	19.8	-14.9	
24 Dec	14.7	13.4	-8.6		24.8	25.0	+0.8	
25 Dec	4.3	-	-		+15.4	-	-	
26 Dec	8.8	10.6	+20.1		25.1	-	-	

on the double fence measurements. From the vertical MRR reflectivity, in Section 4.2.4, Figure 4.2.6, it can be seen, that precipitation was not observed on 21 December 2016 before 9 UTC.

Even though it is assumed that the double fence is the correct measurement it still underlies some uncertainties, such as under-catch during high wind speeds [Wolff, 2018]. A better way to asses the accuracy of the retrieved surface snowfall accumulation could be to compare the results to measurements inside a bush gauge.

Wolff [2018] estimates the under-catchment of double fence gauge compared to bush gauge measurements to 10 %, for outside winds of 9 m s^{-1} (Section 2.3.1). If the double fence gauge underestimate snowfall under high wind condition, would follow that the optimal estimation retrieval results are more than 20 % too low to the true state.

Anyway, the low average difference value for 24 h accumulation, in Table 4.2.2 during the Christmas 2016 event (-4.7 %) follow a much lower average difference between retrieved and observed surface accumulation than at Barrow (36 %) and therefore a very good agreement between observed and retrieved snow accumulation during 21 to 24 December 2016.

In Section 4.2.4, the vertical SWC will be compared to the forecasted MEPS values for the 2016 Christmas storm. Despite the undercatchment of wind related snow precipitation, the double fence measurement give confidence for the retrieved profiles of snow water content. While snow water content is compared to the MEPS forecast, it should be kept in mind that retrieved snow accumulation is underestimated and therefore the vertical SWC may be too low.

4.2.3 MEPS FORECAST AND SURFACE OBSERVATION COMPARISON

One approach of this study is to see if observed surface accumulation was correctly predicted by the newly operational regional weather forecast model MEPS (Section 2.5). Figure 4.2.4 shows observations at the double fence, retrieved snow accumulation, and MEPS forecast for 48 h. Hereafter, MEPS surface precipitation prediction forecast is compared to the double fence gauge observations at Haukeliseter. Accumulation measured by the double fence are presented as red hexagons. Minutely retrieved surface snowfall amount in dash-dotted green. Lines in black and grey show the deterministic and perturbed members for lead time of 48 h. The blue dashed line shows the ensemble mean of all ten members. The ensemble mean of precipitation amount is calculated every three hours, due to the three hourly time resolution of most of the perturbed member. When not all perturbed member data was available from [Norwegian Meteorological Institute \[2016\]](#), like on 23 December 2016 (Figure 4.2.4c), no ensemble mean is calculated. At the bottom of Figure 4.2.4 the associated 10 min average wind of the last hour from the 10 m weather mast at Haukeliseter is presented, to see if surface accumulation observations may be influenced by wind.

In general, Figures 4.2.4a to 4.2.4c show a better agreement between double fence observations and forecast for 48 h forecasts initialised on 21 to 23 December 2016 at 0 UTC. The double fence observation lie for 21, 22, and 23 December 2016 within the spread of the ensemble members (Figures 4.2.4a to 4.2.4c), covering the uncertainty within the measurements (Section 2.5). On the other hand, observations between 24 and 26 December 2016 are too low compared to the ensemble spread (Figures 4.2.4d to 4.2.4f). During 24 and 26 December 2016, the low-pressure system intensifies and gets closer to the Norwegian coast, and influence the local weather in Norway (Section 3.6). Figure 4.2.4d, e, and f indicate a larger estimated surface precipitation amount for all ten ensemble members

compared to observed values at the measurement site between 24 to 26 December 2016.

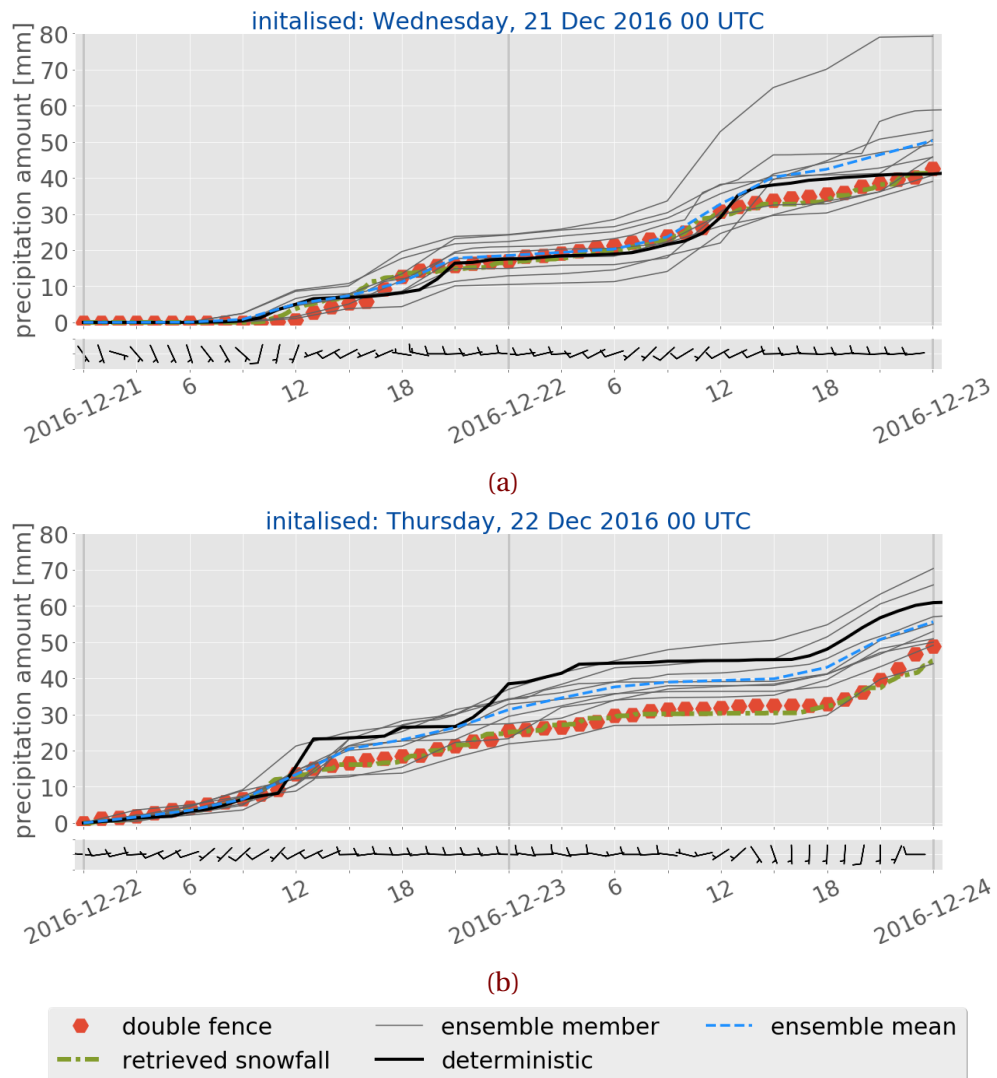


Figure 4.2.4: 48 h surface snowfall accumulation for 21 to 26 December 2016 (a to f). Representing the values from the double fence in red, hexagons; optimal estimation retrieval output at the first noise free level in dash-dotted green; MEPS ensemble member deterministic forecast, initialised at 0 UTC in black and its nine perturbed ensemble members in grey. The ensemble mean of all ten members is shown in dashed blue. Underneath is the associated last hour 10 min average wind from the weather mast at 10 m height. *Continued on next page.*

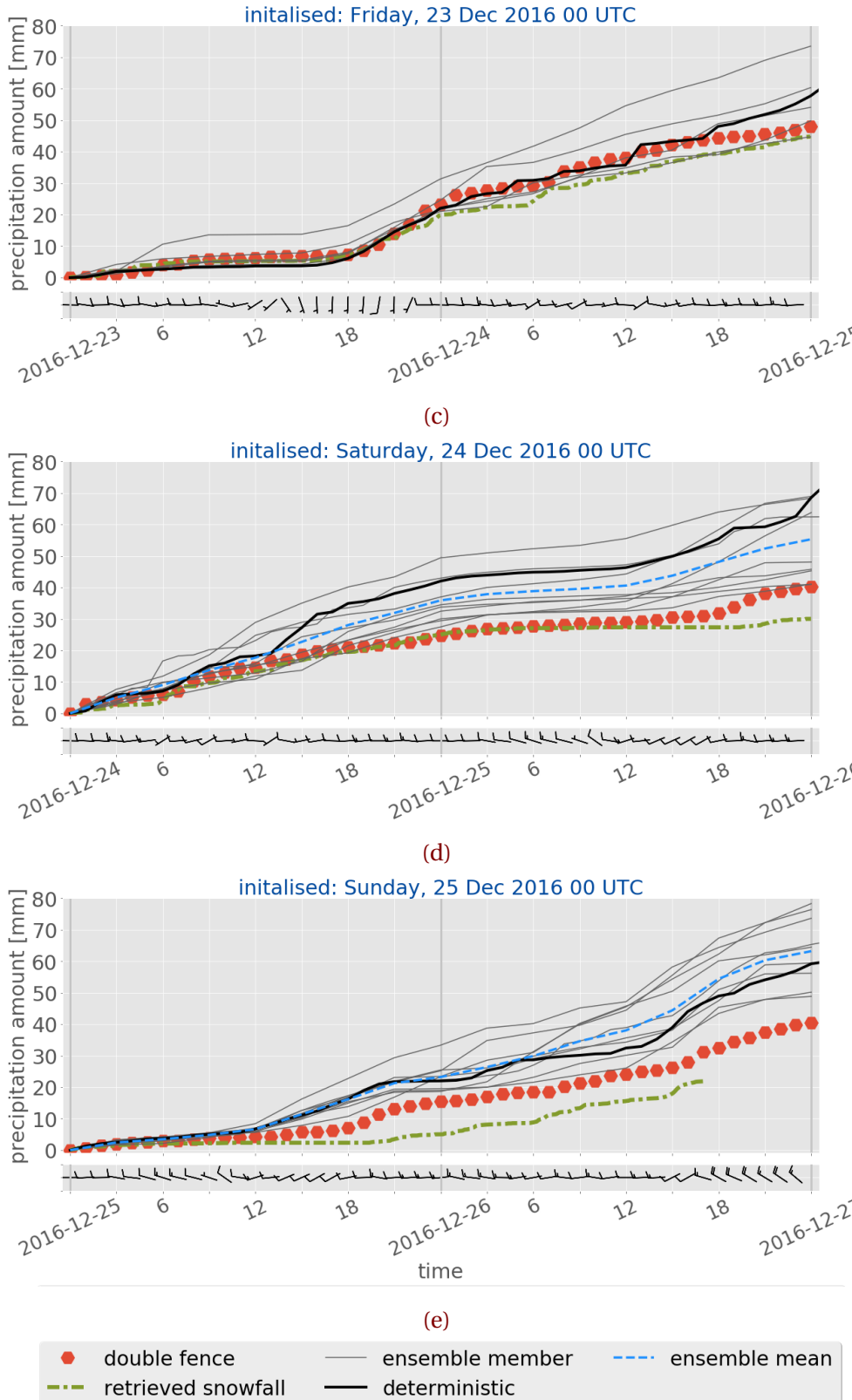


Figure 4.2.4: (Continued from previous page.)

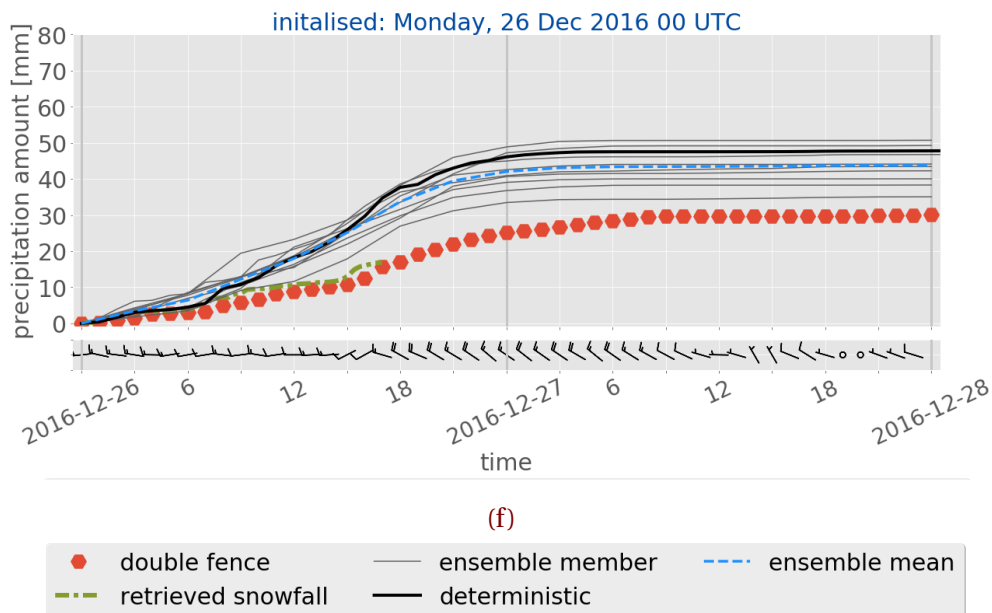


Figure 4.2.4: (Continued from previous page.)

The correlation between 48 h double fence observation and ensemble precipitation forecast is presented in Figure 4.1.2a and b. Showing a better agreement for 21 to 23 December 2016 than initialisation on 24 to 26 December 2016. On 21 to 23 December 2016 the slope of the regression line is relatively close to unity, indicating a good agreement between MEPS forecast and the observations by the double fence. The largest disagreement between surface observations and forecasts is seen on 25 December 2016 with a wet bias up to 15 mm (Figure 4.1.4e). The mean absolute error is not larger than 13 mm for the first three days and increases with intensification of the storm up to 19 mm on 24 December 2016. Initialisations on 24 December 2016 (Figure 4.2.4d) indicate an overestimation of the deterministic surface snowfall prediction already after 13 h forecast time. The deterministic forecast in solid black is much higher and increases faster than the observations. In Figure 4.2.4d at 16 UTC a difference of approximately 15 mm can be seen when compared to the surface measurements. This difference remains almost constantly over the forecast time. Furthermore, all ensemble members seem to overestimate the surface accumulation after 24 h.

Since MEPS performance was better on the previous days one might assume that the double fence measurement is influenced by surface winds. It shows in Figure 4.2.4d

Table 4.2.3: Observations (obs.) and forecasted (MEPS) snowfall amounts for the Christmas storm 2016. Difference refers to the percentage difference between MEPS ensemble members and the double fence observation, averaged over all ensemble member for 12 h and 24 h. The average difference is the value over all days.

Day in 2016	12 h accumulation					24 h accumulation				
	Snowfall		Difference	Average difference	Snowfall	Difference	Average difference			
	obs.	MEPS			obs.					
	[mm]	[%]		[%]	[mm]		[%]			[%]
20 Dec	0.1	0.4	+290.7		0.1	0.4	+302.1			
21 Dec	0.7	5.1	+626.1		17.1	18.5	+8.3			
22 Dec	13.6	13.4	-1.6	+1.3	25.6	31.3	+22.2		+10.8	
23 Dec	6.3	6.6	+4.2		23.3	23.7	+1.8			+32.6
24 Dec	14.7	17.7	+20.4	+59.8	24.8	35.9	+44.8			
25 Dec	4.3	6.7	+55.1		15.4	23.3	+50.8		+54.4	
26 Dec	8.8	17.9	+104.0		25.1	42.1	+67.5			

that the 10 min average wind at 13 UTC increases from 5 m s^{-1} to 10 m s^{-1} (see also Figure 4.1.1i). Wolff [2018] states that the double fence gauge is influenced by wind, and that the double fence gauge underestimates precipitation accumulation within 10 % for winds up to 9 m s^{-1} . Table 4.2.3 shows the difference between the observations and ensemble mean MEPS forecast for 12 h and 24 h. As seen in Table 4.2.3, the average difference error decreases with longer forecast time. For 21 to 26 December 2016 the average difference error is +134.7 %. For longer lead times, 24 h, the average difference error is reduced to +32.6 %. The daily percent difference show to be high for the last three days of the 2016 Christmas extreme event. On 21 December 2016 very large difference error (626.1 mm) is shown. This error is related to the small precipitation amount (0.7 mm) observations at Haukeliseter, which is a known difficulty for precipitation forecasts [Müller et al., 2017]. Generally the forecast accuracy decreases with lead time [Kalnay, 2003].

While the cyclone moves closer to Norway, the forecast inaccuracy of the surface precipitation increases. Overestimation occurs around 12 UTC on 25 December 2016. This

Table 4.2.4: Same as Table 4.2.3, just for an under-catchment of 10 % difference by the double fence gauge.

Day in 2016	12 h accumulation						24 h accumulation					
	Snowfall		Difference	Average difference	Snowfall		Difference	Average difference				
	obs.	MEPS			obs.	MEPS						
	[mm]	[mm]	[%]	[%]	[mm]	[mm]	[%]	[%]	[%]	[%]	[%]	
20 Dec	0.1	0.4	+251.6			0.1	0.4	+261.9				
21 Dec	0.8	5.1	+553.5			19.0	18.5	-2.5				
22 Dec	15.1	13.4	-11.4	-8.8		28.4	31.3	+9.9	-0.3	+19.3		
23 Dec	7.0	6.6	-6.2			25.9	23.7	-8.4				
24 Dec	16.3	17.7	+8.4		+111.2	27.6	35.9	+30.3				
25 Dec	4.8	6.7	+39.6			17.1	23.3	+35.8				
26 Dec	9.8	17.9	+83.6			27.9	42.1	+50.8				

overestimation of the precipitation amount could be associated with the warm sector evolution at Haukeliseter (Section 4.1.1). Afterwards it shows, with increasing lead time the same accumulation is predicted, but too high compared to the double fence observations. The wind at Haukeliseter was higher than 10 m s^{-1} (Figure 4.2.4e before 12 UTC. A relation between high wind and double fence observation could be possible. Assuming an accumulation underestimation of 10 % would lead to a reduction of over estimation to 40.2 % for 12 h (Table 4.2.4). Table 4.2.4 presents the percentage difference between the double fence and MEPS forecasts. Here, it also shows a decrease in forecast accuracy for precipitation accumulation over 24 h. Table 4.2.4 displays a reduction of over estimation for surface accumulation on 24 to 26 December 2016. The average difference is reduced by 16 %. This shows, even though a 10 % under-catchment of the double fence gauge was present, would MEPS overestimate the surface accumulation (12 h: +43.8 %; 24 h: +39 %).

An overestimation of the surface precipitation is also observed on 26 December 2016. While the surface analysis indicates the passage of an occlusion after 15 UTC (Figure 3.6.2n, 3.6.2p, Section 4.1.1), suggests Figure 4.2.4f an overestimation after 12 h lead time. Again, the MEPS ensemble seem to predict the occurrence of precipitation correctly compared

to the double fence, but estimates a too high surface accumulation. The surface wind observation in Figure 4.1.1s suggest also high wind speed up to 17.5 m s^{-1} observations on 26 December 2016. The difference error in Table 4.2.3 is +104 % for 12 h accumulation on 25 December 2016. This shows the highest overestimation for the three days (24 to 26 December 2016). The application of the 10 % under-catchment on the double fence observation would still follow an error of 83.6 % (Tables 4.2.3 and 4.2.4). It seems even though the double fence gauge is influenced by wind, the overestimation of surface accumulation by MEPS is still present.

Whereas the spread between the ensemble members is large in the beginning of 24 December 2016, the variability between the members is narrow for 25 and 26 December 2016 for the first 6 h. The variability between the ensemble members can be compared with a box-whisker plot. A box-whisker-plot shows the time evolution of the distribution of the precipitation amount made of ten ensemble members up to 48 h. Since some ensemble member do not have forecast values every hour the box-whisker-plot in Figure 4.2.5 provides information every 3 h. The red line shows the ensemble mean of all ten members and if the distribution is skewed. The short light green, horizontal line is showing the median, the wide vertical box represents the 25th and 75th percentiles, and minimum and maximum values are indicated by the vertical lines, whiskers.

The box-whisker-plot in Figure 4.2.5 displays the distribution of the ten ensemble members for the respective days. All three days with overestimation seem to have different variability. As expected increases the forecast uncertainty with longer forecast time for precipitation amount.

The variability in Figure 4.2.9 show on 25 December 2016 no large variation between the ensemble members (narrow box-whiskers). This day is also the forecast with the smallest wet bias of the three days with overestimation (Figure 4.1.4e). More variation between the ensemble members is shown on 24 and 26 December 2016 after 3 h. As the correlation for precipitation amount in Figure 4.1.2j suggests, the overestimation is not as high as for 24 and 26 December 2016. On 24 and 25 December 2016 the mean error for the surface accumulation is largest with values up to 7 mm for 12 h (Figure 4.1.5e).

Larger variability is already present after 3 h prediction time in Figure 4.2.5a on 24 December 2016. The spread between the ensemble members (shown by the minimum and maximum whiskers) seems to be wide indicating a larger uncertainty about the amount of surface accumulation. The ensemble mean (red line) is always higher than the median, suggesting

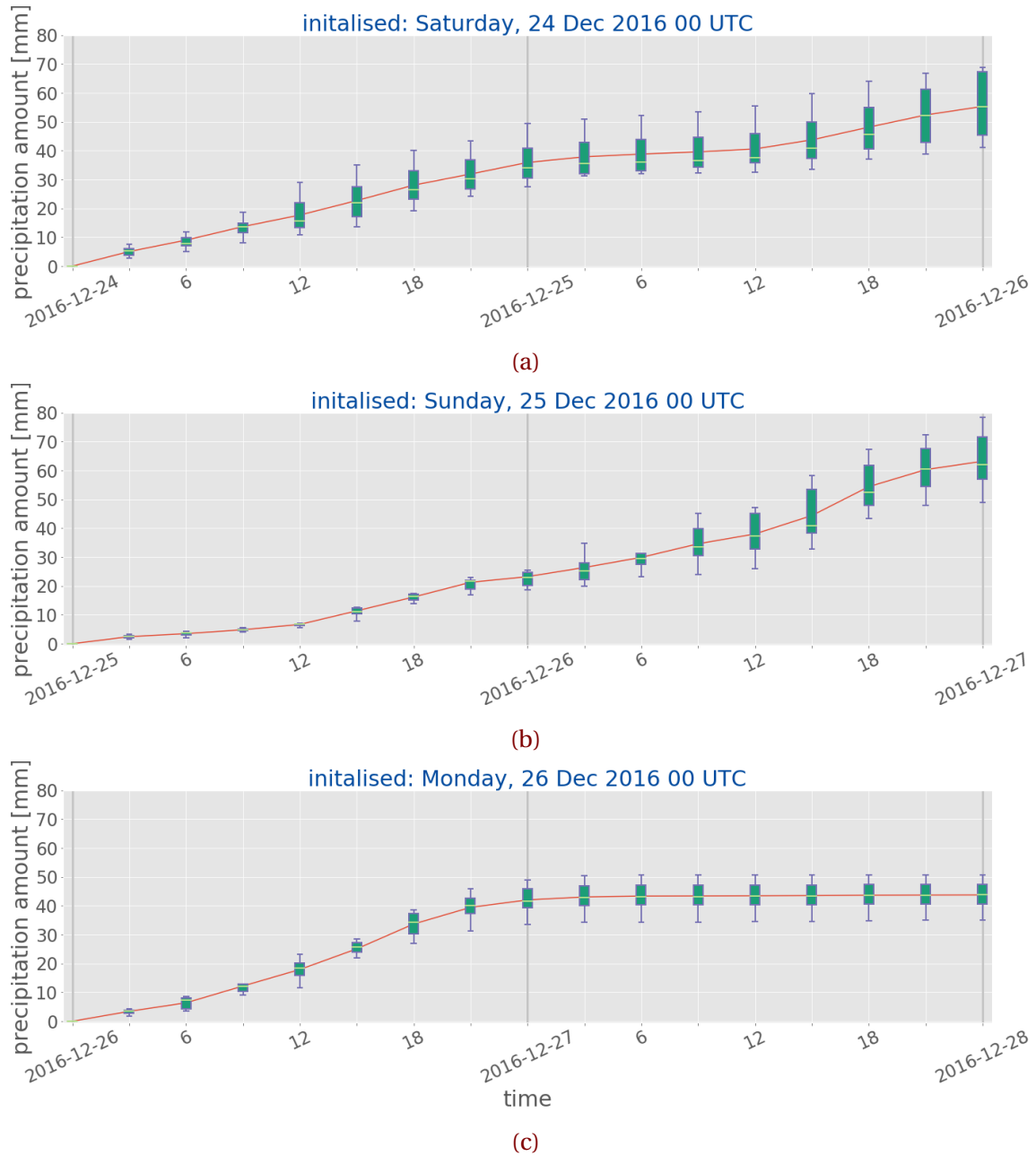


Figure 4.2.5: Box-whisker-plot of the ten ensemble members of MEPS. Red line indicating the ensemble mean, lower and upper whisker the 25th and 75th percentile, respectively. Light green shows the median of all members and the box represents the middle 50 % of scores of the precipitation.

a positively skewed distribution. After 12 h forecast time, the median is closer to the lower 25th percentile, indicating a negative skewness. Also, all upper whiskers in Figure 4.2.5a are longer than the lower ones, which would follow that the ensemble members vary amongst the most positive quartile and that it is very similar for the least positive quartile group.

I believe that the uncertainty appearing already after 3 h (Figure 4.2.5a) could be associated with a too long spin-up time of MEPS. MEPS usually has a spin-up time of about three hours, on 24 December 2016 this might have been longer as a result of poorer initial conditions [Need a reference here, not stated in Müller et al. \[2017\]](#). It seems, that the initial and boundary conditions for MEPS might have not been perfect for initialisations on 24 December 2016 at 0 UTC. As described in Section 2.5 should the perturbed members always lie relatively close to the observations. For a short time (hours) should the forecast member be close together [[Kalnay, 2003](#)]. The deterministic and perturbed members might not to have stabilised yet and show larger variation in Figure 4.2.5a from early on than e.g. on 25 December 2016. More variability between the ensemble members do not necessarily mean, that a forecast is bad, it only shows the uncertainty of the initial conditions. Important is, that the observations, which are going to be used for the initialisation are within the spread of the ensemble member prediction.

The uncertainty might also have been related to the fact that the large-scale situation got more complex. The precipitation amount associated with the transition of an occluded front on 23 December 2016, after 18 UTC, is higher than on the previous days (Figure 4.1.1j and Figure 3.5.1). During 20 to 21 December 2016, the hourly precipitation around 0 UTC is less intense than on 23 December 2016 (Figure 3.6.2e). High accumulation amount over shorter time followed and could have resulted in a larger variability of the MEPS members (Figure 4.2.5). Another possibility is MEPS might have accounted for additional accumulation around 12 UTC on 24 December 2016 and this showed a stronger increase in accretion in Figure 4.2.4d at 13 UTC. I believe it could be associated to a local resolution effect of MEPS at Haukeliseter, which will be further discussed in Section 4.2.5.

Figure 4.2.5b and c show a smaller ensemble member variability on 25 December 2016 and 26 December 2016 than on 24 December 2016. The box-whiskers are narrower for the first 30 h in Figure 4.2.5b, but slightly larger after 6 h forecast time for initialisations on 26 December 2016. Section 4.1.1 presented a good agreement between observations and

forecast of large scale features in terms of pressure, temperature and wind direction. While the occlusion on 26 December 2016 was more intuitive (Figures 4.1.1p to 4.1.1s) than the warm front development on 25 December 2016 (Figure 4.1.1k, l, m, n). The mean error in Figure 4.1.4 for each variable shows to be best on 25 December 2016 (Figure 4.1.5a,b,c, d, and e).

On 25 December 2016 the overestimation started to occur around 13 UTC in Figure 4.2.4e, and may be related to the delayed temperature MEPS forecasted temperature increase in Figure 4.1.1l. As Figure 4.2.5b shows, the variability in the forecast increases after 15 h prediction time. In general, median and mean agree well for the entire period of a 48 h lead time. After 39 h the mean is much higher than the median and closer to the lower 25th percentile in Figure 4.2.5b. It seems, that all ten ensemble members agree well on the prediction and nevertheless MEPS overestimates the surface accumulation. The MEPS surface forecasts on 25 December 2016 suggest that MEPS did not expect the occurrence of a warm front (Figures 4.1.1k to 4.1.1n). However, the surface accumulation prediction could suggest that MEPS expected more precipitation around 12 UTC. Maybe MEPS has expected a weak warm-front passage and therefore more precipitation. The fact that the temperature is rising and therefore the phase is changing from snow to liquid precipitation (Figure 4.1.3) may have led to MEPS expecting more liquid precipitation rather than mixed phase precipitation and hence MEPS predicted more surface accumulation.

Between 15 UTC and 18 UTC on 26 December 2016, the core of the low-pressure system passes over Haukeliseter Figures 4.1.1p to 4.1.1s. The box-whiskers in Figure 4.2.5c indicate a larger variability after 6 h prediction while the precipitation amount forecast is overestimating at 12 UTC. The forecast precipitation amount is similar to the double fence observations, but overestimated. Variability of all ensemble members increases at 6 h lead time, but then decreases again in Figure 4.2.5c.

Since the box-whisker-plot in Figure 4.2.5b and c (25 and 26 December 2016) show less variability in the beginning it is assumed that spin-up time issues are less likely, but not totally excluded. It could be related to an error in the initialisation state, even though it does not show within the variability at the beginning. In Figure 4.2.4e and f, the ensemble mean agrees well with the deterministic forecast, which is an indication of a symmetrical spread around the deterministic run. Again, the ensemble mean is the best statistical solution over a longer timespan and does not necessarily mean to be the best for an extreme event such as the Christmas storm 2016.

The overestimation of accumulated precipitation during 24 and 26 December 2016 might be related local topography as well as to the complex development of the low-pressure system north-west of Norway on 24 December 2016. Furthermore could it be related to the 10 % under-catchment by the double fence gauge under high wind condition.

According to Müller et al. [2017] strong precipitation events are better predicted with AROME-MetCoOp than with ECMWF. In Section 2.2 it was described, that during 21 to 27 December 2016 56.9 % of the total December 2016 accumulation of precipitation were observed. In December 2014, the 12 h precipitation mean absolute error in AROME-MetCoOp was below 1.5 mm [Müller et al., 2017]. For the 2016 Christmas storm the mean absolute error is not larger than 5 mm for the first 12 h of accumulation on 24 and 26 December 2016 (Figure 4.1.5e). Therefore, the assumption follows that on 26 December 2016 the overestimation might be correlated to the <10 mm problem described by Müller et al. [2017]. The 12 h and 24 h accumulation is presented in Table 4.2.3 for Haukeliseter and shows that 12 h observed accretion was less than 10 mm for 25 and 26 December 2016. The mean error for 12 h accumulation in fact shows a wet bias during 24 and 26 December 2016.

4.2.4 COMPARISON OF SNOW WATER CONTENT IN THE VERTICAL

Frontal boundary passages were observed at the surface several times throughout the extreme storm in December 2016. MEPS is able to predict the large scale features and related surface changes for initialisation more than 24 h before (Section 4.1.1). In winter 2016 three additional instruments were installed to estimate the vertical snow water content at Haukeliseter. This unique approach gives the opportunity to compare the vertical forecasts of SWC to vertical solid precipitation observations.

Previous studies such as Joos and Wernli [2012] motivate to make accurate surface measurements more available to improve mesoscale models.

Passages of occluded fronts and a warm sector were observed on 23, 26, and 25 December 2016, respectively. Figure 4.2.6 shows the reflectivity from the MRR at Haukeliseter for these three days. Figure 4.2.6c presents only values until 17 UTC, because of the temperature change and hence a precipitation shift followed liquid drops freezing on the MRR dish and the signal got attenuated.

More consistent storm structure with higher reflectivity values indicate the transition of the

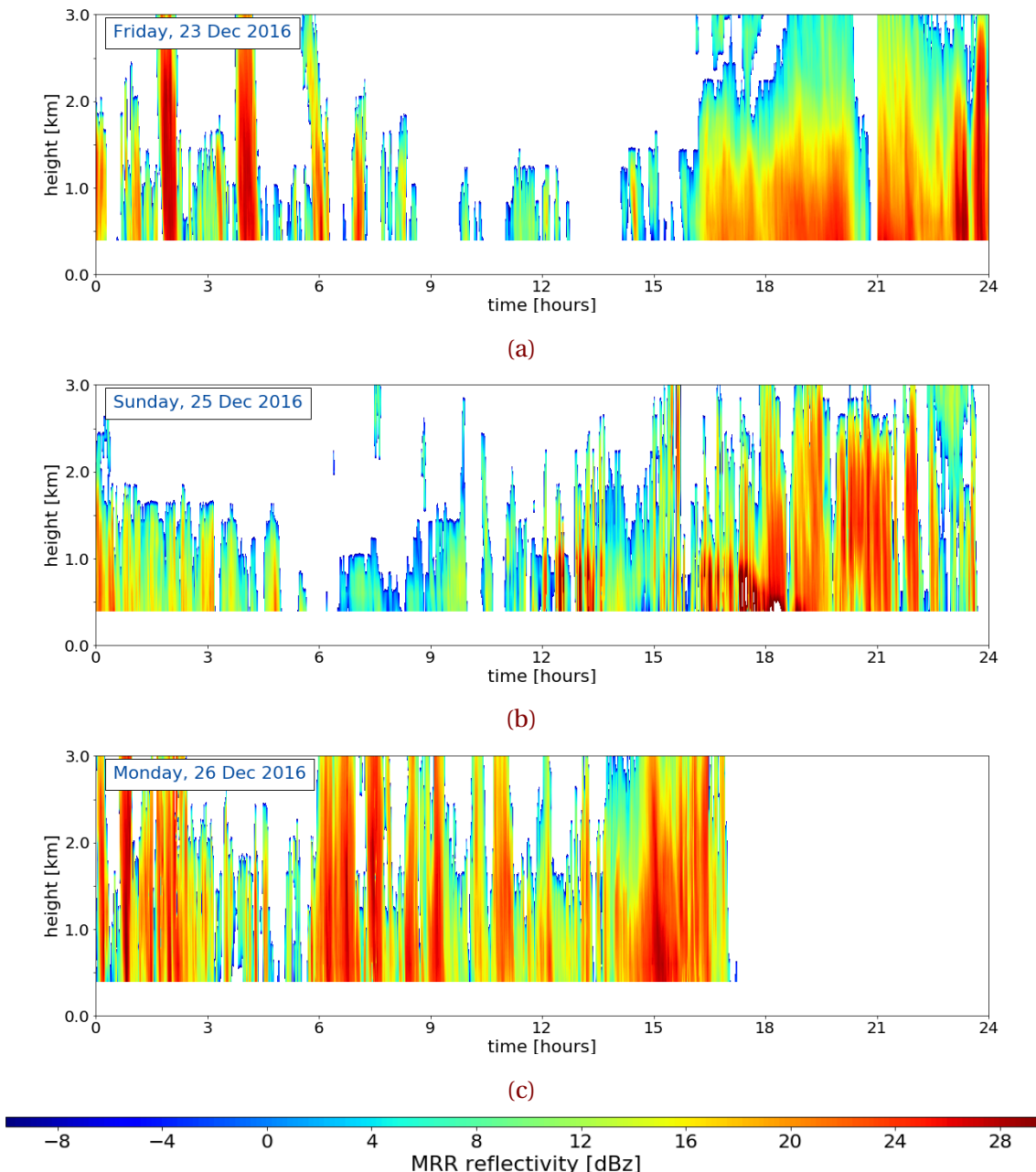


Figure 4.2.6: MRR reflectivity for the days when a front or an occlusion passed through at Haukeliseter. dBZ reflectivity according to the colour bar, with weaker precipitation in blue and more intense precipitation in red. **a:** Friday, 23 December 2016, **b:** Sunday, 25 December 2016, and **c:** Monday, 26 December 2016.

boundaries in Figure 4.2.6. While on 23 and 26 December 2016 the reflectivity did not pass values larger than 28 dBZ shows Figure 4.2.6b high reflectivity values larger than 30 dBZ (compare for approximation Table 2.3.1). These high values indicate the observation of possible liquid precipitation. Images from the MASC were able to verify observed liquid drops during 12 UTC to 21 UTC (Figure 4.1.3).

On 23 December 2016, the surface observations allow to assume that the occluded front passed through between 12 UTC to 21 UTC (Figure 4.1.1f, g, h). The vertical observations at Haukeliseter show intense reflectivity and therefore more intense precipitation after 16 UTC (Figure 4.2.6a). Another occlusion passed through on 26 December 2016 shortly before 15 UTC which lasted until 21 UTC indicated by a more consistent storm structure and high reflectivity in Figure 4.2.6c around 15 UTC. The high reflectivity on both days shows the passage of the occlusion and the associated precipitation. On 23 December 2016, the wind is from the south, upslope (Figure 4.1.1h, Figure 2.1.1c) which led to a more consistent storm structure in Figure 4.2.6a. Figure 4.1.1m and n indicate strong wind observations from the west which led to a consistent, but shorter storm structure in Figure 4.2.6b at 15 UTC on 25 December 2016. The orographic influenced wind and therefore a possible relation to the precipitation will be further assessed in Section 4.2.5.

Figure 4.2.7 presents the reflectivity of the MRR and the snow water content retrieved from the reflectivity as well as the 48 h forecast values. Minutely MRR reflectivity and retrieved snow water content can be seen in Figure 4.2.7a, d, j, and m. Figure 4.2.7b, e, k, n show in the upper panel the hourly averaged values from the retrieved SWC and in the lower panel the ensemble mean of the instantaneous forecast values every hour over all ensemble member. Three hourly averaged retrieved values are then presented in the upper panel of Figure 4.2.7c, f, l, and o, the lower panel are the ensemble mean forecast values every three hours.

Figure 4.2.7e (lower panel) shows the one hourly averaged forecast values over all ensemble members, neglecting not existing values on 23 December 2016. Forecasts initialised 48 h (22 December 2016) prior predict the consistent storm structure and therefore the passage of the front (Figure 4.2.7b, c). The consistent structure of retrieved snowfall after 16 UTC is predicted for initialisations less than 24 h before the occurrence of the occlusion (Figure 4.2.7d, e, and f). Even the three hourly resolved averaged forecast values show a

response on the occurrence of the storm (Figure 4.2.7f, lower panel). The duration of the passage is between 16 UTC to 23 UTC (Figure 4.2.7a to f). MEPS is able to estimate the snow water content for time resolutions of 3 h in Figure 4.2.7c, f.

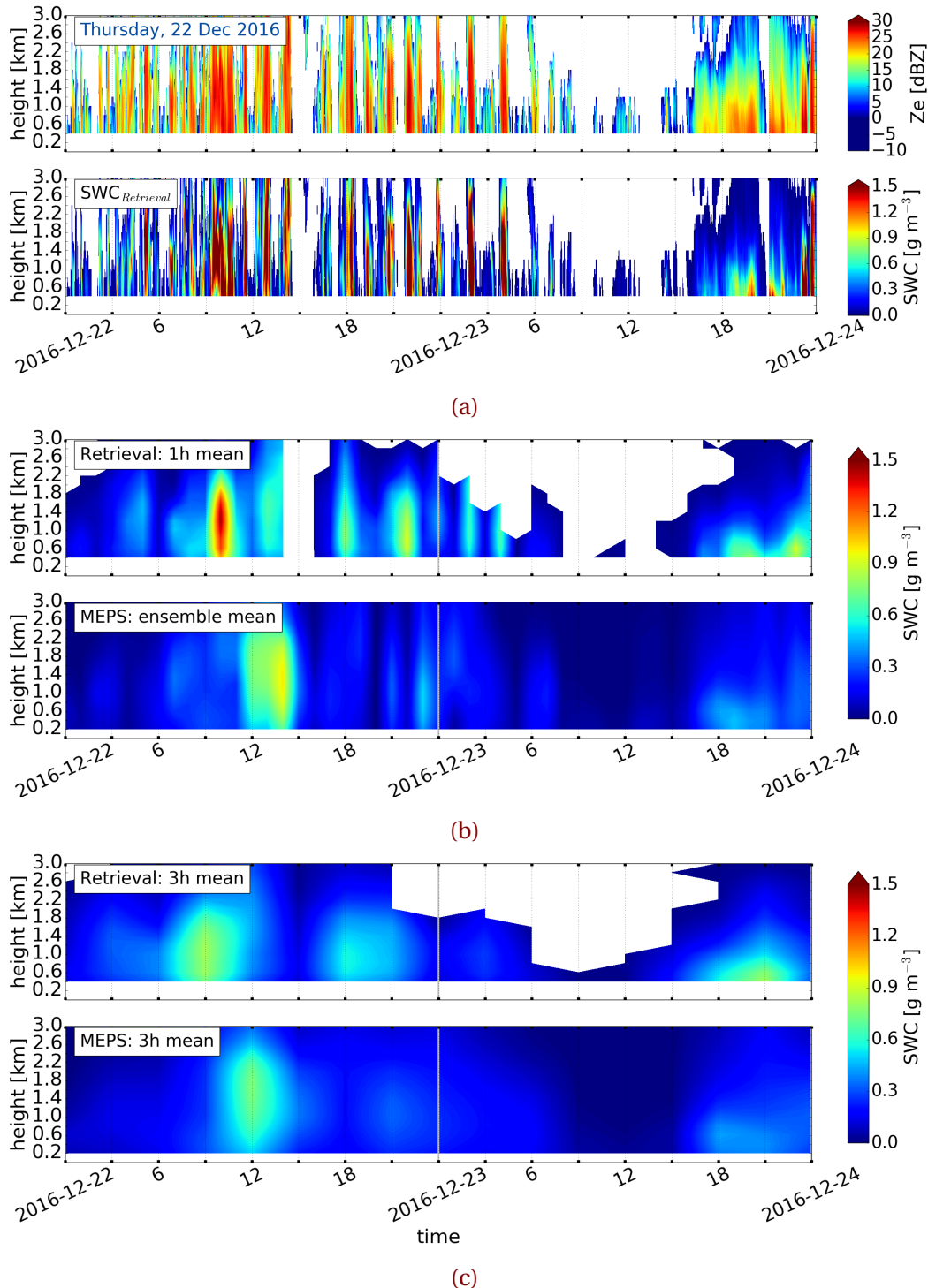


Figure 4.2.7: Initialisation on 22 December 2016 at 0 UTC. From top to bottom: (a) MRR reflectivity for 48 h, minutely retrieved SWC. (b) Hourly averaged retrieved SWC, lower panel instantaneous hourly averaged forecast of all ensemble member SWC, neglecting missing values. (c) Three hourly averaged retrieved SWC, lower panel instantaneous three hourly averaged forecast of all ensemble member SWC. *Continued on next page.*

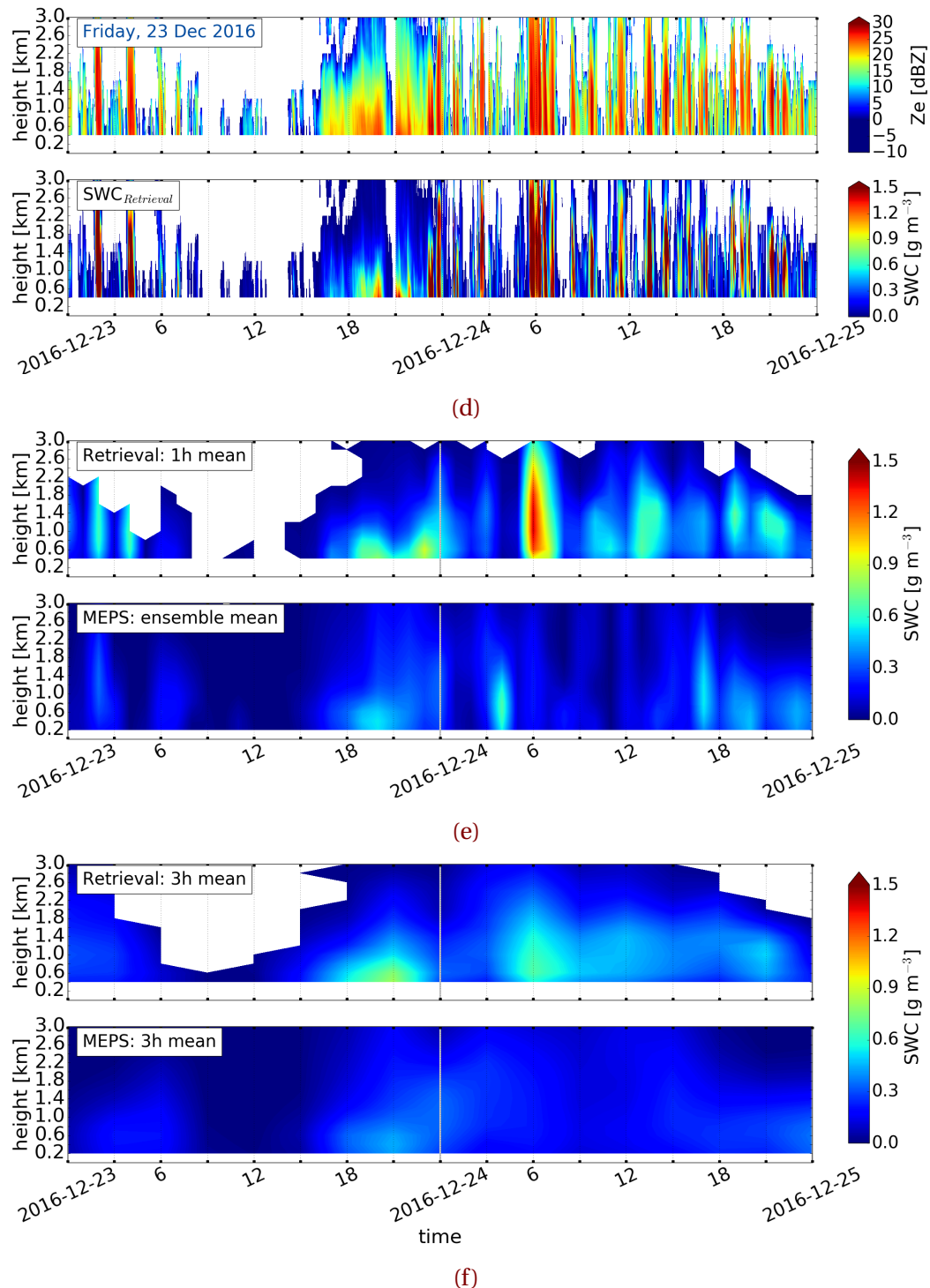


Figure 4.2.7: (Continued from previous page.) Initialisation 23 December 2016 at 0 UTC.

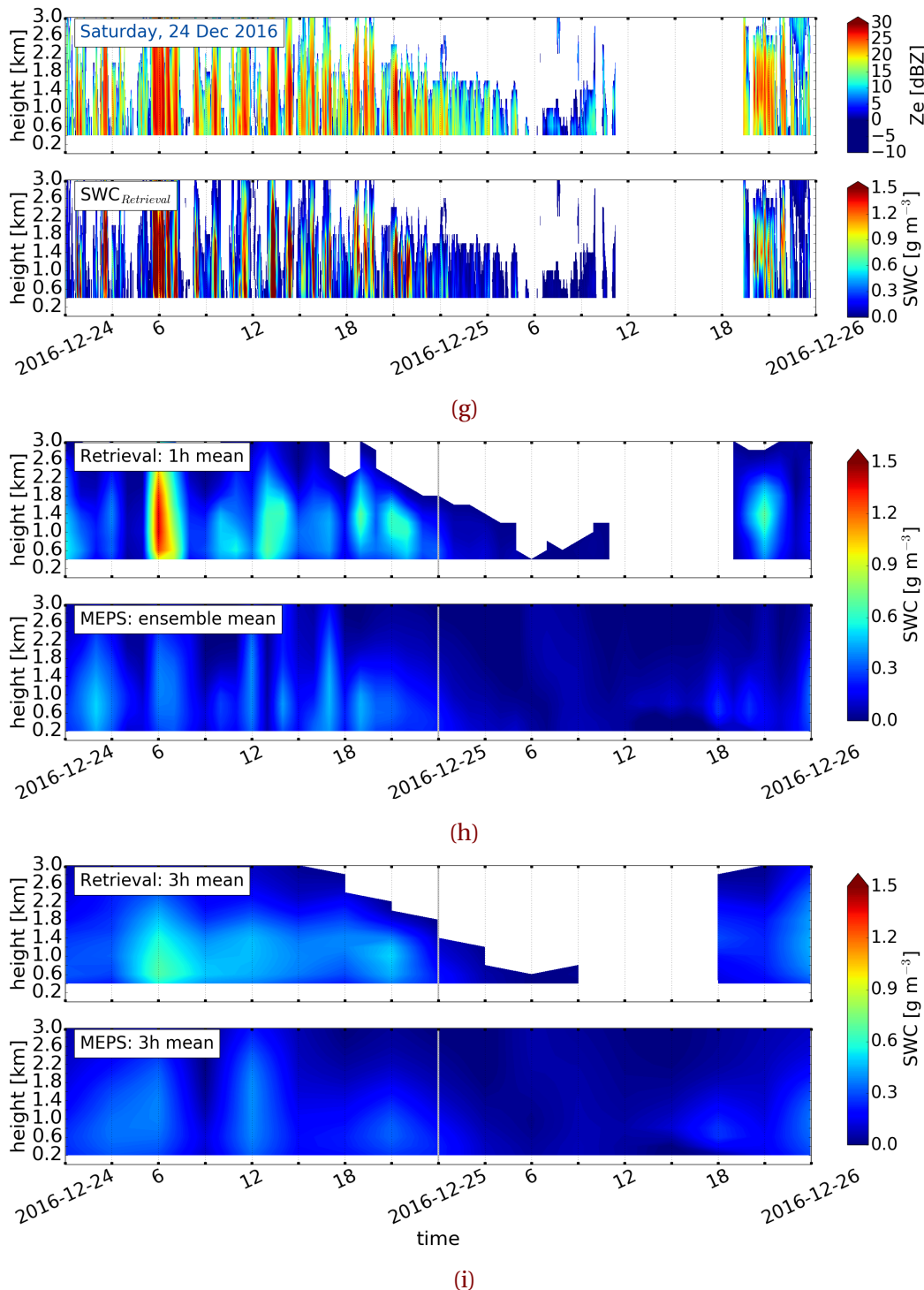


Figure 4.2.7: (Continued from previous page.) Initialisation 26 December 2016 at 0 UTC.

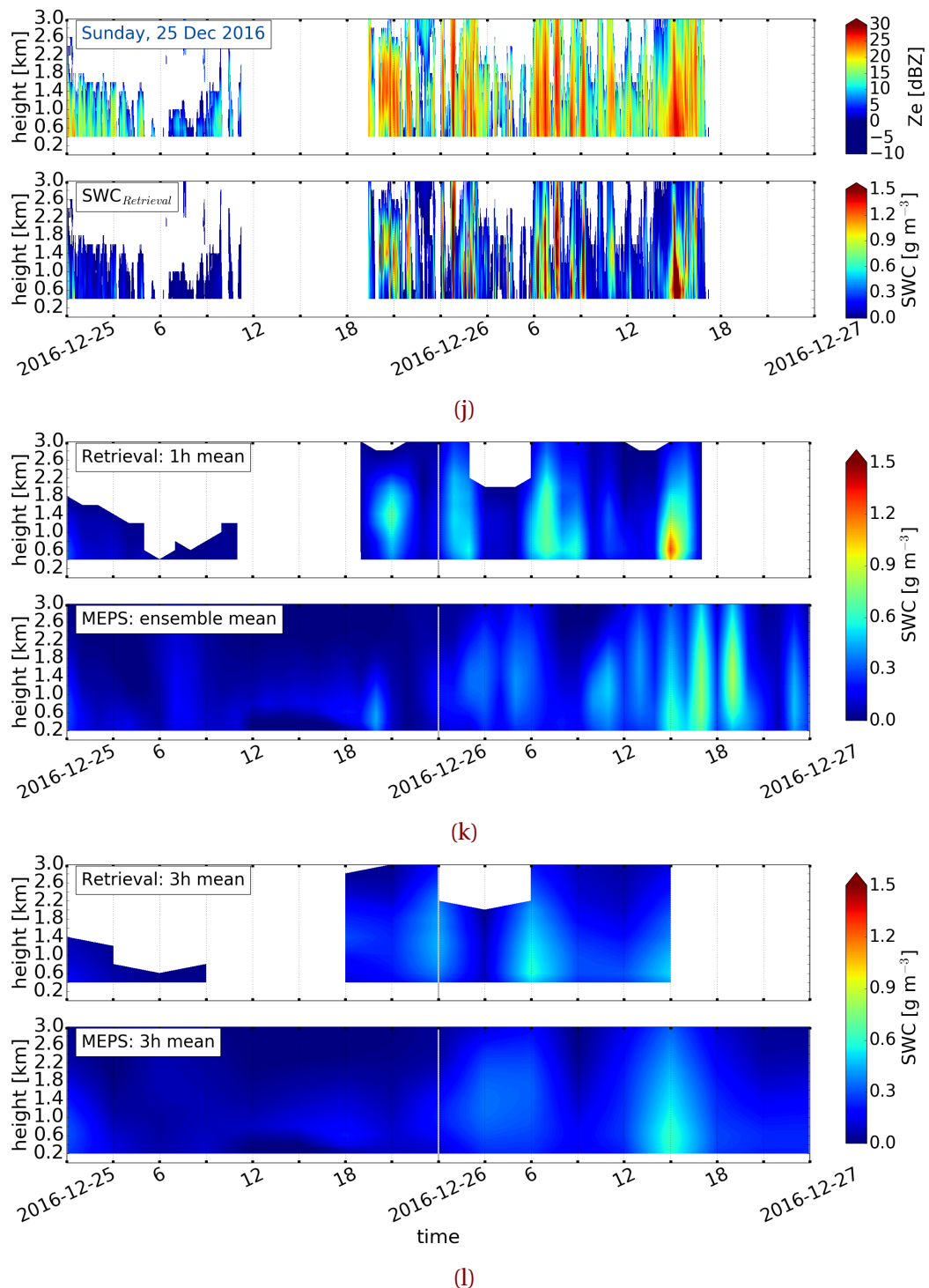


Figure 4.2.7: (Continued from previous page.) Initialisation 25 December 2016 at 0 UTC.

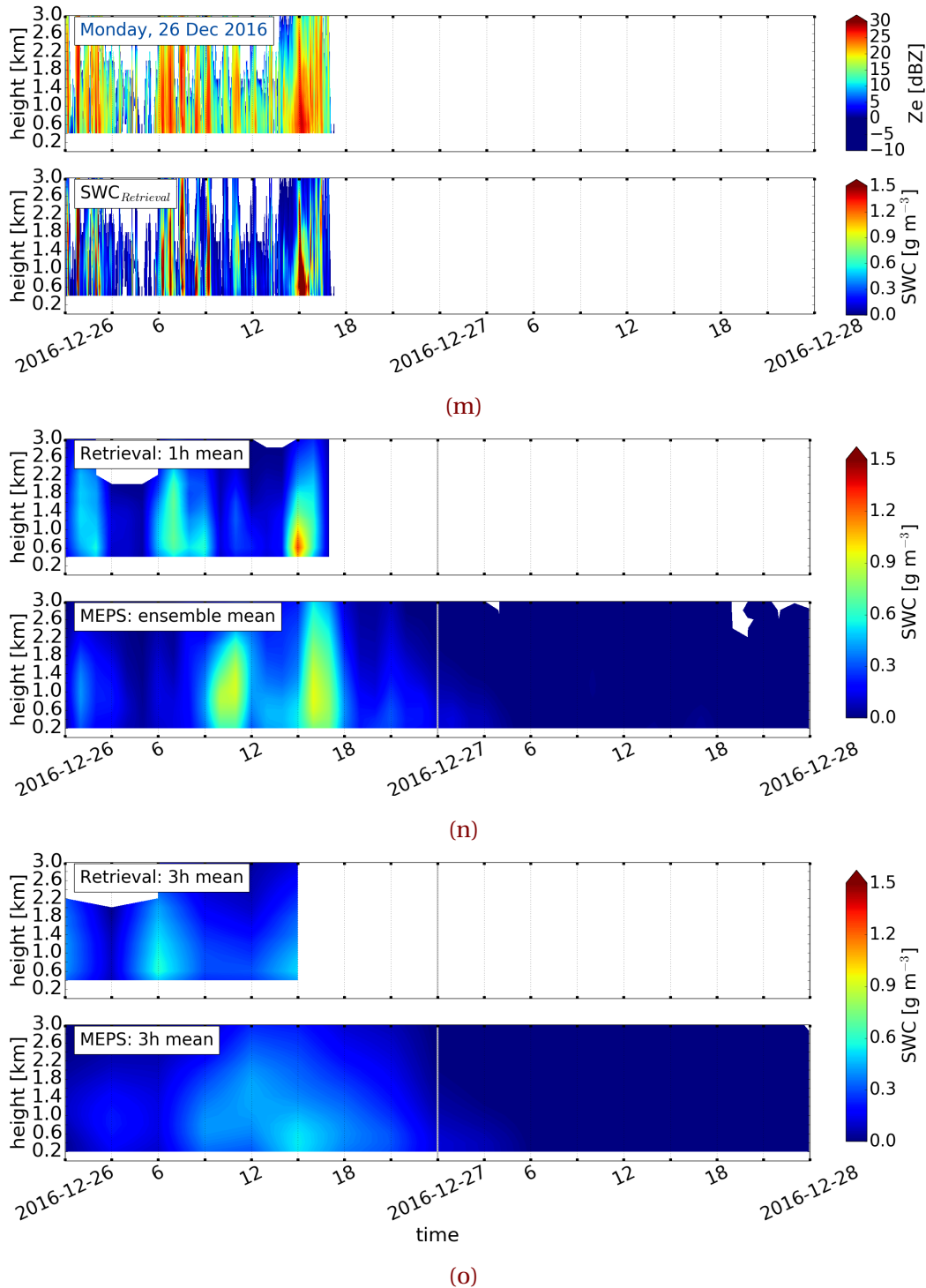


Figure 4.2.7: (Continued from previous page.) Initialisation 26 December 2016 at 0 UTC.

In general, the forecasted instantaneous snow water content amount is weaker than the retrieved values for predictions on 23 December 2016. Hourly averages, only using the deterministic forecast and the first ensemble member show no occurrence of the occlusion passage on either day (??). The variation of each initialisation ensemble member is given in Figure B.2.1 for the respective day In Figure B.2.1b the prediction for the occlusion passage is quite weak for all ensemble members

In the evening of 23 December 2016, the first perturbed ensemble member does not exist and hence little snow water content is predicted for the ensemble means especially for the hourly resolved mean Figure B.1.1b). A comparison with 25 and 26 December 2016 show the same result, when only the deterministic forecast and first perturbed member is used Figure B.1.1e and f.

On 26 December 2016, only retrieves snow water content until the passage of the occlusion is observed (Figures 4.1.1p to 4.1.1t. The average of all ensemble members (Figure 4.2.7n) as well as the three-hourly instantaneous SWC (Figure 4.2.7o) predict the frontal passage. Initialisations already 39 h prior let assume that intense precipitation over a short time will occur (Figure 4.2.7k, l). The variation of all members in Figure B.2.1e and f indicate that almost all perturbed members would have predicted the precipitation around 16 UTC, but the ensemble mean weakens the result. On 25 and 26 December 2016 high predicted SWC values are calculated for the deterministic forecast, than for any other ensemble member. This bias might have led to an overestimation at the surface on 26 December 2016, where the deterministic forecast indicates higher values than the perturbed members (Figure 4.2.4f). But in Figure B.1.1e and f the amount of snow water content is very weak. Better estimations for predicted snowfall amount are displaye for the use of all ten ensemble member with either hourly or three hourly time resolution to creat the ensemble mean. Still, the instantaneous average values of all ensemble members are much weaker than the retrieved SWC.

In the observations on 25 December 2016, patterns of possible liquid precipitation (Figure 4.1.3) related to warm temperatures (Figure 4.1.1l) and high reflectivity (Figure 4.2.6b) are shown, between 12 UTC to 21 UTC. High reflectivity values in Figure 4.2.6b are present around 18 UTC with layer thickness up to 1.2 km. To see if liquid precipitation is predicted, the atmospheric cloud condensed water content and rainfall amount in model levels is summed (Figure 4.2.8). Figure 4.2.8a and b show liquid water content for initialisations on 24 December 2016 or 25 December 2016, respectively. Positive surface temperatures

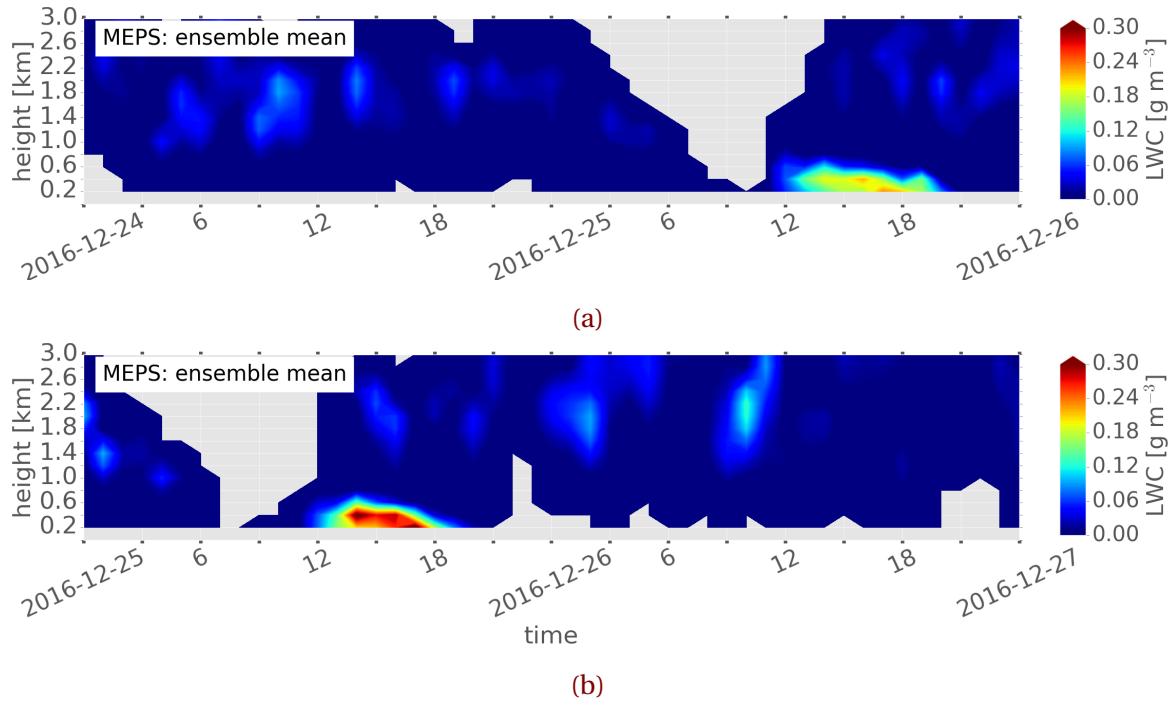


Figure 4.2.8: 200m hourly averaged LWC forecast from MEPS with all ensemble members, neglecting missing values. Initialised on 24 December 2016 and 25 December 2016 at 0 UTC. Liquid water content according to the colorbar.

were forecasted between 12 UTC and 21 UTC (Figure 4.1.11). Initialisations more than 24 h prior show already the occurrence of the liquid layer (Figure 4.2.8a). Figure 4.2.8a or b show also a narrow liquid layer thickness up to 800 m.

In Norwegian mountainous terrain this is an important forecast ability, since precipitation change can lead to a high risk for people. The avalanche danger increases with the precipitation change especially during high wind speeds [Hansen et al., 2014]. Since MEPS forecasts the liquid layer correctly in thickness and duration it seems to be a good interaction between the surface model temperature and the temperature assimilation. This follows a high accuracy of MEPS and the positive impact of using a high resolution convective scheme model.

For the first glance operates MEPS well when compared to vertical observations, even though weaker ensemble mean estimates occur compared to the observations. One pos-

Table 4.2.5: Interpretation of the coefficient of variation for SWC.

Size of CV [%]	Interpretation variability
0 to <25	negligible
25 to <50	low
50 to <75	moderate
75 to <100	high
100 to ∞	very high

sibility to assess the variability of all ensemble member is with the use of the coefficient of variation (CV) described in Section 2.6.4. Figures 4.2.9a to 4.2.9d show the coefficient of variation for SWC.

The grey line in Figure 4.2.9 presents the ensemble mean of the hourly predicted SWC values. The darker the shading in Figure 4.2.9 the smaller the variation of the SWC relative to the mean.

MEPS data does not exist for all ten ensemble members on 23 December 2016. No coefficient of variation is calculated for this day, since only six perturbed members were available. Therefore, the initialisation on 22 December 2016 is used to validate the forecast. The interpretation of the coefficient of variation for SWC is presented in Table 4.2.5.

All ensemble members agree well with the occurrence of the up-slope storm on 23 December 2016 after 15 UTC (Figure B.2.1b). For prediction initialised on 22 December 2016 the verification in Figure 4.2.9a shows little variability below 50 % and show a good agreement on the occurrence of snow precipitation. All ten ensemble members forecast the up-slope to occur after 16 UTC, compare Figure B.2.1b and c. The comparison of only six ensemble members in Figure B.2.1c, let assume that the variability between all ensemble members during the up-slope storm is low, but not as certain as for an initialisation on 22 December 2016 at 0 UTC. The deterministic forecast (EM0) and ensemble member one in Figure B.2.1b indicate peaks of high SWC before 8 UTC. The retrieved SWC on 23 December 2016 had two peaks, one at around 2 UTC and another at 4 UTC. The deterministic forecast, initialised on 22 December 2016 predicted a peak at 2 UTC, 6 UTC and 8 UTC, where the first perturbed ensemble member (EM1) has a strong SWC at 7 UTC.

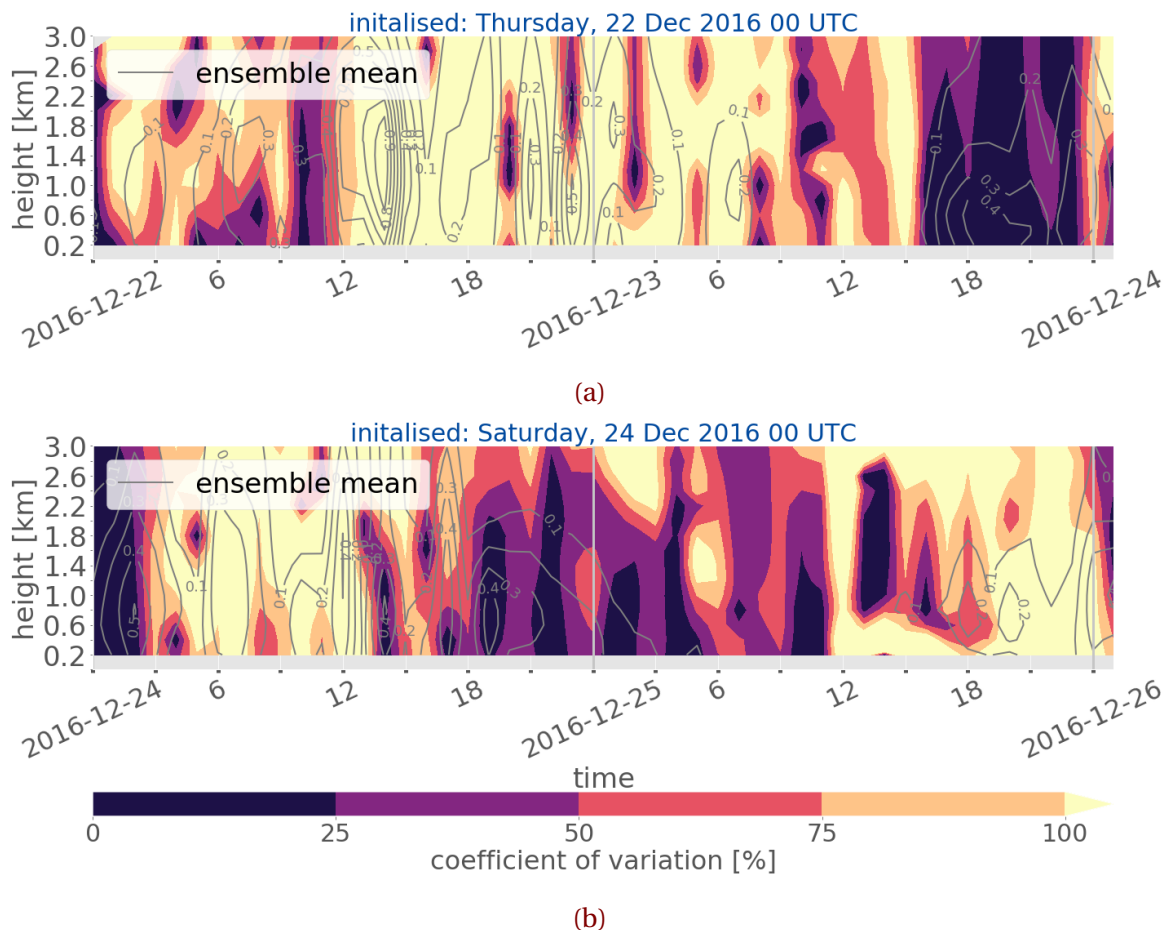


Figure 4.2.9: SWC variation of the ten ensemble members of MEPS. The lighter the colour according to the colour bar the higher the variation between the perturbed ensemble members. In grey the ensemble mean of all ten members. For initialisations on 22 and 24 December 2016. *Continued on next page.*

Overall seems a combination of the deterministic and first ensemble member of the 22 December 2016 initialisation to be a good forecast when comparing to the retrieved SWC in Figures 4.2.7a to 4.2.7d.

A larger variability between the ensemble members is shown for the evolution of the occlusion on 26 December 2016 in Figure 4.2.9d. In general, the 25 December 2016 was a very weak snow storm with strong liquid precipitation observed between 12 UTC and 18 UTC. Initialisations on 25 December 2016 (Figure 4.2.9c) present a lower variability for the transition after 15 UTC on 26 December 2016 than initialisations less than 24 h prior.

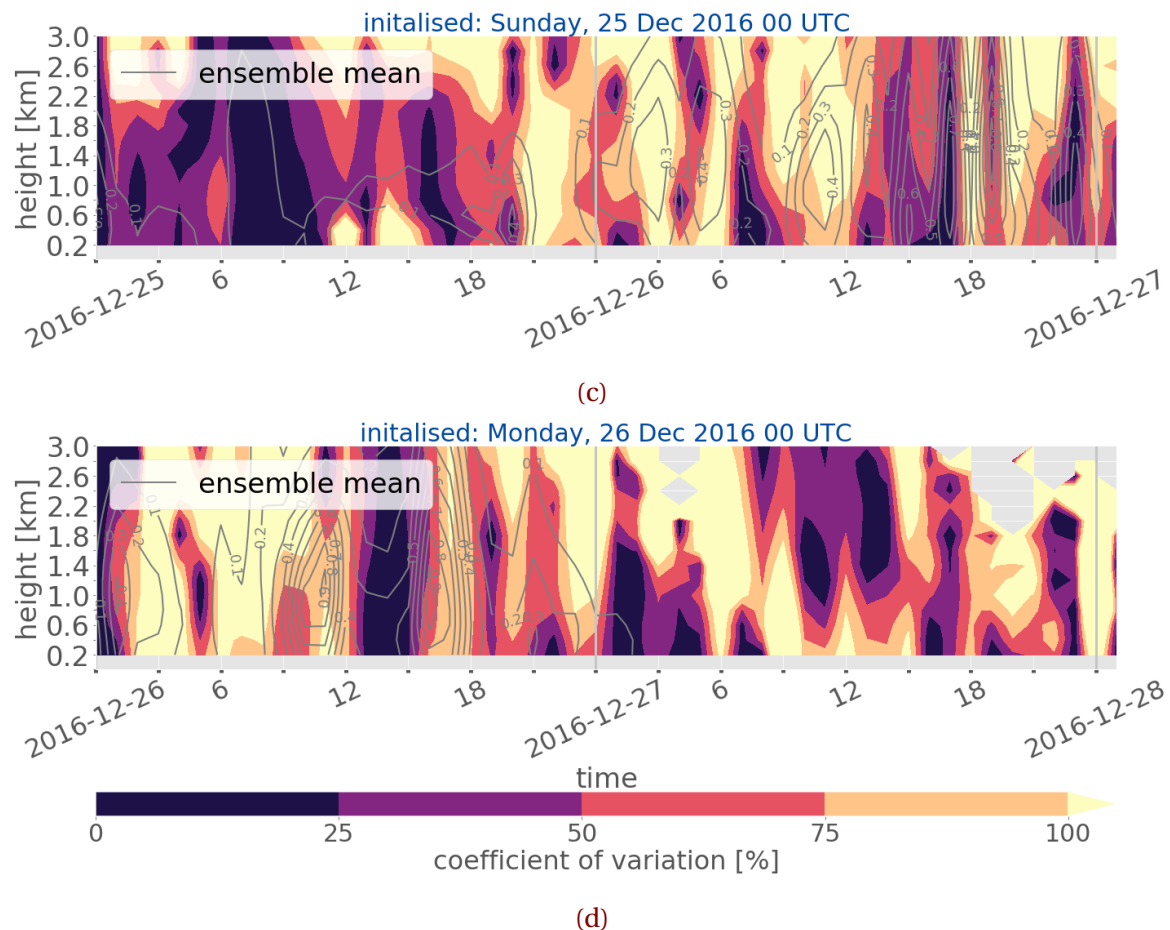


Figure 4.2.9: (Continued from previous page.) Initialisation 25 and 26 December 2016.

Therefore, an increase of variability after shorter time is given rather than long lead time (48 h). Figures 4.2.7g to 4.2.7i and Figures 4.2.7j to 4.2.7l give a low value of predicted SWC in the course of a day. As Figure 4.2.9b indicates is the forecast accuracy very high up to 1.8 km until noon, this is when liquid precipitation was measured. The depth of the liquid layer was up to 0.8 km in Figure 4.2.8a and 4.2.8b. The variation coefficient (Figure 4.2.9b and 4.2.9c) has a large disagreement below 0.8 km, but above the variability is between the members not existing or low. Initialisation on 24 December 2016 show weak snow water content peak in Figure 4.2.7h and i at 18 UTC, which had a moderate variability (Table 4.2.5, Figure 4.2.9b). Afterwards it is very high. Initialisation on 25 December 2016 the forecast variability is low until noon (Figure 4.2.9c). While liquid precipitation was monitored the variability in the lower layer is first very high and shortly before 18 UTC not

existing. A high agreement for the SWC peak at 20 UTC up to 0.8 km exists in Figure 4.2.9c and decreases to be moderate above.

Figure 4.2.7k and l would suggest a continues pulsing of the storm. The two peaks around 18 UTC (Figure 4.2.7k) are predicted with a negligible and moderate variability in ???. The SWC peaks at around 3 UTC and 5 UTC show a very high variability. Figure B.2.1e displays that four out of ten ensemble members would agree with the peaked event around 5 UTC. Whereas the peak at 3 UTC is dominated by the strong predicted SWC of the deterministic forecast, which follows the high variation in Figure 4.2.9c. Initialisation on 26 December 2016 follow that the SWC peak at 1 UTC is related to a moderate variability of the ensemble members. Low forecast accuracy is shown for the SWC between 9 UTC to 12 UTC and the one between 15 UTC to 18 UTC has a low to moderate variability between the members. When looking at Figure B.2.1f might this disagreement be related to the colourful variation of the vertical predicted SWC. There seems to be no agreement between the different members about the incidence of the SWC peaks. The high conflict for the CV before noon is most likely related to the high SWC of the deterministic SWC.

Again, this is not a fair comparison since hourly instantaneous values are used and there might be a time delay of half an hour about the development of boundaries which would follow it is not seen in the model forecast.

One question to answer in this work is if the operational model MEPS estimates large scale features correctly. As discussed here and in Section 4.1.1 it seems that the model is able to cover the development of large scale features and its associated precipitation. Even with the intensification of the storm MEPS seem to be able to predict extreme events for vertical snowfall such as the 2016 Christmas extreme event, but might have some issues predicting transitions of frontal boundaries as well as associated precipitation at the surface.

MEPS is also able to distinguish between liquid and solid precipitation in layer thickness and duration for time resolution of one hour. This can be a major advantage since a change in temperature and associated precipitation transformation can lead to high safety issues in the Norwegian mountains, especially during winter. With the knowledge more than 24 h prior can risk notice be send out to the population and rescue teams can prepare in advance. Furthermore, roads and train tracks can be closed to increase the safety.

The here presented results are a first look, trying to compare a mesoscale ensemble member forecast system (MEPS) with vertical in-situ measurement for snowfall.

The next section will go into detail, how the local orography at Haukeliseter may influence frozen precipitation, and how MEPS's representation of the topography may affect it.

4.2.5 OROGRAPHIC INFLUENCE ON PRECIPITATION

The Haukeliseter site is suspended to high wind speeds during the winter. The previous results in Section 4.1.1, 4.2.3, 4.2.4 have shown, that wind plays an important role for the precipitation at Haukeliseter. The mountain plateau is surrounded by higher mountains to the west and more open to the south east (Figure 4.2.10a), this orography seems to influence the vertical precipitation pattern. The correlation between wind speed observations and forecast show an overestimation of predicted wind speed throughout the event (Figure 4.1.1d, i, n and s). Müller et al. [2017] already mentioned the weakness of too strong wind prediction in AROME-MetCoOp, the previous operational deterministic version of MEPS.

Figure 4.2.10b shows the MEPS resolution and its 2.5 km grid cells around the Haukeliseter site. The complex terrain and its representation in MEPS might have followed the overestimation of accumulation. In this thesis the closest grid point to the Haukeliseter measurement site is used. Alternatively, the use of an average of the grid points surrounding the Haukeliseter site could lead to a solution that is closer to the truth and must be evaluated further.

On 21 and 23 December 2016 wind directions from the south-east and south were observed, respectively. As earlier discussed in Section 4.1.1 and 4.2.4 the wind change is associated with the occlusion passage on 23 December 2016 (Figure 3.6.2a and 3.6.2c). The wind direction on 21 December 2016 in Figure 4.1.1c change was also related to the large scale synoptic flow but is not associated to a frontal boundary. A comparison with the large scale weather analysis from ECMWF shows, that the large scale surface wind is from the south-west at 6 UTC on 21 December 2016 (not shown) and has changed to west at 12 UTC (Figure 3.6.1d). The observations at the Haukeliseter site show between 6 UTC and 12 UTC wind from south-east, while the predicted wind direction is from south in Figure 4.1.1c. The local wind direction influenced the precipitation pattern in the vertical on 21 and 23 December 2016, in the matter that a more consistent storm structure was observed and predicted between 9 UTC to 12 UTC (Figures 4.2.11a to 4.2.11c).

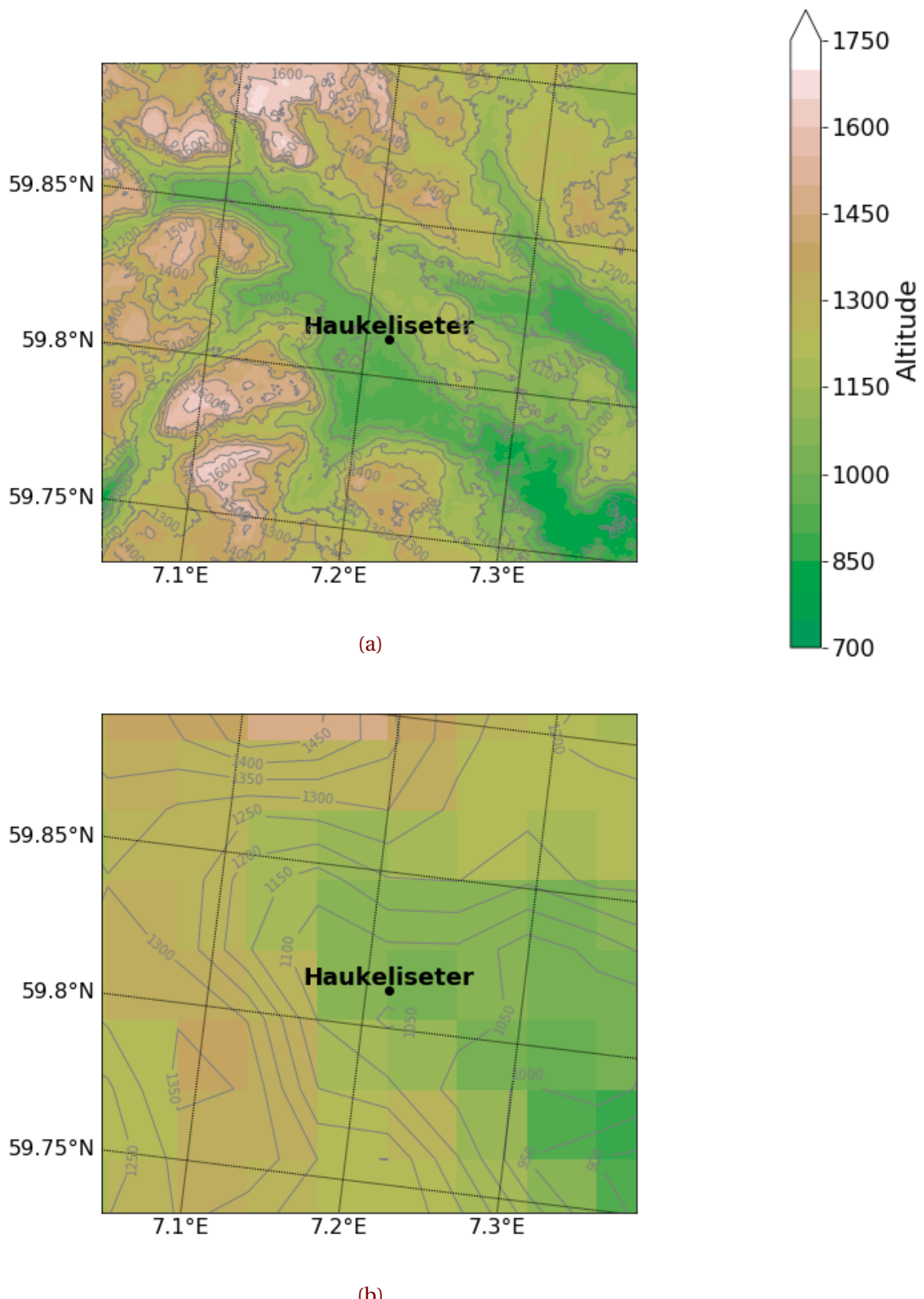


Figure 4.2.10: Topography around Haukeliseter. In **a** the DTM 10 Terrain Model (UTM33) from Geonorge [2018]. Contours and shading according to the colorbar. **b:** Representation of the topography around the measurement site Haukeliseter in MEPS. Contours and shading present the elevation of the grid cells.

Both days show a more consistent storm structure with not as intense snow water content than for storm patterns from the west such as on 24 December 2016 (Figures 4.2.7g to 4.2.7i). Figure 4.2.10a presents the local topography around Haukeliseter and Figure 4.2.10b shows the topography resolved by MEPS. MEPS is able to cover some of the complex structure around the site (Figure 4.2.10b), with the higher mountain to the west and the valley to the south-east (Figure 4.2.10a). The forecast model seems to forecast the wind direction overall well, only on 21 December 2016 before 10 UTC is a south-west instead of a south-east wind predicted. It displays that even if the large scale wind is from the south-west the local wind is rather from the south or south-east (Figure 3.6.1d).

Figure 4.1.2f shows a good correlation for west winds, but on the other side, southerly winds seem to be troublesome to predict for MEPS. Figure 4.1.2e indicates an unbalance for south-westerly winds. While south-easterly winds (along the valley) are observed at Haukeliseter predicts MEPS the 10 m wind to be south-westerly.

Figure 4.2.10 shows the comparison between the orography and the resolved topography by MEPS. Observed south-easterly winds are forced along the valley, directed in south-east. MEPS resolves it in the way, that the wind is south-westerly. Figure 4.2.10b displays a high mountain to the west of the station and a small one to the south. 10 m wind predicted by MEPS is predicted to blow between these two elevations.

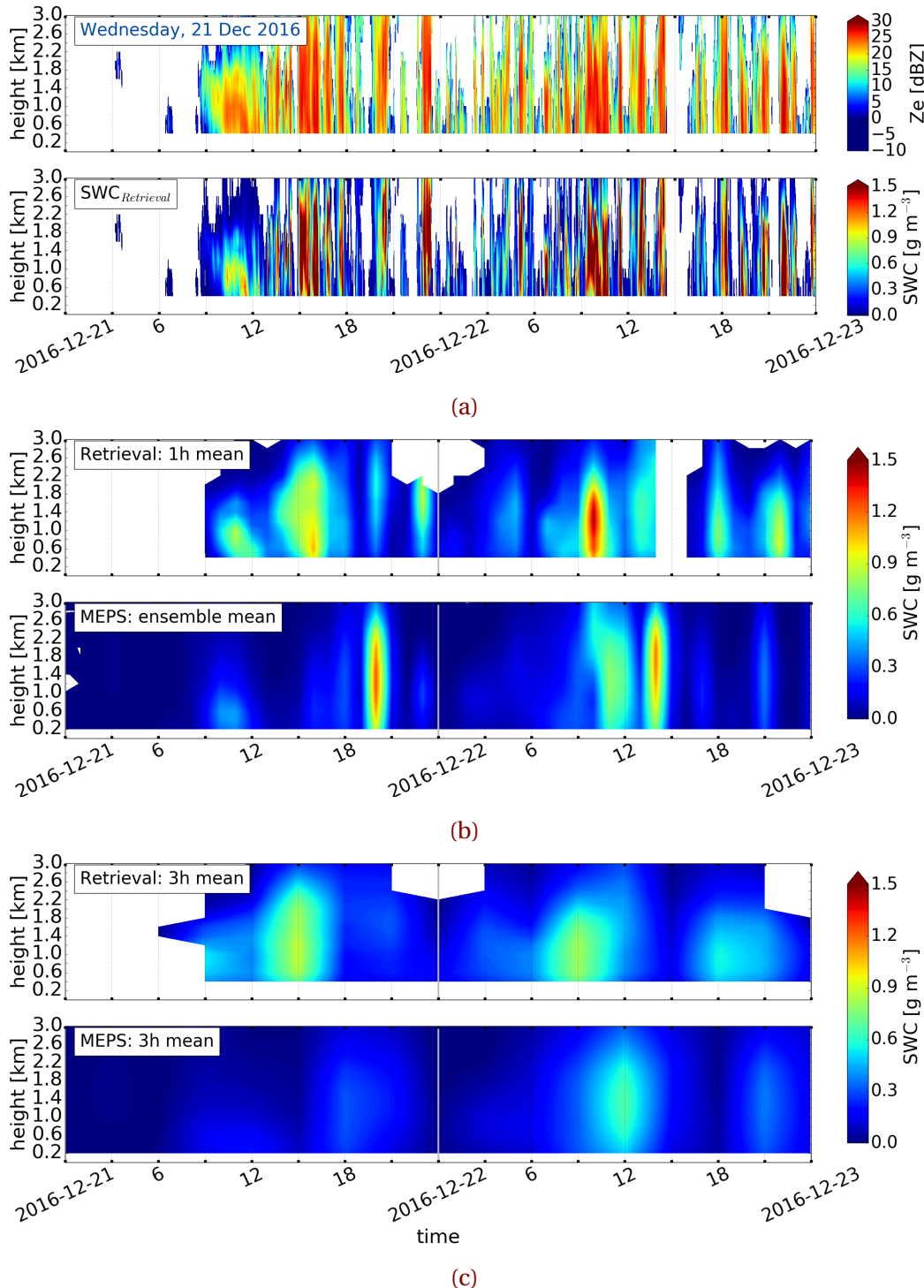


Figure 4.2.11: Initialisation 21 December 2016 0 UTC. (a,g) Upper panel: MRR reflectivity for 48 h, lower panel minutely retrieved SWC. (b, h) Upper panel: hourly averaged retrieved SWC, lower panel instantaneous hourly averaged forecast of all ensemble member SWC, neglecting missing values. (c, i) Upper panel three hourly averaged retrieved SWC, lower panel instantaneous three hourly averaged forecast of all ensemble member SWC.

As Figure 4.2.11b indicates is the model able to cover almost the exact timing of the up-slope storm pattern. The variability of each ensemble member is presented in Figure B.2.1a. It shows that almost all ensemble member agree on the occurrence of the storm pattern during 9 UTC to 12 UTC.

Wind from the west and therefore over high mountains (1500 m) always follow a pulsing with more intense vertical precipitation e.g. on 24 December 2016, Figure 4.2.7g and 4.2.7j). This effect might be related to wave breaking at the mountain and result into a pulsing precipitation pattern. More precipitation events need to be studied to understand this effect around the Haukeliseter site. MEPS does not cover all pulses related to west wind during the course of a day. This is related to the short occurrence of the pulses as well as to the time resolution of the forecast values. Since the prediction values exist only every hour the model might miss some of the high pulses 30 min before or after the frozen precipitation.

One outcome of the presented study is that MEPS is able to resolve the local topography and predicts the wind direction correctly. The variability between the ensemble members is smaller for precipitation related to south-easterly winds (Figure 4.2.9a, c, d). It did not cover the south-east wind direction on 21 December 2016 (Figure 4.1.1c), which must be related to the local topography.

It seems more intuitive for the model to force large scale south-westerly flow into south direction rather than the observed wind direction along the south-easterly directed valley. As seen in Figure 4.2.10 the wind must go along the 7.2° longitude, since a higher (1500 m to 1650 m) elevation is to the west and a 1350 m high mountain to the east. True prediction of wind direction leads to the correct estimation of frozen precipitation patterns, such as up-slope (south-easterly wind) and pulsing (west wind).

Section 4.2.3 describes the overestimation of surface snow accumulation during the intensification of the extreme storm. MEPS forecast in Figure 4.2.4d, e, and f show more ground accumulation than it is observed for 24 to 26 December 2016. One approach was to see, if the wind might have had an influence on the surface measurement of the double fence, which did not show to be true, even if 10 % under-catch by the double fence gauge is

assumed (Table 4.2.4). A comparison of the hourly values of MEPS, show neither on 24 nor on 25 nor 26 December 2016 high vertical snow amount compared to the estimated SWC (Figure 4.2.7h, 4.2.7k, and n). Figure B.2.1 shows values of very intense instantaneous snow water content for individual ensemble members, but no prominent sign of overestimation when the surface miscalculation was present.

During 24 to 26 December 2016 the wind was constantly from the west with higher wind speeds observed than during 21 to 23 December 2016 (Figure 4.1.1). Figure 4.1.2e and f indicate a better correlation for the forecasted and observed wind directions when precipitation overestimation occurred (24 to 26 December 2016). During 24 and 26 December 2016, observed wind speeds were higher up to 18 ms^{-1} than on the previous days. As Figure 4.1.2g and h present is the correlation between observation and forecasts lower for high wind speeds. The high wind speeds from the west followed a pulsing storm pattern with changing intense and less intense snowfall (e.g. 22 and 24 December 2016, Figures 4.2.7a to 4.2.7c, g, h, i). MEPS is able to forecast the pulsing pattern for initialisations longer than 24 h prior. Since the model estimates the wind direction correctly for west wind and local mountain affects it follows that there seems to be an interaction issue between frozen precipitation and the surface accumulation. Hourly vertical instantaneous values could have led to a misinterpretation of the here presented results. Furthermore, this study presents only a first look for a comparison between observed profiles of precipitation to MEPS forecast for an extreme event.

The ensemble variability in Figure 4.2.9 show that the ensemble members are divided about the existence of the exact precipitation pulsing.

While the wind direction of MEPS has a good agreement, at least for west wind, shows the wind speed larger values over all days (Figures 4.1.2e to 4.1.2h). Although MEPS includes ten perturbed ensemble members the insufficiency of AROME-MetCoOp too high wind prediction in extreme situations is not resolved. As Müller et al. [2017] mentioned are higher wind speeds in general better forecasted in AROME-MetCoOp than in ECMWF, which is an advantage for small scale forecast models. Especially in Norway, where the topography changes from sea to mountains.

REFERENCES

- Barnett, T. P., Adam, J. C., and Lettenmaier, D. P. Potential impacts of a warming climate on water availability in snow-dominated regions. *Nature*, 438(7066):303–309, November 2005. ISSN 1476-4687. doi: [10.1038/nature04141](https://doi.org/10.1038/nature04141). URL <https://www.nature.com/articles/nature04141>.
- Caniaux, G., Redelsperger, J.-L., and Lafore, J.-P. A Numerical Study of the Stratiform Region of a Fast-Moving Squall Line. Part I: General Description and Water and Heat Budgets. *J. Atmos. Sci.*, 51(14):2046–2074, July 1994. ISSN 0022-4928. doi: [10.1175/1520-0469\(1994\)051<2046:ANSOTS>2.0.CO;2](https://doi.org/10.1175/1520-0469(1994)051<2046:ANSOTS>2.0.CO;2). URL [https://journals.ametsoc.org/doi/abs/10.1175/1520-0469\(1994\)051%3C2046:ANSOTS%3E2.0.CO;2](https://journals.ametsoc.org/doi/abs/10.1175/1520-0469(1994)051%3C2046:ANSOTS%3E2.0.CO;2).
- Christensen, M. W., Behrangi, A., L'ecuyer, T. S., Wood, N. B., Lebsack, M. D., and Stephens, G. L. Arctic Observation and Reanalysis Integrated System: A New Data Product for Validation and Climate Study. *Bull. Amer. Meteor. Soc.*, 97(6):907–916, January 2016. ISSN 0003-0007. doi: [10.1175/BAMS-D-14-00273.1](https://doi.org/10.1175/BAMS-D-14-00273.1). URL <https://journals.ametsoc.org/doi/10.1175/BAMS-D-14-00273.1>.
- Colle, B. A., Garvert, M. F., Wolfe, J. B., Mass, C. F., and Woods, C. P. The 13–14 December 2001 IMPROVE-2 Event. Part III: Simulated Microphysical Budgets and Sensitivity Studies. *J. Atmos. Sci.*, 62(10):3535–3558, October 2005. ISSN 0022-4928. doi: [10.1175/JAS3552.1](https://doi.org/10.1175/JAS3552.1). URL <https://journals.ametsoc.org/doi/abs/10.1175/JAS3552.1>.
- Cooper, S. J., Wood, N. B., and L'Eucyer, T. S. A variational technique to estimate snowfall rate from coincident radar, snowflake, and fall-speed observations. *Atmos. Meas. Tech.*, 10(7):2557–2571, July 2017. ISSN 1867-8548. doi: [10.5194/amt-10-2557-2017](https://doi.org/10.5194/amt-10-2557-2017). URL <https://www.atmos-meas-tech.net/10/2557/2017/>.

- Dahlgren, P. A Comparison Of Two Large Scale Blending Methods. page 16, 2013. URL <http://metcoop.org/memo/2013/02-2013-METCOOP-MEMO.PDF>.
- Dando, P. Introducing the octahedral reduced Gaussian grid, June 2016. URL <https://software.ecmwf.int/wiki/display/FCST/Gaussian+grids>.
- Doviak, R. J. and Zrnic, D. S. *Doppler Radar and Weather Observations*. Courier Corporation, 1993. ISBN 978-0-486-45060-5. Google-Books-ID: ispLkPX9n2UC.
- eklima. Norwegian Meteorological Institute, 2016. URL http://sharki.oslo.dnmi.no/portal/page?_pageid=73,39035,73_39049&_dad=portal&_schema=PORTAL.
- Farestveit, E. 80.000 mista radioen under ekstremvêret, December 2016. URL <https://www.nrk.no/hordaland/80.000-mista-radioen-under-ekstremveret-1.13294980>.
- Field, C. B., Barros, V. R., Dokken, D. J., Mach, K. J., Mastrandrea, M. D., Bilir, T. E., Chatterjee, M., Ebi, K. L., Estrada, Y. O., Genova, R. C., Girma, B., Kissel, E. S., Levy, A. N., MacCracken, S., Mastrandrea, P. R., and White, L. L. Summary for policymakers. In: Climate Change 2014: Impacts, Adaptation, and Vulnerability. Part A: Global and Sectoral Aspects. Contribution of Working Group II to the Fifth Assessment Report of the Intergovernmental Panel on Climate Change. Cambridge: Cambridge University Press, page 34, 2014.
- Færaas, A., Rommetveit, A., Duesund, J., and Senel, E. «Urd» har nådd orkan styrke – flytter seg mot Østlandet, December 2016. URL http://www.yr.no/artikkel/_urd_-har-nadd-orkan-styrke--flytter-seg-mot-ostlandet-1.13292245.
- Garrett, T. J., Fallgatter, C., Shkurko, K., and Howlett, D. Fall speed measurement and high-resolution multi-angle photography of hydrometeors in free fall. *Atmos. Meas. Tech.*, 5(11):2625–2633, November 2012. ISSN 1867-8548. doi: [10.5194/amt-5-2625-2012](https://doi.org/10.5194/amt-5-2625-2012). URL <https://www.atmos-meas-tech.net/5/2625/2012/>.
- Garvert, M. F., Woods, C. P., Colle, B. A., Mass, C. F., Hobbs, P. V., Stoelinga, M. T., and Wolfe, J. B. The 13–14 December 2001 IMPROVE-2 Event. Part II: Comparisons of MM5 Model Simulations of Clouds and Precipitation with Observations. *J. Atmos.*

- Sci.*, 62(10):3520–3534, October 2005. ISSN 0022-4928. doi: 10.1175/JAS3551.1. URL <https://journals.ametsoc.org/doi/10.1175/JAS3551.1>.
- Geonor Inc. T-200b All Weather Precipitation – Rain Gauge, 2015. URL <http://geonor.com/live/products/weather-instruments/t-200b-weather-precipitation-rain-gauge/>.
- Geonorge. DTM 10 Terrengmodell (UTM33) - Kartverket - Kartkatalogen, May 2018. URL <https://kartkatalog.geonorge.no/metadata/uuid/dddbb667-1303-4ac5-8640-7ec04c0e3918>.
- Goodison, B. E., Louie, P. Y. T., and Yang, D. WMO Solid Precipitation Measurement Intercomparison: Final Report. Instruments and Observing Methods Rep. 67, WMO/TD-No. 872,. *World Meteorological Organization, Geneva, Switzerland*, page 318, 1998.
- Gowan, T. M., Steenburgh, W. J., and Schwartz, C. S. Validation of Mountain Precipitation Forecasts from the Convection-Permitting NCAR Ensemble and Operational Forecast Systems over the Western United States. *Wea. Forecasting*, 33(3):739–765, June 2018. ISSN 0882-8156, 1520-0434. doi: 10.1175/WAF-D-17-0144.1. URL <http://journals.ametsoc.org/doi/10.1175/WAF-D-17-0144.1>.
- Hansen, B. B., Isaksen, K., Benestad, R. E., Kohler, J., Pedersen, Ø. Ø., Loe, L. E., Coulson, S. J., Larsen, J. O., and Varpe, Ø. Warmer and wetter winters: characteristics and implications of an extreme weather event in the High Arctic. *Environ. Res. Lett.*, 9(11):114021, 2014. ISSN 1748-9326. doi: 10.1088/1748-9326/9/11/114021. URL <http://stacks.iop.org/1748-9326/9/i=11/a=114021>.
- Hansen, B. B., Aanes, R., Herfindal, I., Kohler, J., and Sæther, B.-E. Climate, icing, and wild arctic reindeer: past relationships and future prospects. *Ecology*, 92(10):1917–1923, October 2011. ISSN 1939-9170. doi: 10.1890/11-0095.1. URL <https://esajournals.onlinelibrary.wiley.com/doi/abs/10.1890/11-0095.1>.
- Homleid, M. and Tveter, F. T. Verification of operational weather prediction models september to november 2015. *METInfo Rep*, 16:2016, 2016. URL https://www.met.no/publikasjoner/met-info/met-info-2016/_attachment/download/b0463915-

- cba0-42ac-8539-4233ae2bf01c:3d71565a27f88085373199a33ab8569151c144e9/
MET-info-22-2016.pdf.
- Hudak, D., Barker, H., Rodriguez, P., and Donovan, D. The Canadian CloudSat Validation Project. *4th ERAD*, September 2006. URL <http://www.crahi.upc.edu/ERAD2006/proceedingsMask/00165.pdf>. Barcelona, Spain.
- Joos, H. and Wernli, H. Influence of microphysical processes on the potential vorticity development in a warm conveyor belt: a case-study with the limited-area model COSMO. *Q. J. Royal Meteorol. Soc.*, 138(663):407–418, January 2012. ISSN 00359009. doi: [10.1002/qj.934](https://doi.org/10.1002/qj.934). URL <http://doi.wiley.com/10.1002/qj.934>.
- Kalnay, E. *Atmospheric modeling, data assimilation and predictability*. Cambridge University Press, Cambridge, 2003. ISBN 978-0-521-79179-3.
- Kochendorfer, J., Nitu, R., Wolff, M., Mekis, E., Rasmussen, R., Baker, B., Earle, M. E., Reverdin, A., Wong, K., Smith, C. D., Yang, D., Roulet, Y.-A., Buisan, S., Laine, T., Lee, G., Aceituno, J. L. C., Alastrué, J., Isaksen, K., Meyers, T., Brækkan, R., Landolt, S., Jachcik, A., and Poikonen, A. Analysis of single-Alter-shielded and unshielded measurements of mixed and solid precipitation from WMO-SPICE. *Hydrol. Earth Syst. Sci.*, 21(7):3525–3542, July 2017. ISSN 1607-7938. doi: [10.5194/hess-21-3525-2017](https://doi.org/10.5194/hess-21-3525-2017). URL <https://www.hydrol-earth-syst-sci.net/21/3525/2017/>.
- Kulie, M. S. and Bennartz, R. Utilizing Spaceborne Radars to Retrieve Dry Snowfall. *J. Appl. Meteor. Climatol.*, 48(12):2564–2580, January 2009. ISSN 1558-8424. doi: [10.1175/2009JAMC2193.1](https://doi.org/10.1175/2009JAMC2193.1). URL <http://journals.ametsoc.org/doi/abs/10.1175/2009JAMC2193.1>.
- Kulie, M. S., Milani, L., Wood, N. B., Tushaus, S. A., Bennartz, R., and L’Ecuyer, T. S. A Shallow Cumuliform Snowfall Census Using Spaceborne Radar. *J. Hydrometeor.*, 17(4):1261–1279, February 2016. ISSN 1525-755X. doi: [10.1175/JHM-D-15-0123.1](https://doi.org/10.1175/JHM-D-15-0123.1). URL <https://journals.ametsoc.org/doi/abs/10.1175/JHM-D-15-0123.1>.
- Køltzow, M. A. MetCoOp EPS - A convection permitting ensemble prediction system, October 2017.

- L'Ecuyer, T. S. AOS 441 - Satellite and Radar Meteorology. January 2017. URL <https://lecuyer.aos.wisc.edu/aos441>.
- Liu G. Deriving snow cloud characteristics from CloudSat observations. *J. Geophys. Res. Atmos.*, 113(D8), September 2008. ISSN 0148-0227. doi: [10.1029/2007JD009766](https://doi.org/10.1029/2007JD009766). URL <https://agupubs.onlinelibrary.wiley.com/doi/abs/10.1029/2007JD009766>.
- Lorenz, E. N. Atmospheric Predictability as Revealed by Naturally Occurring Analogues. *J. Atmos. Sci.*, 26(4):636–646, July 1969. ISSN 0022-4928. doi: [10.1175/1520-0469\(1969\)26<636:APARBN>2.0.CO;2](https://doi.org/10.1175/1520-0469(1969)26<636:APARBN>2.0.CO;2). URL <https://journals.ametsoc.org/doi/abs/10.1175/1520-0469%281969%2926%3C636%3AAPARBN%3E2.0.CO%3B2>.
- Markowski, P. and Richardson, Y. *Mesoscale Meteorology in Midlatitudes*. John Wiley & Sons, September 2011. ISBN 978-1-119-96667-8. Google-Books-ID: MDeYosfLLEYC.
- Martin, J. E. *Mid-Latitude Atmospheric Dynamics: A First Course*. Wiley, May 2006. ISBN 978-0-470-86466-1.
- Matrosov, S. Y. Modeling Backscatter Properties of Snowfall at Millimeter Wavelengths. *J. Atmos. Sci.*, 64(5):1727–1736, May 2007. ISSN 0022-4928. doi: [10.1175/JAS3904.1](https://doi.org/10.1175/JAS3904.1). URL <https://journals.ametsoc.org/doi/abs/10.1175/JAS3904.1>.
- McCumber, M., Tao, W.-K., Simpson, J., Penc, R., and Soong, S.-T. Comparison of Ice-Phase Microphysical Parameterization Schemes Using Numerical Simulations of Tropical Convection. *J. Appl. Meteor.*, 30(7):985–1004, July 1991. ISSN 0894-8763. doi: [10.1175/1520-0450-30.7.985](https://doi.org/10.1175/1520-0450-30.7.985). URL <https://journals.ametsoc.org/doi/abs/10.1175/1520-0450-30.7.985>.
- Meehl, G. A., Karl, T., Easterling, D. R., Changnon, S., Pielke, R., Changnon, D., Evans, J., Groisman, P. Y., Knutson, T. R., Kunkel, K. E., Mearns, L. O., Parmesan, C., Pulwarty, R., Root, T., Sylves, R. T., Whetton, P., and Zwiers, F. An Introduction to Trends in Extreme Weather and Climate Events: Observations, Socioeconomic Impacts, Terrestrial Ecological Impacts, and Model Projections. *Bull. Amer. Meteor. Soc.*, 81(3):413–416, March 2000. ISSN 0003-0007. doi: [10.1175/1520-0477\(2000\)081<0413:AITTIE>2.3.CO;2](https://doi.org/10.1175/1520-0477(2000)081<0413:AITTIE>2.3.CO;2). URL [https://journals.ametsoc.org/doi/abs/10.1175/1520-0477\(2000\)081%3C0413:AITTIE%3E2.3.CO;2](https://journals.ametsoc.org/doi/abs/10.1175/1520-0477(2000)081%3C0413:AITTIE%3E2.3.CO;2).

- MetCoOp Wiki. Description of MEPS, December 2017. URL <https://metcoop.smhi.se/dokuwiki/nwp/metcoop/>.
- METEK, M. M. G. Micro Rain Radar MRR-2, October 2010. URL <http://metek.de/wp-content/uploads/2014/05/Metek-Micro-Rain-Radar-MRR-2-Datasheet.pdf>.
- Meteo France. The Meso-NH Atmospheric Simulation System: Scientific Documentation, Part III: Physics, January 2009.
- Meteorologene. "Her kommer #Urd! Selve Lavtrykksenteret treffer Møre og Romsdal, men den sterkeste vinden kommer sør for Stad. #SørNorge" 26 December 2016, 9:34am, 2016. URL <https://twitter.com/Meteorologene>.
- Müller, M., Homleid, M., Ivarsson, K.-I., Køltzow, M. A. Ø., Lindskog, M., Midtbø, K. H., Andrae, U., Aspelien, T., Berggren, L., Bjørge, D., Dahlgren, P., Kristiansen, J., Randriamampianina, R., Ridal, M., and Vignes, O. AROME-MetCoOp: A Nordic Convective-Scale Operational Weather Prediction Model. *Wea. Forecasting*, 32(2):609–627, January 2017. ISSN 0882-8156. doi: [10.1175/WAF-D-16-0099.1](https://doi.org/10.1175/WAF-D-16-0099.1). URL <http://journals.ametsoc.org/doi/abs/10.1175/WAF-D-16-0099.1>.
- Newman, A. J., Kucera, P. A., and Bliven, L. F. Presenting the Snowflake Video Imager (SVI). *J. Atmos. Oceanic Technol.*, 26(2):167–179, February 2009. ISSN 0739-0572. doi: [10.1175/2008JTECHA1148.1](https://doi.org/10.1175/2008JTECHA1148.1). URL <https://journals.ametsoc.org/doi/abs/10.1175/2008JTECHA1148.1>.
- Noh, Y.-J., Liu, G., Seo, E.-K., Wang, J. R., and Aonashi, K. Development of a snowfall retrieval algorithm at high microwave frequencies. *J. Geophys. Res.*, 111(D22), November 2006. ISSN 2156-2202. doi: [10.1029/2005JD006826](https://doi.org/10.1029/2005JD006826). URL <https://agupubs.onlinelibrary.wiley.com/doi/abs/10.1029/2005JD006826>.
- Norin, L., Devasthale, A., L'Ecuyer, T. S., Wood, N. B., and Smalley, M. Intercomparison of snowfall estimates derived from the CloudSat Cloud Profiling Radar and the ground-based weather radar network over Sweden. *Atmos. Meas. Tech.*, 8(12):5009–5021, December 2015. ISSN 1867-8548. doi: [10.5194/amt-8-5009-2015](https://doi.org/10.5194/amt-8-5009-2015). URL <https://www.atmos-meas-tech.net/8/5009/2015/>.

- Norwegian Meteorological Institute. MET Norway Thredds Service, 2016. URL <http://thredds.met.no/thredds/catalog/meps25epsarchive/catalog.html>.
- Olsen, A.-M. and Granerød, M. Ekstremværrapport. Hendelse: Urd 26. desember met. info. no. 18/2017 ISSN X METEOROLOGI Bergen, - PDF, September 2017. URL <http://docplayer.me/48734203-Ekstremvaerrapport-hendelse-urd-26-desember-met-info-no-18-2017-issn-x-meteorologi-bergen.html>.
- Palerme, C., Kay, J. E., Genthon, C., L'Ecuyer, T., Wood, N. B., and Claud, C. How much snow falls on the Antarctic ice sheet? *The Cryosphere*, 8(4):1577–1587, August 2014. ISSN 1994-0424. doi: 10.5194/tc-8-1577-2014. URL <https://www.the-cryosphere.net/8/1577/2014/>.
- Palerme, C., Genthon, C., Claud, C., Kay, J. E., Wood, N. B., and L'Ecuyer, T. Evaluation of current and projected Antarctic precipitation in CMIP5 models. *Clim. Dyn.*, 48(1-2): 225–239, January 2017. ISSN 0930-7575, 1432-0894. doi: 10.1007/s00382-016-3071-1. URL <https://link.springer.com/article/10.1007/s00382-016-3071-1>.
- Pedersen, K. and Rommetveit, A. Hva er et «ekstremvær»?, November 2013. URL http://www.yr.no/artikkelen/hva-er-et-_ekstremvaer___-1.7890946.
- Peel, M. C., Finlayson, B. L., and McMahon, T. A. Updated world map of the Köppen-Geiger climate classification. *Hydrology and Earth System Sciences Discussions*, 4(2):439–473, March 2007. URL <https://hal.archives-ouvertes.fr/hal-00298818>.
- Pinty, J.-P. and Jabouille, P. A mixed-phased cloud parameterization for use in a mesoscale non-hydrostatic model: Simulations of a squall line and of orographic precipitation. pages 217–220. Amer. Meteor. Soc., 1998.
- Putkonen, J. and Roe, G. Rain-on-snow events impact soil temperatures and affect ungulate survival: RAIN-ON-SNOW EVENTS IMPACT SOIL TEMPERATURES. *Geophysical Research Letters*, 30(4), February 2003. ISSN 00948276. doi: 10.1029/2002GL016326. URL <http://doi.wiley.com/10.1029/2002GL016326>.
- Rinehart, R. E. *Radar for Meteorologists: Or You, Too, Can be a Radar Meteorologist*. Rinehart Publications, 2010. ISBN 978-0-9658002-3-5. Google-Books-ID: VqatcQAACAAJ.

- Rutz, J. J., Steenburgh, W. J., and Ralph, F. M. Climatological Characteristics of Atmospheric Rivers and Their Inland Penetration over the Western United States. *Mon. Wea. Rev.*, 142(2):905–921, January 2014. ISSN 0027-0644. doi: 10.1175/MWR-D-13-00168.1. URL <http://journals.ametsoc.org/doi/abs/10.1175/MWR-D-13-00168.1>.
- Ruud, S., Carr Ekroll, H., Bakke Foss, A., Torgersen, H. O., and Annar Holm, P. To tonn tungt skilt blåste ned da ekstremværet traff Oslo og Østlandet i natt, December 2016. URL <https://www.aftenposten.no/article/ap-2z6wy.html>.
- Schirle, C. Characterization of snowfall at high latitudes using an optimal estimation-based retrieval algorithm. Private Communication, 2018.
- Schwartz, C. S. Reproducing the September 2013 Record-Breaking Rainfall over the Colorado Front Range with High-Resolution WRF Forecasts. *Wea. Forecasting*, 29(2): 393–402, January 2014. ISSN 0882-8156. doi: 10.1175/WAF-D-13-00136.1. URL <https://journals.ametsoc.org/doi/abs/10.1175/WAF-D-13-00136.1>.
- Skofronick-Jackson, G. M., Kim, M.-J., Weinman, J. A., and Chang, D.-E. A physical model to determine snowfall over land by microwave radiometry. *IEEE Geosci. Remote Sens. Lett.*, 42(5):1047–1058, May 2004. ISSN 0196-2892. doi: 10.1109/TGRS.2004.825585.
- Stephens, G. L. *Remote Sensing of the Lower Atmosphere: An Introduction*. Oxford University Press, 1994. ISBN 978-0-19-508188-6. Google-Books-ID: 2FcRAQAAIAAJ.
- Stimberis, J. and Rubin, C. M. Glide avalanche response to an extreme rain-on-snow event, Snoqualmie Pass, Washington, USA. *Journal of Glaciology*, 57(203): 468–474, 2011. ISSN 0022-1430, 1727-5652. doi: 10.3189/002214311796905686. URL <https://www.cambridge.org/core/journals/journal-of-glaciology/article/glide-avalanche-response-to-an-extreme-rainonsnow-event-snoqualmie-pass-washington-usa/2B6E48BD92F0700B7BEA02EF156E203F>.
- Stocker, T. F., Qin, D., Plattner, G.-K., Tignor, M. M. B., Allen, S. K., Boschung, J., Nauels, A., Xia, Y., Bex, V., and Midgley, P. M. Working Group I Contribution to the Fifth Assessment Report of the Intergovernmental Panel on Climate Change. *Cambridge: Cambridge University Press*, page 14, 2013.

- Sun, J. Convective-scale assimilation of radar data: progress and challenges. *Quarterly Journal of the Royal Meteorological Society*, 131(613):3439–3463, 2005. ISSN 1477-870X. doi: 10.1256/qj.05.149. URL <https://rmets.onlinelibrary.wiley.com/doi/abs/10.1256/qj.05.149>.
- Wolff, M. A. WMO Solid Precipitation Intercomparison Experiment (WMO-SPICE), Ch. 4.2.4 Precipitation measurements in areas with high winds and/or complex terrain. unpublished, 2018.
- Wolff, M. A., Brækkan, R., Isaksen, K., and Ruud, E. A new testsite for wind correction of precipitation measurements at a mountain plateau in southern Norway. In *Proceedings of WMO Technical Conference on Meteorological and Environmental Instruments and Methods of Observation (TECO–2010). Instruments and Observing Methods Report*, 2010.
- Wolff, M. A., Isaksen, K., Brækkan, R., Alfnes, E., Petersen-Øverleir, A., and Ruud, E. Measurements of wind-induced loss of solid precipitation: description of a Norwegian field study. *Hydrol. Res.*, 44(1):35–43, February 2013. ISSN 0029-1277, 2224-7955. doi: 10.2166/nh.2012.166. URL <http://hr.iwaponline.com/content/44/1/35>.
- Wolff, M. A., Isaksen, K., Petersen-Øverleir, A., Ødemark, K., Reitan, T., and Brækkan, R. Derivation of a new continuous adjustment function for correcting wind-induced loss of solid precipitation: results of a Norwegian field study. *Hydrol. Earth Syst. Sci.*, 19(2):951–967, February 2015. ISSN 1607-7938. doi: 10.5194/hess-19-951-2015. URL <https://www.hydrol-earth-syst-sci.net/19/951/2015/>.
- Wood, N. B. *Estimation of snow microphysical properties with application to millimeter-wavelength radar retrievals for snowfall rate*. Ph.D., Colorado State University, 2011. URL https://dspace.library.colostate.edu/bitstream/handle/10217/48170/Wood_colostate_0053A_10476.pdf?sequence=1&isAllowed=y.
- Wood, N. B., L'Ecuyer, T. S., Vane, D. G., Stephens, G. L., and Partain, P. Level 2c snow profile process description and interface control document. Technical Report, 2013. URL http://www.cloudsat.cira.colostate.edu/sites/default/files/products/files/2C-SNOW-PROFILE_PDICD.P_R04.20130210.pdf.

- Wood, N. B., L'Ecuyer, T. S., Heymsfield, A. J., and Stephens, G. L. Microphysical Constraints on Millimeter-Wavelength Scattering Properties of Snow Particles. *J. Appl. Meteor. Climatol.*, 54(4):909–931, January 2015. ISSN 1558-8424. doi: 10.1175/JAMC-D-14-0137.1. URL <http://journals.ametsoc.org/doi/10.1175/JAMC-D-14-0137.1>.

APPENDIX B: RESULTS

B.1 HOURLY AVERAGES ENSEMBLE MEMBER ZERO AND ONE

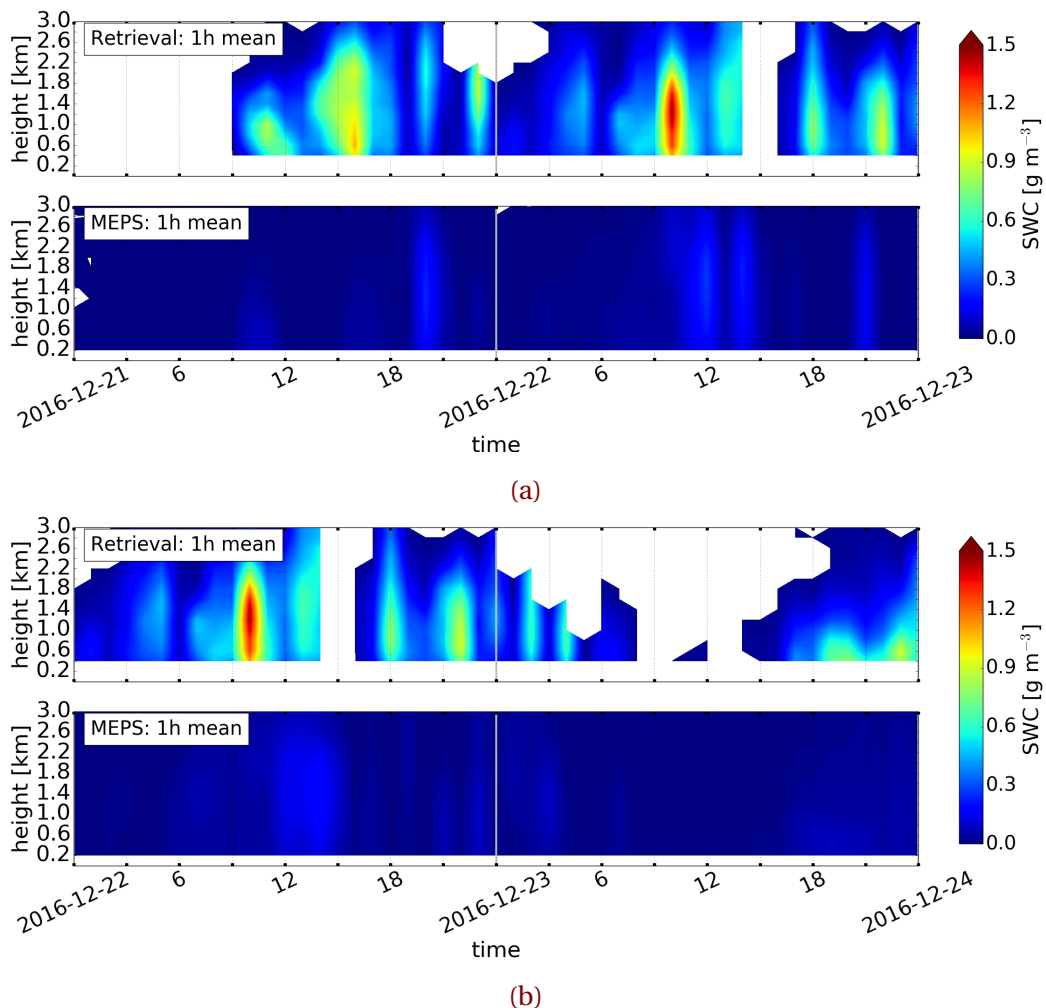
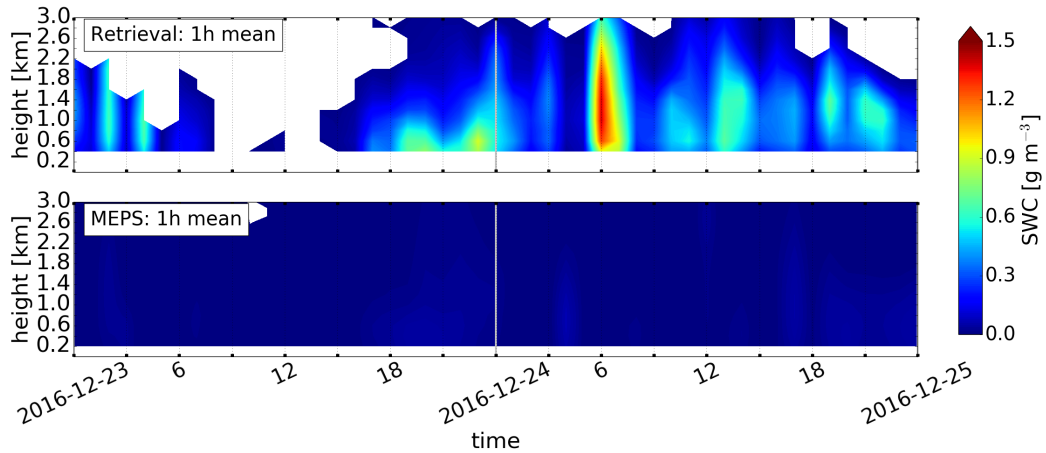
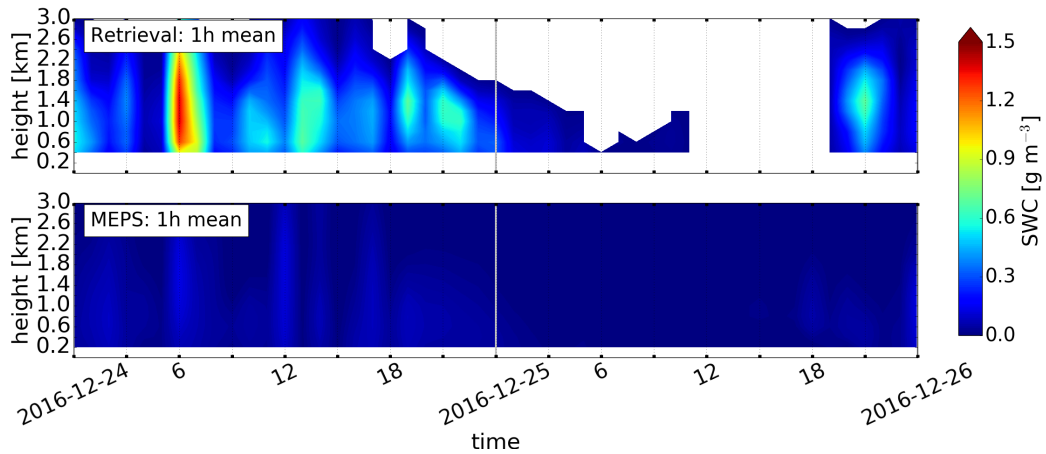


Figure B.1.1: Upper panel: hourly averaged retrieved SWC, lower panel instantaneous hourly averaged SWC forecast of deterministic and first ensemble member. Initialised 21 December 2016 and 22 December 2016 at 0 UTC.

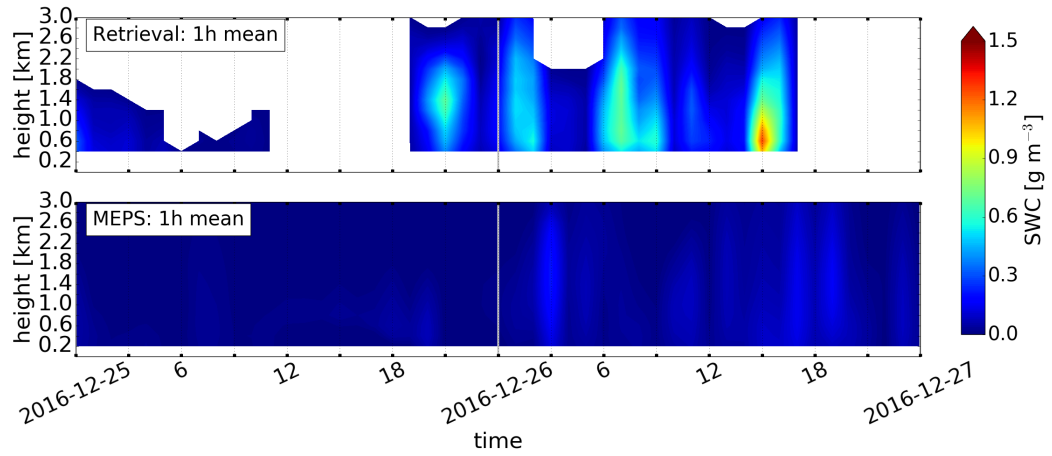


(c)

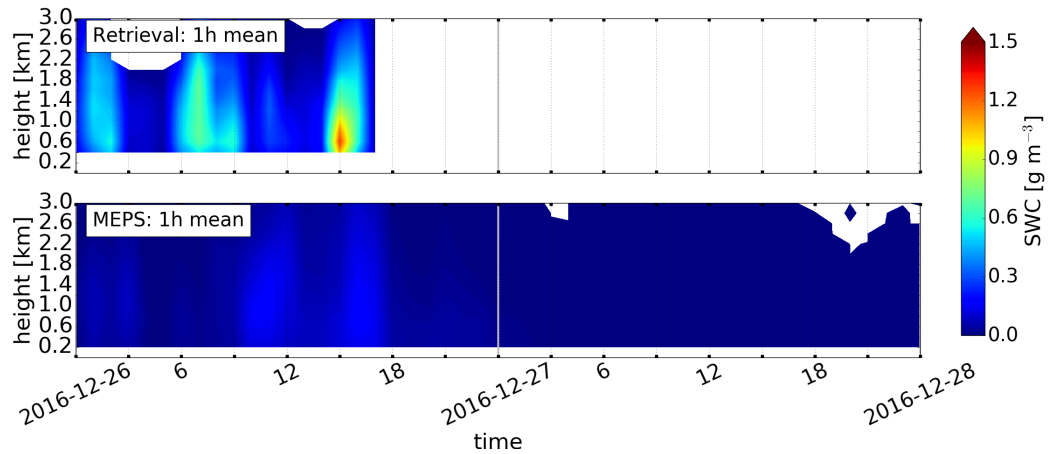


(d)

Figure B.1.1: (Continued from previous page.) Initialised 23 December 2016 and 24 December 2016 at 0 UTC.



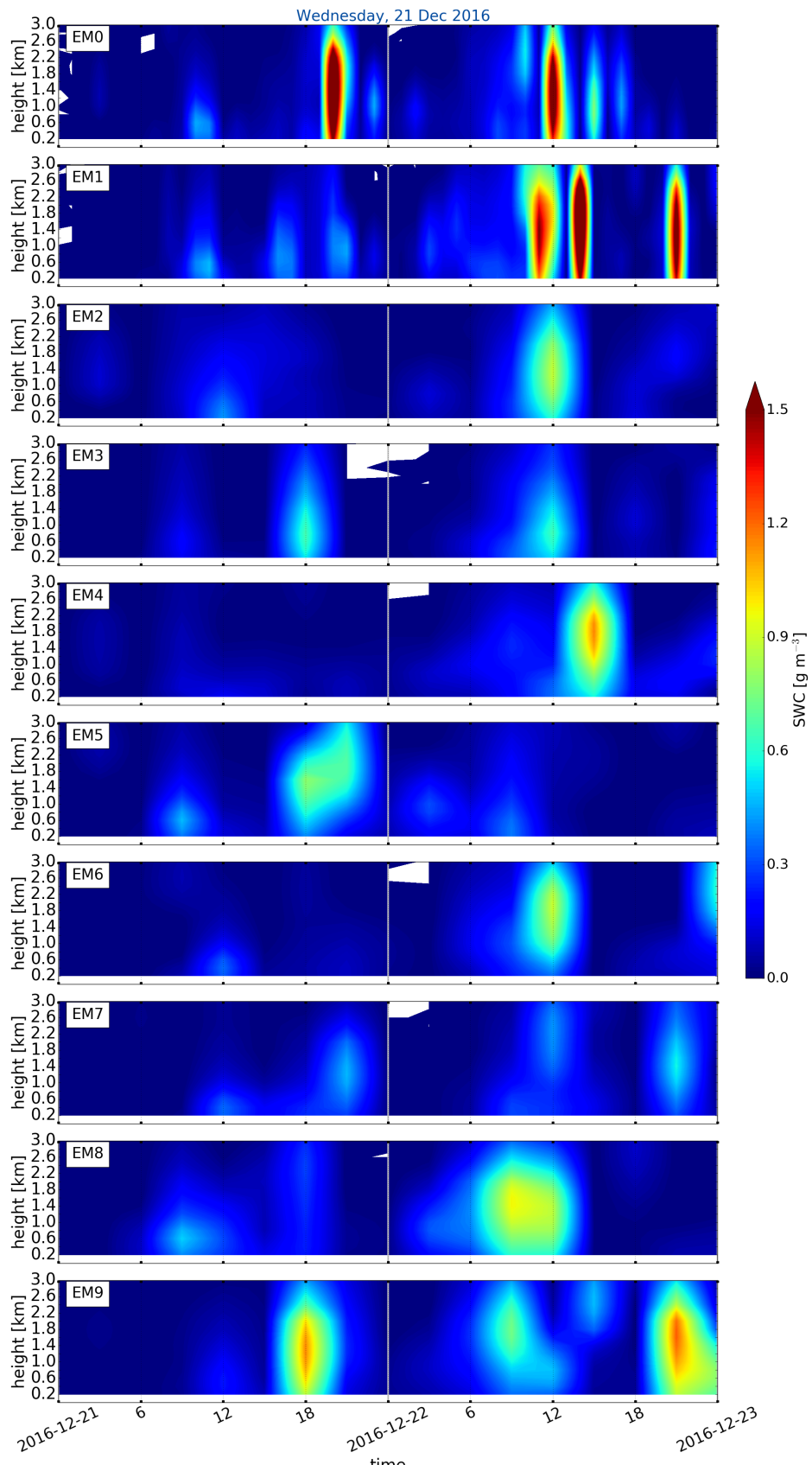
(e)



(f)

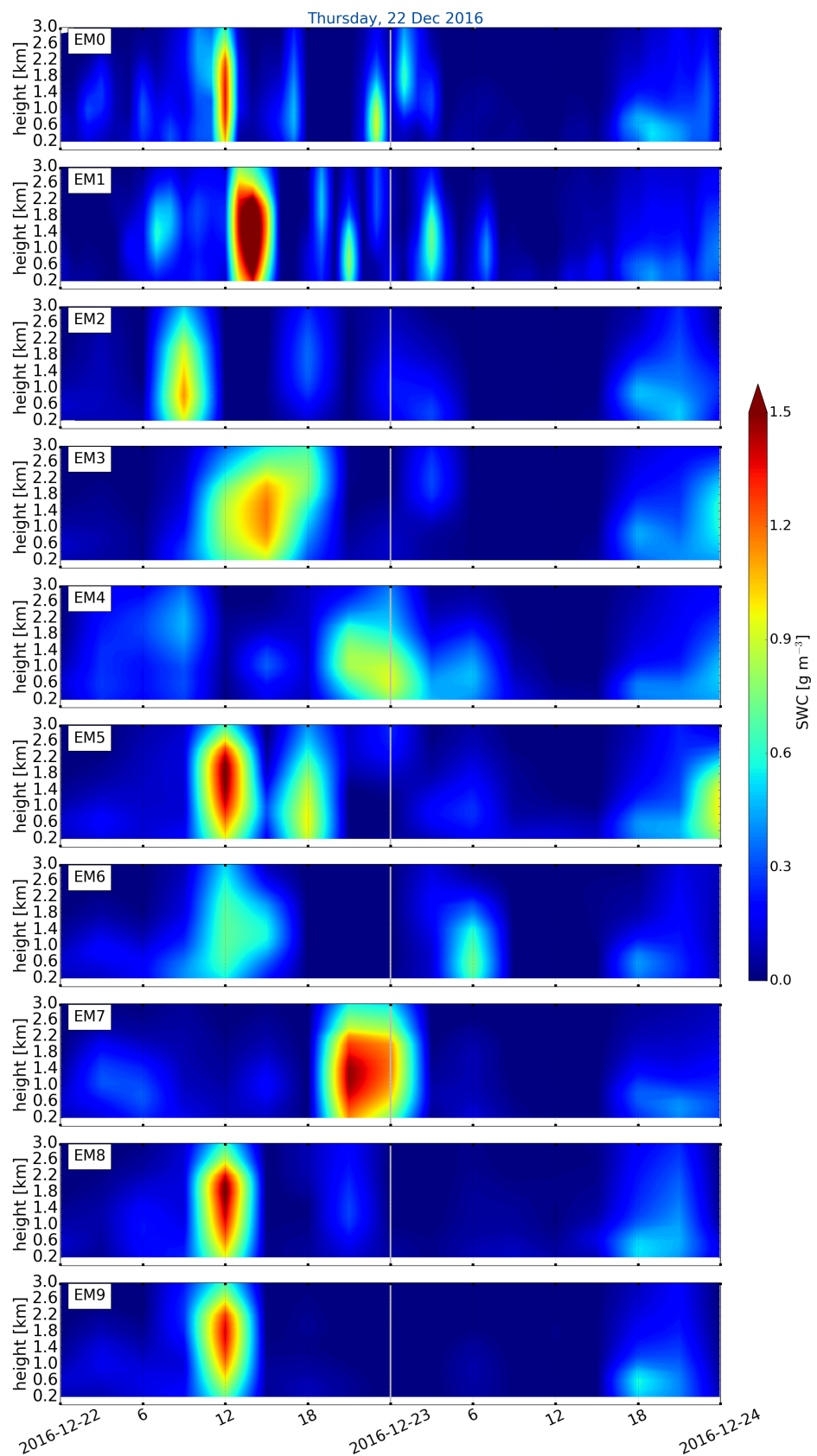
Figure B.1.1: (Continued from previous page.) Initialised 25 December 2016 and 26 December 2016 at 0 UTC.

B.2 VERTICAL SWC - ALL ENSEMBLE MEMBER



(a)

Figure B.2.1: Vertical SWC of each individual ensemble member from 0 to 9 forecast for 48 h. Initialised 21 December 2016 at 0 UTC.



(b)

Figure B.2.1: (Continued from previous page.) Initialised 22 December 2016 at 0 UTC.

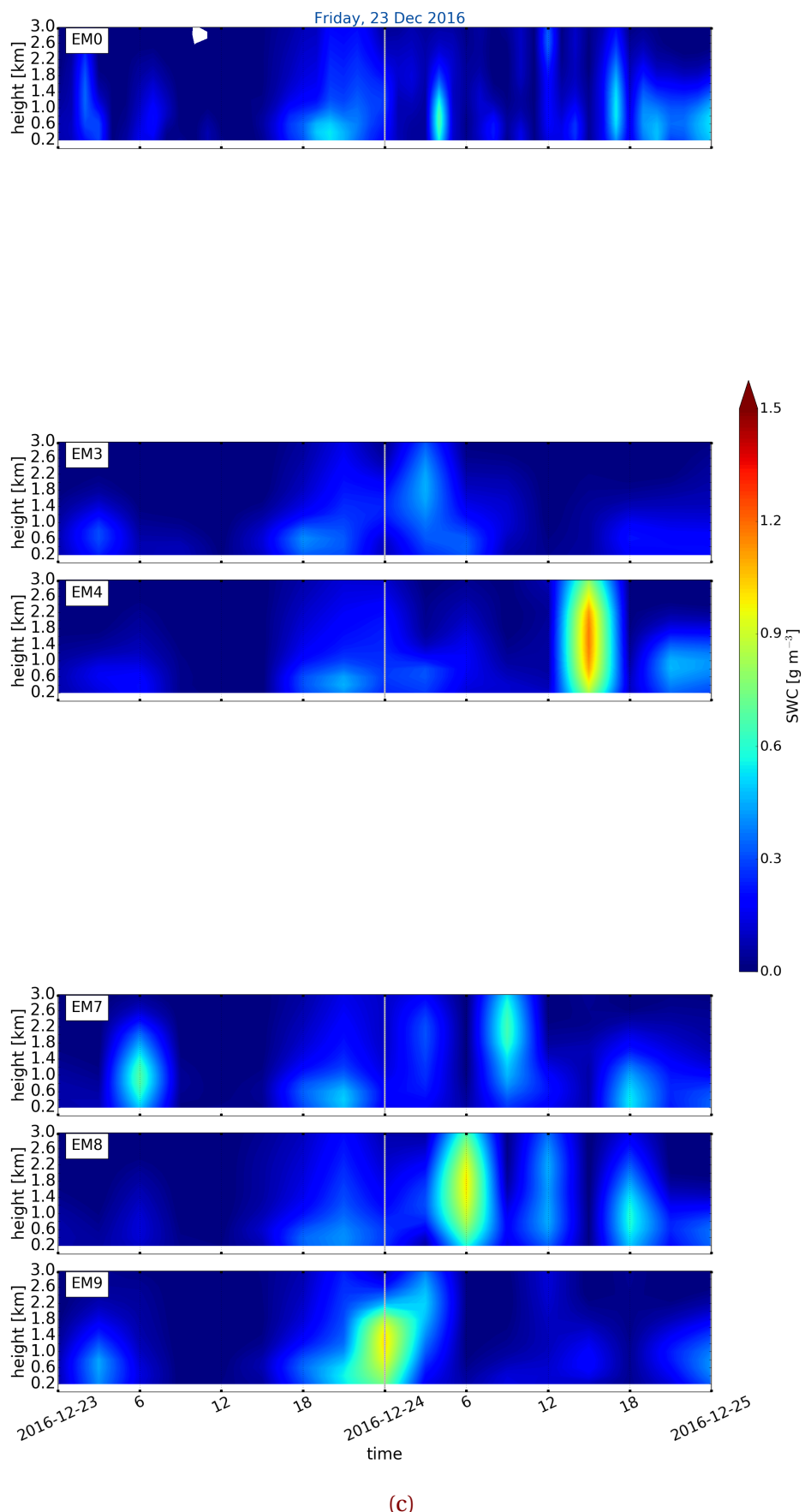
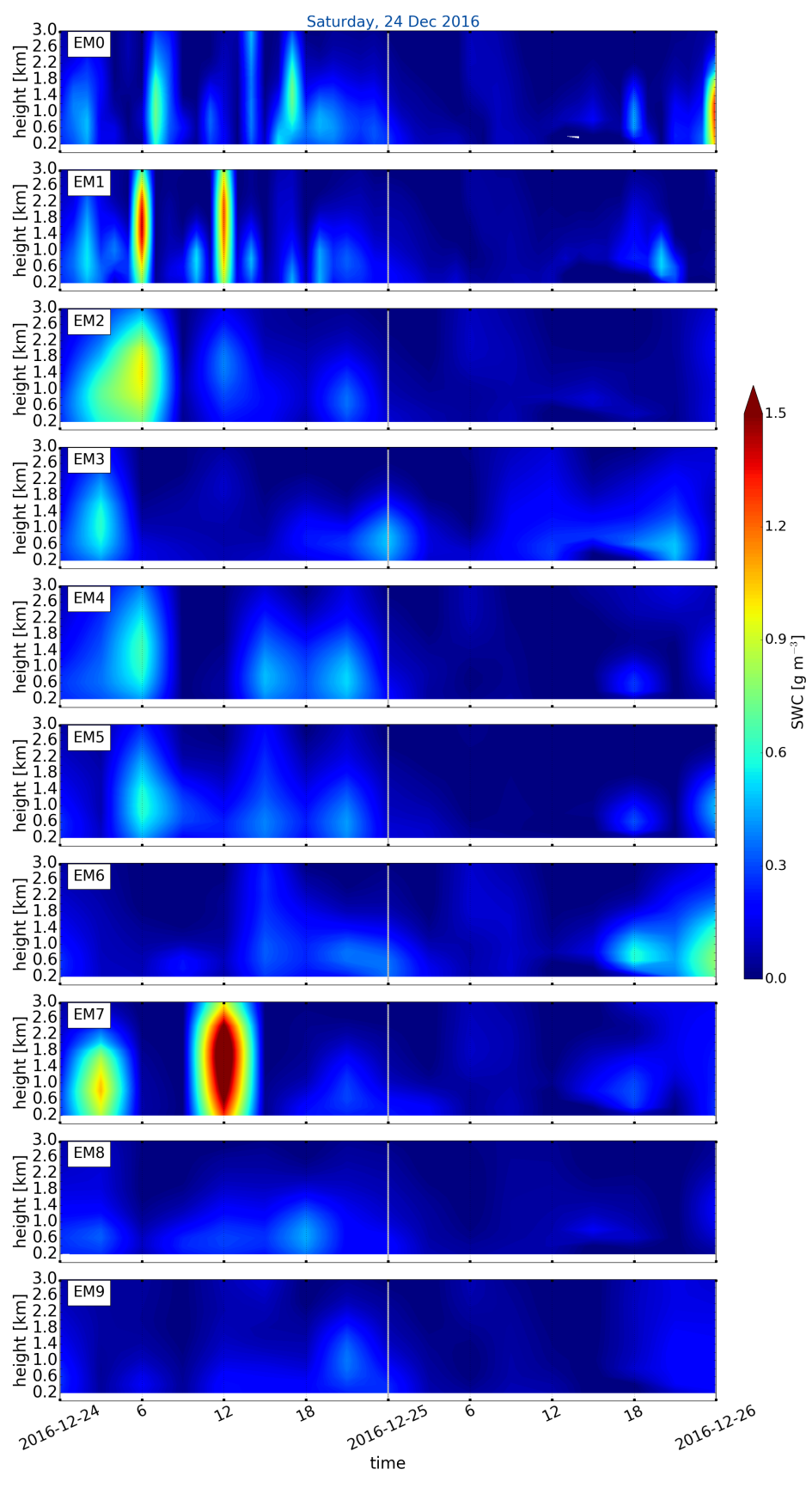


Figure B.2.1: (Continued from previous page.) Initialised 23 December 2016 at 0 UTC.



(d)

Figure B.2.1: (Continued from previous page.) Initialised 24 December 2016 at 0 UTC.

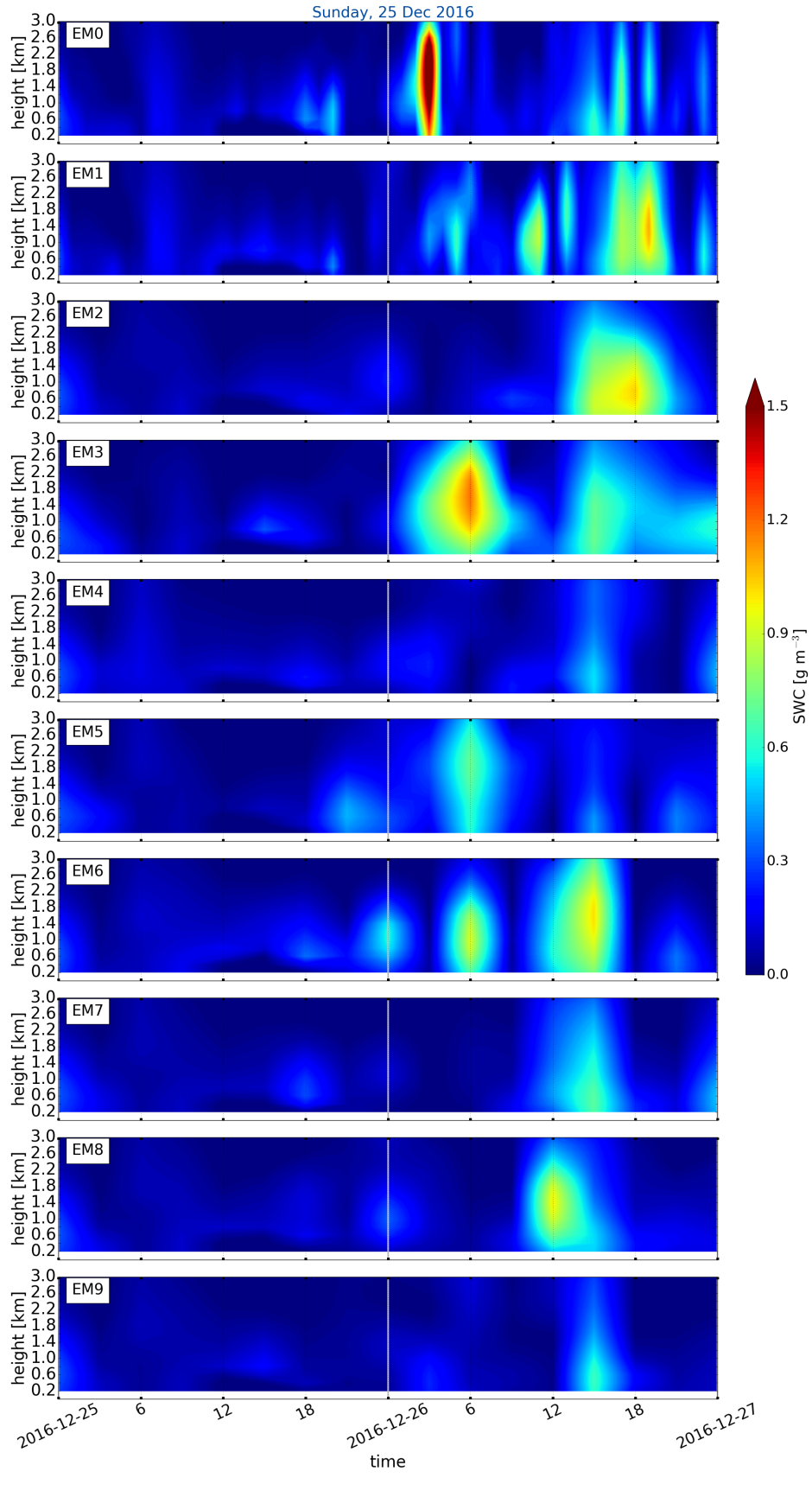
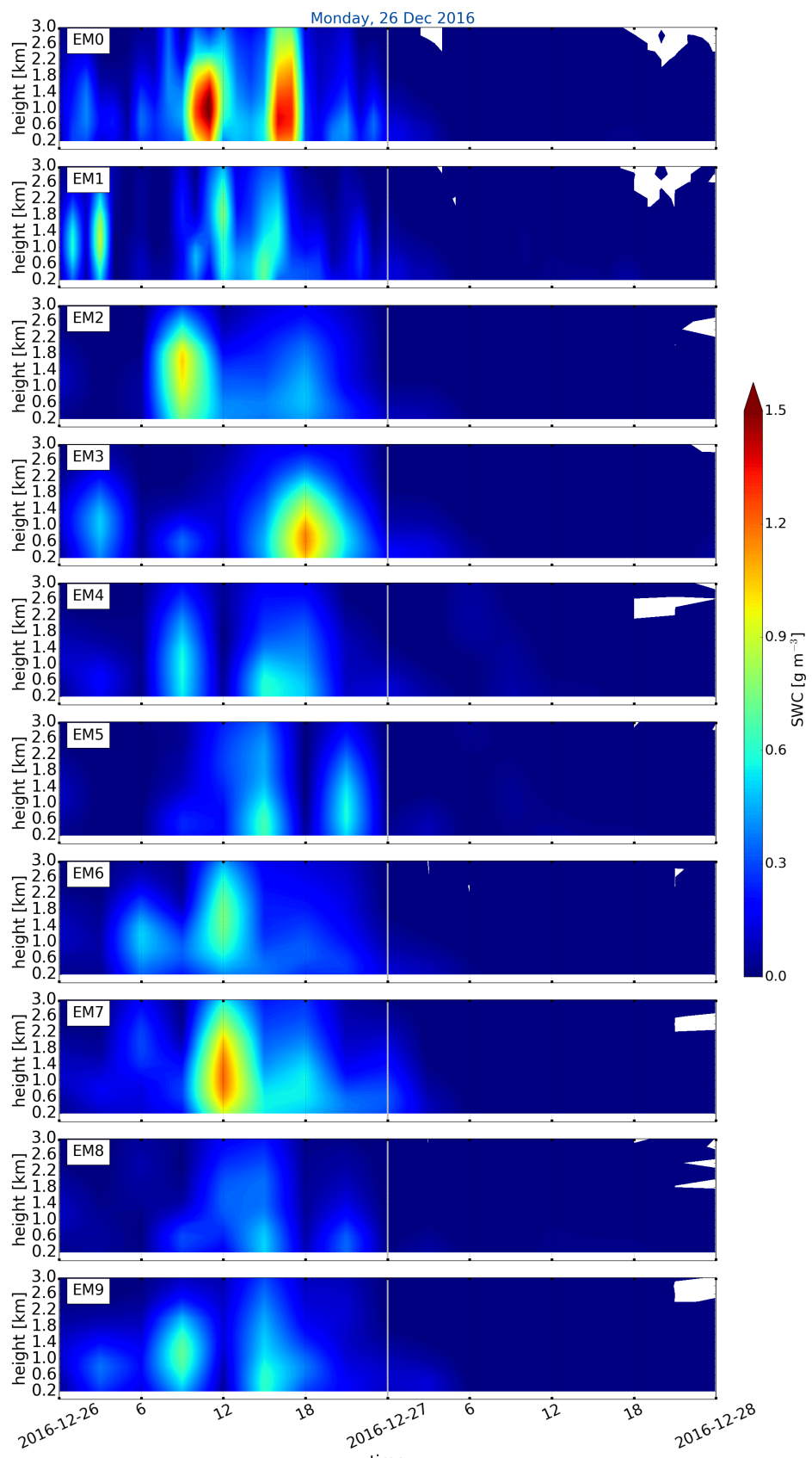


Figure B.2.1: (Continued from previous page.) Initialised 25 December 2016 at 0 UTC



(f)

Figure B.2.1: (Continued from previous page.) Initialised 26 December 2016 at 0 UTC.

